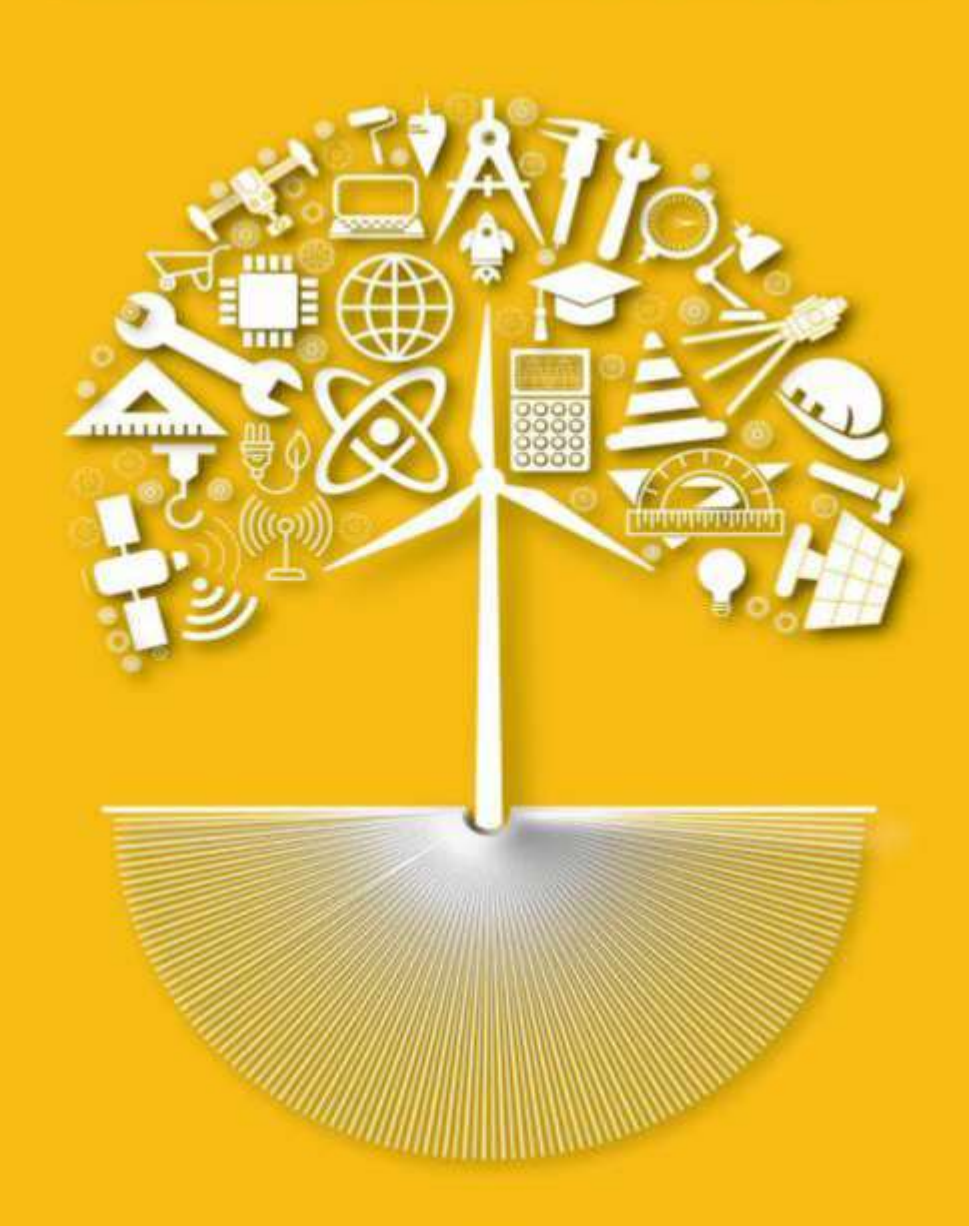


# ETHIOPIAN INTERNATIONAL JOURNAL OF ENGINEERING AND TECHNOLOGY

- "exploration of novel knowledge" —



ISSN (E): 2959-3921, ISSN (P): 2959-393X



m www.amu.edu.et



eijet@amu.edu.et



Volume - 2

ISSUE - 2

December - 2024



# ETHIOPIAN INTERNATIONAL JOURNAL OF ENGINEERING AND TECHNOLOGY (EIJET)

ISSN (E): 2959-3921, ISSN (P): 2959-393X VOLUME-2, ISSUE-2

> DECEMBER, 2024 ARBA MINCH, ETHIOPIA

# **Editorial Team**

# Editor in Chief

**Durga Prasad Sharma**, Ph.D, (Professor), Cloud Computing, Intelligent Autonomic Systems, Software Engineering, and Distributed Green Computing. **Email:** sharma.dp@amu.edu.et, Arba Minch University, Ethiopia.

**ORCID ID:** <a href="https://orcid.org/0000-0002-1654-901X">https://orcid.org/0000-0002-1654-901X</a>

Google Scholar: <a href="https://scholar.google.com/citations?user=jFrf5VsAAAAJ&hl=en">https://scholar.google.com/citations?user=jFrf5VsAAAAJ&hl=en</a>

### Co-Editor in Chief

**Samuel Kefale** (Asst. Prof), Electrical Power System Engineering, Renewable Energy, Electrical Machines, AI in Power Systems. **Email:** samuel.kefale@amu.edu.et, Arba Minch University, Ethiopia.

**ORCID** iD: <a href="https://orcid.org/0000-0003-1105-1084">https://orcid.org/0000-0003-1105-1084</a>

Google Scholar:

https://scholar.google.co.uk/citations?hl=en&user=FY6t2FsAAAAJ&view\_op=list\_works

# Editorial Manager

Addisu Mulugeta, (Asst. Prof), Machine Learning, Data Science, Big Data Analytics, Data Mining, Data Warehousing. Email: addisu.mulugeta@amu.edu.et, Arba Minch University, Ethiopia.

**ORCID iD:** <u>https://orcid.org/0000-0002-6548-9359</u>

Google Scholar: <a href="https://scholar.google.com/citations?user=YOti-8wAAAA]&hl=en">https://scholar.google.com/citations?user=YOti-8wAAAA]&hl=en</a>

# Language Editor

Endalkachew Hailu Guluma, Ph.D., (Asst. Professor), English Language and Literature, Literary and Cultural Studies, Environmental Humanities, Indigenous Knowledge Studies, Folkloristics. Email: endalkachew.hailu@amu.edu.et, Arba Minch University, Ethiopia.

**ORCID ID:** <u>https://orcid.org/0000-0002-6772-4391</u>

Google Scholar: <a href="https://scholar.google.com/citations?user=6nsRrO0AAAA]&hl=en">https://scholar.google.com/citations?user=6nsRrO0AAAA]&hl=en</a>

# Layout Editor

Chirotaw Kentib, Computer Science,

Email: chirotaw.kentib@amu.edu.et, Arba Minch University, Ethiopia.

# **Associate Editors**

**Muluneh Lemma Woldesemayat,** PhD in Electrical Engineering, Specialization: Power Electronics & Drives, Research Interest: Electric Vehicles, Renewable Energy, Power Systems, Arba Minch University, Email: muluneh2006@yahoo.com, Arba Minch, **Ethiopia** 

**Anchit Bijalwan**, PhD in Computer Science & Engineering, Specialization: Network Security & Forensics, Research Interest: Botnet Analysis, AI in Healthcare, Cybersecurity, British University Vietnam, Email: anchit.b@buv.edu.vn, Hanoi, **Vietnam** 

**Mohammed Abebe**, PhD in Computer Engineering, Specialization: Machine Learning, Research Interest: AI in Healthcare, Phishing Detection, Speech Recognition, Arba Minch University, Email: moshethio@gmail.com, Arba Minch, **Ethiopia** 

**Bisrat Gissila,** PhD in Geotechnical Engineering, Specialization: Ground Improvement, Research Interest: Landslide Mitigation, Soil Stabilization, Slope Stability, Arba Minch University, Email: Bisratgissila@gmail.com, Arba Minch, **Ethiopia** 

**Jitendra Kumar Verma**, PhD in Computer Science & Technology, Specialization: Cloud Computing, Research Interest: Energy-Efficient Cloud Systems, IoT, AI, Indian Institute of Foreign Trade, Email: jkverma@iift.edu, Kakinada, **India** 

**Nisha Sharma**, PhD in IT Security, Specialization: Cybersecurity, Research Interest: Wormhole Attacks in MANETs, Network Security, Splunk, State of Missouri (ITSD), Email: Nisha.SharmaJC@gmail.com, Jefferson City, **USA** 

**Rajesh Ravi,** PhD in Mechanical Engineering (Automotive), Specialization: Waste Heat Recovery, Research Interest: Biofuels, Emission Control, Heat Exchangers, Université Internationale De Rabat, Email: rajesh4mech@gmail.com, Rabat, **Morocco** 

Mesay Samuel Gondere, PhD in Computing & IT, Specialization: Artificial Intelligence, Research Interest: NLP, Amharic OCR, Deep Learning, Arba Minch University, Email: mesay.samuel@amu.edu.et, Arba Minch, Ethiopia

Mario Alessandro Bochicchio, PhD in Computer Science, Specialization: eHealth & Data Management, Research Interest: Digital Health, AAL, Big Data, University of Bari, Email: mario.bochicchio@uniba.it, Bari, Italy

**S. Balakumar**, PhD in Electrical Engineering, Specialization: Renewable Energy, Research Interest: Solar & Wind Energy, Power Electronics, Power System Optimization, Arba Minch University, Email: balakumar25dec@gmail.com, Arba Minch, **Ethiopia** 

Worku Jimma, PhD in Health Information Management, Specialization: Health Informatics, Research Interest: Health Information Systems, Knowledge Management, Infodemic Management, Jimma University, Email: worku.jimma@gmail.com, Jimma, Ethiopia

**Hiwot Tsegaye**, PhD in Civil Engineering, Specialization: Infrastructure Materials, Research Interest: Sustainable Construction Materials, Crushed Brick Reuse, High-Performance Concrete, Arba Minch University, Email: hiwitsegsh@gmail.com, Arba Minch, **Ethiopia** 

**J. Isaac JoshuaRamesh Lalvani**, PhD in Mechanical Engineering, Specialization: Automotive Engineering, Research Interest: Alternate Fuels, Biofuels, Hybrid Vehicles, Arba Minch University, Email: isaac.jrl@amu.edu.et, Arba Minch, **Ethiopia** 

**Vasudeva Rao,** PhD in Civil Engineering, Specialization: Geotechnical Engineering, Soil Remediation, Expansive Soils, Arba Minch University, Email: vasudevarao\_9@yahoo.com, Visakhapatnam, **Ethiopia** 

Vandna Rani Verma, PhD in Computer Science & Engineering, Specialization: Complexity Reduction of Software, Energy Efficient Wireless Networks, Galgotias College of Engineering & Technology, Email: profvandna@gmail.com, Greater Noida, India

**Nuredin Edris**, PhD in Architecture, Specialization: Healing Architecture, User Perception in Hospital Design, Wollega University, Email: nuredinidris51@gmail.com, Wollega, **Ethiopia** 

**Zeleke Lulayehu Tadesse**, PhD in Civil Engineering, Specialization: Seismic Response & Soil-Structure Interaction of Buildings, Arba Minch University Institute of Technology, Email: zeleke.lulayehu@amu.edu.et, Arba Minch, **Ethiopia** 

**Efrem Girma,** PhD in Construction Engineering & Management, Specialization: Construction Project Management, Project Performance, BIM, Arba Minch University, Email: ephremg41@gmail.com, Arba Minch, **Ethiopia** 

**Fescha Sahile,** PhD in Construction Engineering, Specialization: Geotechnical Engineering, Construction Materials, Concrete Technology, Arba Minch University, Email: sahile21@gmail.com, Arba Minch, **Ethiopia** 

**Kibreab Adane,** PhD in Computing & IT, Specialization: Artificial Intelligence, Cybersecurity, AI in Cybersecurity, Machine Learning, Arba Minch University, Email: kibreab.adane@amu.edu.et, Arba Minch, **Ethiopia** 

**Solomon Neway,** PhD in Automotive Engineering, Specialization: Vehicle Emissions, Sustainable Transportation, EV Technology, Arba Minch University, Email: solomonnewayjida@gmail.com, Arba Minch, **Ethiopia** 

Yalisho Girma, PhD in Electrical Power Engineering, Specialization: Power Electronics, Renewable Energy, Power Distribution, Arba Minch University, Email: yalisho.girma@amu.edu.et, Arba Minch, Ethiopia

Negussie Tadege Demeke, PhD in Material Science, Arba Minch University, Email: kibreab.adane@amu.edu.et, Arba Minch, Ethiopia

# **Advisory Board**

Alemayehu Chufamo, PhD in Chemical Engineering, Specialization: Process Engineering, Micro/Milli Channels, Phase Transfer Catalysis, Arba Minch University, Email: alemayehuc@gmail.com, Arba Minch, Ethiopia

Sumit Gautam, PhD in Computer Science, Specialization: Mobility Management & AI, Research Interest: Heterogeneous Networks, AI, Product Innovation, LG Soft India, Email: sumit.gautam@ieee.org, Bengaluru, India

Rakesh Kumar Sharma, PhD in Computer Science, Specialization: Cybersecurity, Data Mining, Spatial Decision Support Systems, University of Maryland Eastern Shore, Email: rsharma@umes.edu, Fruitland, United States

Mesfin Abebe, PhD in Software Engineering, Specialization: Artificial Intelligence, Machine Learning, Deep Learning, Autonomous Systems, Adama Science and Technology University, Email: mesfin.abebe@astu.edu.et, Adama, Ethiopia

**Beakal Gizachew**, PhD in Computer Science and Engineering, Specialization: Artificial Intelligence, Energy Efficiency in SDN, Machine Learning, Addis Ababa University, Email: beakal.gizachew@aait.edu.et, Addis Ababa, **Ethiopia** 

**Girma Neshir,** PhD in Information Retrieval, Specialization: Adaptive Systems, Sentiment Analysis, Transfer Learning, Addis Ababa Science and Technology University, Email: girma.neshir@aastu.edu.et, Addis Ababa, **Ethiopia** 

**Prathap Mani**, PhD in Computing, Specialization: Computer Networks, Cybersecurity, Blockchain, IoT, American University of Kurdistan, Email: prathap.mani@auk.edu.krd, Duhok, **Iraq** 

**Lissanework Sileshi Alemu,** PhD in Urban & Regional Planning, Specialization: Urban Management & Planning, Residential Satisfaction, Urban Renewal, Ethiopian Civil Service University, Email: lisaethfirst@yahoo.com, Addis Ababa, **Ethiopia** 

**Padmanabhan**, PhD in Mechanical Engineering, Specialization: Gearbox Design Optimization, Energy, Design, Optimization, Vel Tech Rangarajan Sagunthala R&D Institute of Science and Technology, Email: padmanabhan.ks@gmail.com, Chennai, **India** 

**P. Mangaiyarkarasi**, PhD in Electrical Engineering, Specialization: Power Systems, Voltage Security Assessment, Hybrid Optimization, University College of Engineering, Panruti, Email: mangaisowneya@gmail.com, Panruti, **India** 

# **About the EIJET**

The Ethiopian International Journal of Engineering and Technology (EIJET) is a non-profit peer-reviewed open-access academic research Journal of Arba Minch Institute of Technology under Arba Minch University, Ethiopia. The Journal is indexed in the Asian Science Citation Index (ASCI), Google Scholar, and Academia database. The scope of the Journal covers multidisciplinary and cross-disciplinary areas of study in engineering and technology. The peer-reviewed International Journal publishes all types of quality research papers, case studies, review papers, experimental and empirical papers, and shortened thesises/ dissertations in the broad area of engineering and technology.

The Journal is specifically dedicated to publish novel research contributions and innovative research outcomes in the following fields of engineering and technology: -

- Intelligent Computing and Information Technology,
- Mechanical and Metallurgy Engineering,
- Architectural Design and Town Planning,
- Civil and Transport Engineering Systems,
- Electrical Engineering and Power Electronics,
- Emerging areas of Renewable Energy
- Papers related to allied disciplines, emerging technologies, and future-generation engineering will be given priority for publication.

The Journal publishes papers from worldwide sources, especially for covering the emerging issues of engineering and technology from developing and developed countries. The Papers from African continent countries having localized problem-solving research will be given priority.

# **Table of Contents**

About EIJETVIII	[
Enhancing Accuracy of Fault Detection System and Reducing Outage Time with GIS: A Case Study of Arba Minch Electrical Distribution System	
Esayas Zarba <sup>1</sup> , Samuel Kefale <sup>1*</sup> and Andinet Anjamo <sup>1</sup>	1
Structural Reliability Studies on Pulverized Glass Powder Concrete Subjected to Bending Forces with Natural Aggregate17	
Kolo, D. N <sup>1*</sup> ., Aguwa, J. I. <sup>1</sup> , Hadi, A. M <sup>1</sup> ., Shehu, M <sup>1</sup> ., and Ashraf, M. L.M <sup>2</sup>	7
Effect of Fine Fractions on Engineering Properties of Sandy Soils in Southern Ethiopia's Gamo Zone	
Paulos Sisay Shido <sup>1*</sup> , Democracy Dilla Dirate <sup>1</sup> , and Dr. Bisrat Gissila <sup>1</sup>	6
Synthesis of Nano-Biocomposite for Light-Weight Structural Applications41	Ĺ
Nehemiah Mengistu Zeleke* <sup>1</sup> , Devendra Kumar Sinha <sup>1</sup> , Santosh Kumar <sup>2</sup> 4	1
Analyzing Mechanical Property and the Corresponding Power Output of Bamboo Plant for the Construction of Vertical Axis Wind Turbine Blade68	
Elias Alemu <sup>1*</sup> and Degnet Abose <sup>2</sup> 6	8
Integrating Sustainability Frameworks for Assessment of Environmental Performance in Higher Education Institutions Via Energy, Fuel, and Waste Management Audits	
Tsegaye Getachew Alenka <sup>1*</sup> , Mulugeta Tadese Wotango <sup>2</sup> , Sileshi Kore Dube <sup>3</sup>	9

Volume 2, Issue 2, 2024

Copyright and License Grant: CC By 4.0 🙃 0



DOI: https://doi.org/10.59122/164CFC12

ISSN (E): 2959-3921 (P): 2959-393X

# **Enhancing Accuracy of Fault Detection System and Reducing Outage Time** with GIS: A Case Study of Arba Minch Electrical Distribution System

Esayas Zarba<sup>1</sup>, Samuel Kefale<sup>1\*</sup> and Andinet Anjamo<sup>1</sup> <sup>1</sup>Faculty of Electrical and Computer Engineering, Arba Minch University, Ethiopia \*Corresponding Author's Email: anikeed1@gmail.com

### **Abstract**

Fault detection and location in electrical distribution systems are critical for maintaining a reliable electric power supply and minimizing outage time. The Arba Minch District distribution department of Ethiopian Electric Utility (EEU) currently employs a manual trial-and-error approach for fault detection and location of the faults, is not only inefficient, time-consuming, and ineffective in the current state of the arts but crucial for resolving faults. This study evaluates the current approach and proposes an enhanced system utilizing Geographic Information System (GIS) technology to improve fault detection and location in the Arba Minch distribution system, specifically at the Shecha feeder. The implementation of GIS-based fault detection and location aims to address the limitations of the manual method and mitigate economic losses associated with feeder faults. By synchronization of the ETAP circuit and ETAP GIS network, the location of the fault visualized in the ETAP-GIS system. The GIS system achieved a 99.11% reduction in fault detection and location time relative to the conventional method. In this research by optimizing fault detection and locating time, the System's Average Interruption Duration Index (SAIDI) for the feeder significantly reduced from 216.36 to 1.93 hours/customer per fault. Consequently, the GIS system also eliminated economic losses associated with energy unsupplied (24,784.58 kWh and 13,625.41 kVArh) and non-collected revenue (42,000 ETB for 1 hour, 78,288 ETB for 1.864 hours, and 231,000 ETB for 5.5 hours). The results demonstrate the potential of GIS technology in enhancing fault detection and location, ultimately improving the reliability and efficiency of the distribution system.

Keywords: Distribution systems, ETAP, Fault Detection, Fault Location, GIS, SAIDI

#### I. Introduction

Electric power is vital for economic progress in a country. It encompassing generation, transmission, and distribution systems to deliver electricity to users. In the developing countries such as Ethiopia the disruptions in the distribution network are commonplace and present significant obstacles. The electricity distribution system consists of primary distribution feeders, distribution transformers, distributors, and service lines. Electricity produced at plants converted to lower voltage at substations, carried via primary

Received: 25 July 2024; Revised: 9 October 2024; Accepted: 26 October 2024; Published: November 2024.

Volume 2, Issue 2, 2024

DOI: https://doi.org/10.59122/164CFC12

Copyright and License Grant: CC By 4.0 (a)



distribution feeders to distribution transformers, and further decreased in voltage. In the current system the low-voltage power links to distributors or directly to consumer loads. Service lines transporting low-voltage electricity link to distributors and furnish power to users. Distributors classified as distributors and subdistributors, are establishing an effective framework for delivering electricity to consumers [1].

In 2013, Ethiopia restructured its electric power sector, leading to the formation of two distinct entities: Ethiopian Electric Power (EEP) and Ethiopian Electric Utility (EEU). EEP primarily handles electricity generation and transmission at voltages above 66 kV, while EEU oversees sub-transmission systems up to 66 kV and the distribution of electricity to end-users. Power transformers of varying capacities supply distribution transformers, typically deployed at standard medium voltage levels of 33 kV and 15 kV. The distribution grid follows a radial layout, with distribution transformers of various ratings stepping down the voltages of 33 kV and 15 kV to deliver 400 volts for three-phase systems and 230 volts for single-phase consumers [2].

In the current scenario the power demand on the distribution system continually changes [3]. To handle this, change the structure of distribution networks is undergoing profound changes. These networks are becoming increasingly intricate with the integration of new technologies, while the electricity demand continues to rise steadily [4]. Electrical circuit failures and disruptions to normal circuit functioning stem from physical faults, often triggered by over- currents, over- voltages, short circuits, open circuits, and damaged devices. Short circuits or overloads, the primary culprits, create abnormal connections or disturbances and divert current from its intended path. Short circuit faults exhibit either low or significant impedance.

Activation of a protective device in response to a short circuit fault may lead to service interruptions for utility customers. Conversely, high impedance faults with ample impedance to thwart protective devices may not cause outages, but they can still induce power quality issues and potential harm to utility equipment [5].

Effective fault detection and location are fundamental to the operation of electrical distribution systems. Traditional methods, such as impedance-based and traveling wave techniques, have been widely employed but often fall short in terms of accuracy and response time, especially in complex network environments [6], [7]. These limitations necessitate the development of more advanced solutions.

Modern smart grids and smart cities rely on efficient fault management for optimal functionality. This involves swiftly identifying and isolating faults, strategically deploying backup resources to restore power to affected customers, and minimizing the impact of outages. By automating fault location and service restoration, smart grids can significantly improve reliability and decrease revenue losses caused by

Volume 2, Issue 2, 2024

DOI: https://doi.org/10.59122/164CFC12



interruptions. These interruptions, often due to weather events, equipment malfunctions, road work, and other factors, make up about 80% of all customer disruptions in electric power distribution networks [5]. The reliability of electrical distribution systems is heavily dependent on effective fault detection and location techniques. Historically, identifying faults in distribution networks has been a challenge for utility companies. Extensive research has focused on developing fault location methods to expedite service restoration, reduce outage time, and ultimately lower associated costs [8]. Traditional methods for detecting faults, like impedance-based and traveling wave techniques, have widely used. However, these methods can struggle with accuracy and speed, especially in large and intricate networks [9]. These traditional methods are gradually supplemented by more advanced technologies to address their limitations.

ETAP GIS offers a significant advantage in fault detection by seamlessly integrating electrical one-line diagrams with geographical maps, providing a comprehensive and dynamic tool for accessing, analyzing, and managing geospatial information. GIS provides a robust framework for integrating spatial data with real-time monitoring, facilitating precise fault localization and rapid response. By leveraging GIS, utilities can visualize the network topology, analyze spatial relationships, and efficiently deploy resources to fault locations [10],[11]. Compared to AI-based systems, which require extensive data and specialized knowledge, and IoT-enabled fault passage indicators, which depend on reliable communication networks and robust security measures, ETAP GIS stands out for combining geospatial and electrical data effectively [12]. This makes it particularly valuable for utilities looking to improve their fault detection capabilities while maintaining a clear and intuitive overview of their electrical network.

Incorporating GIS into fault detection systems has shown significant promise. For instance, GIS-based systems can process and visualize large volumes of data, offering insights into the spatial distribution of faults and their impacts on the network [5]. ETAP GIS can handle various network configurations and complexities making it suitable for different types of electrical distribution systems, whether urban or rural.

The Arba Minch distribution system, located in southern Ethiopia presents unique challenges due to its diverse topography and rapidly expanding infrastructure. The region's increasing demand for reliable electricity necessitates innovative solutions for fault management. In Arba Minch, traditional methods are employed to pinpoint outage areas in the 11kV and 15kV distribution network using earth fault indicators installed at distribution substations. Technical staff patrol the suspected faulty feeder and inspect the fault indicator's status to identify the faulty section of the feeder. Subsequently, they perform necessary isolation operations before restoring supply to consumers. Occasionally, switching operations are necessary to pinpoint the faulty section. Moreover, faults typically detected only when customers report outages, after



Volume 2, Issue 2, 2024

which onsite fault location techniques utilized for LV feeders. This fault location process is time-consuming and may subject feeder cables to stress from frequent switching actions or high voltage surges from surge wave generators.

This paper explores the application of GIS technology in enhancing fault detection and the location of the faults within the Arba Minch distribution system. By utilizing GIS, the research seeks to demonstrate improvements in fault detection accuracy, localization detection speed, and overall system efficiency.

#### II. **Materials and Methods**

## A. Data Collection

The information gathered includes the ratings and loads of each transformer, the GPS coordinates of all transformers, some suspension poles, and all poles with angles along the Arba Minch Shecha feeder as shown in Fig. 1. This data was collected through primary methods like surveys, observations, and measurements. Transformer loads were measured using Clamp meters and Energy analyzers. The GPS coordinates of transformers, poles, and line lengths were obtained through surveys and GPS GARMIN measurements at EEU Arba Minch District. Secondary data, such as outage times of faults and information needed to identify these faults, were acquired through interviews with the Arba Minch substation and the Arba Minch district distribution operation department.

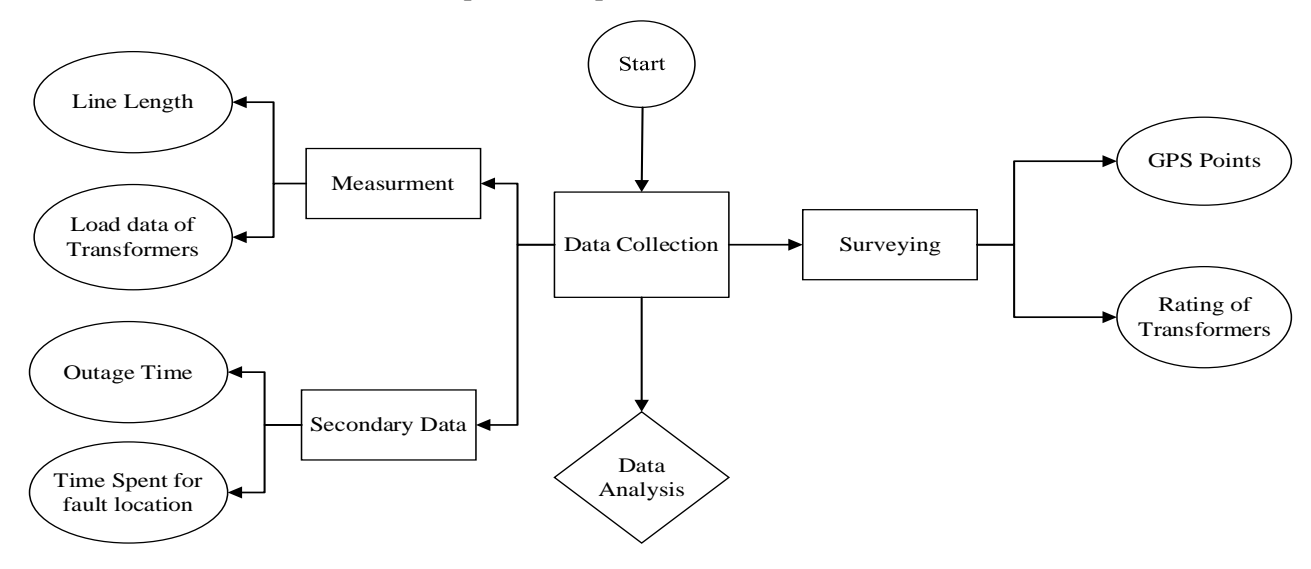


Fig. 1.: Data collection methods

The types of overhead line conductors are all alloyed aluminum conductors (AAAC) with the crosssectional are sizes of 50 mm<sup>2</sup> and 95 mm<sup>2</sup>. There are 31 public and 31 private transformers with ratings 25, 50, 100, 200, 315, 500, 630, 800 and 1250 KVA. The three-year data of fault duration greater than an hour



is taken from the Arba Minch substation and the time required to find the corresponding fault is collected from the Arba Minch District distribution operation department. The Arba Minch substation is depicted in the single-line diagram shown in Fig. 2.

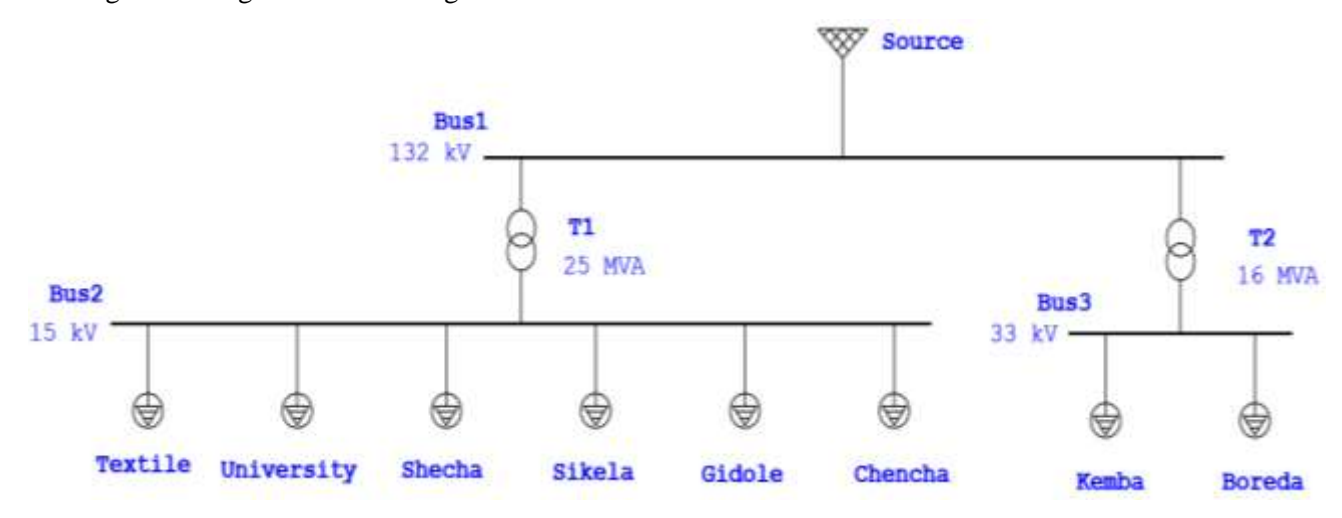


Fig. 2.: Single line diagram of Arba Minch substation

Fig. 3., which was created using real data, depicts the single-line diagram of the Shecha feeder,. The feeder comprises 62 distribution transformers (T1-T62), four section switches (SS1, SS2, SS3, and SS4), and 177 buses, including 115 main buses and 62 load buses. The network also includes 114 lines.

DOI: https://doi.org/10.59122/164CFC12

Copyright and License Grant: CC By 4.0





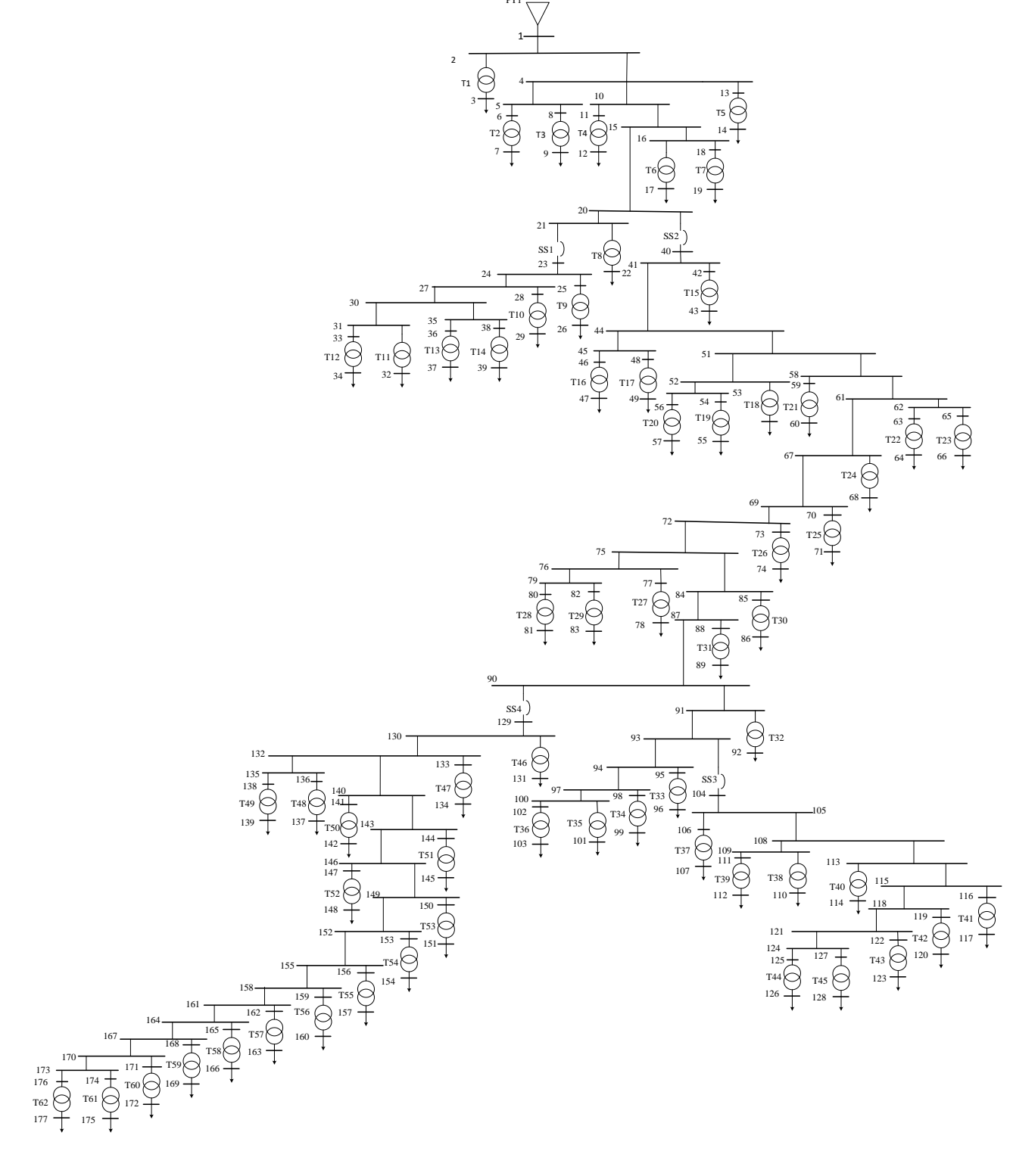
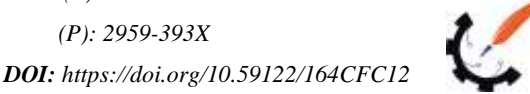


Fig. 3.: The single -line- diagram of Shecha feeder



Copyright and License Grant: CC By 4.0 (a)



Volume 2, Issue 2, 2024

# B. Work Flow of the System

The overall block diagram that shows the complete work of the study is shown in Fig. 4.

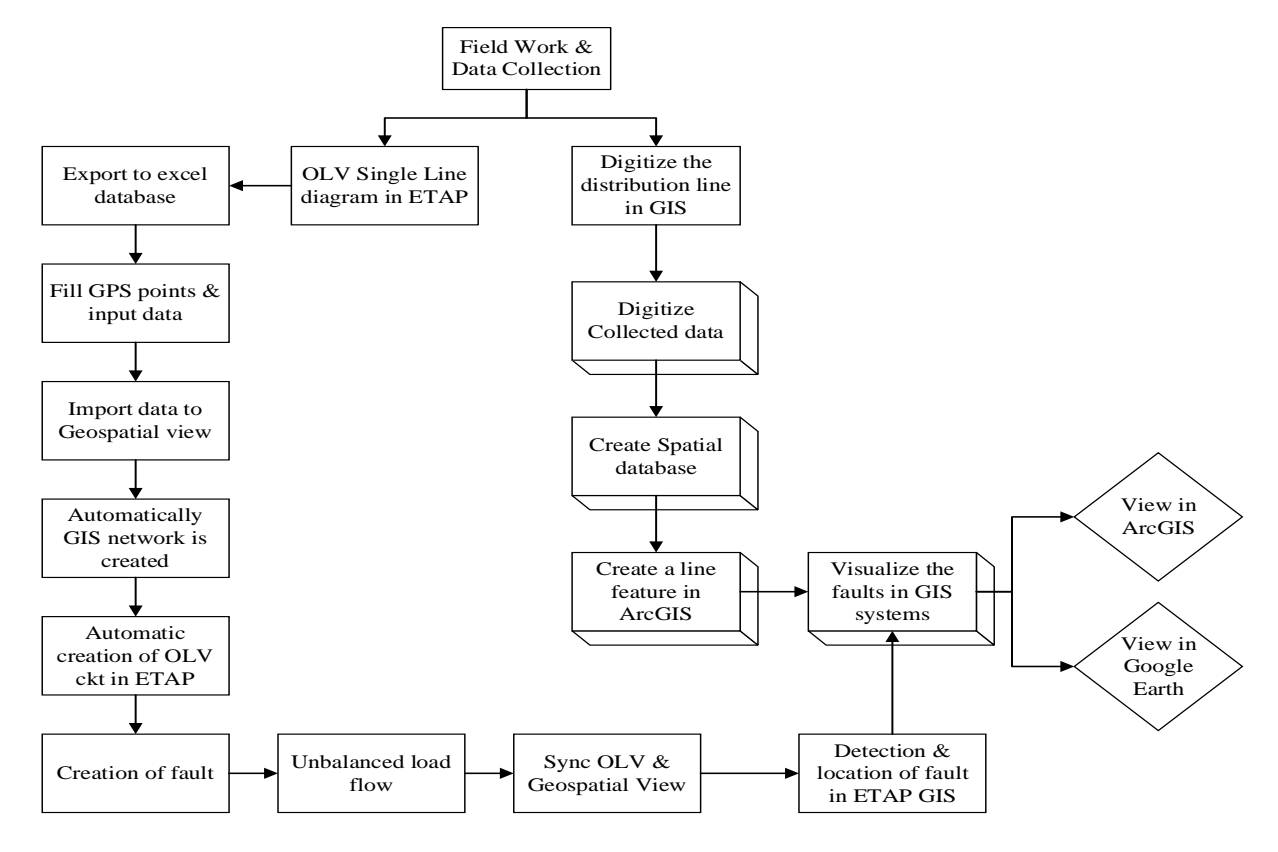


Fig. 4.: Overall block diagram of the system

# C. ETAP GIS Map

When an electrical system's GIS (Geographic Information System) map is available, data can be seamlessly transferred to ETAP (Electrical Transient Analyzer Program), eliminating the need for manual input and significantly reducing the potential for errors. This seamless data transfer facilitates the creation of one-line diagrams and ensures the accuracy of data used in system studies.

By integrating electrical one-line diagrams with corresponding geographical maps of power generation, transmission, and distribution systems, the ETAP GIS Map provides a dynamic tool for accessing, analyzing, and managing geospatial information. ETAP's one-line diagrams offer a logical representation of the electrical connections within a complex GIS map. These maps typically utilize one or more geometric networks, which represent one-dimensional linear networks such as utility or electrical power distribution networks through geometric shapes.



Volume 2, Issue 2, 2024

The components of the geometric network are associated with corresponding ETAP elements, resulting in a detailed and accurate illustration of the electrical system. During the initial data transfer process, ETAP generates electrical one-line diagrams using topology data from the geometric network and its features. These diagrams incorporate both default values and library data from ETAP. This combined information is then employed for conducting power system studies, including Power Flow Studies and Fault Analysis. The data flow process between ETAP and ETAP GIS is depicted in Fig. 5.

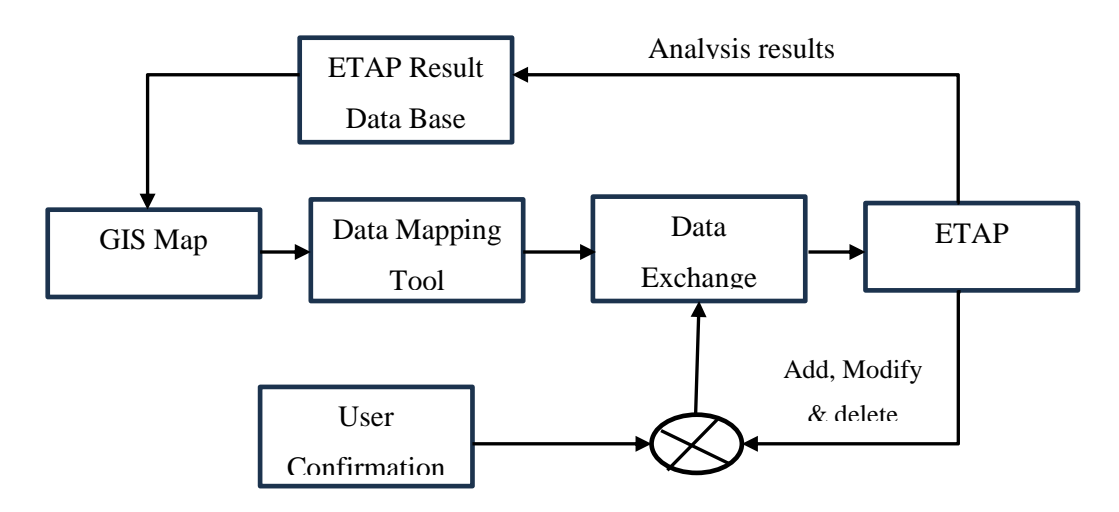


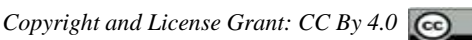
Fig. 5.: ETAP and GIS map data flow

# D. GIS-based Fault Detection and Location Identification Methods

GIS platforms integrate various data sources, including network diagrams, equipment specifications, and sensor data. This integration provides a comprehensive view of the power distribution network. To effectively implement methods for improving the detection and location of faults, a range of devices are utilized to gather information about the fault's nature and its location. These devices are connected to network components like switch-disconnectors or circuit breakers, which can be found in both overhead and underground networks, on conductors or electrical towers. These devices, known as protection relays, are also referred to as Intelligent Electronic Devices (IEDs) when connected to circuit breakers, or Fault Passage Indicators (FPIs) when connected to switch-disconnectors. The key distinction between these devices is that while IEDs can identify a fault and promptly send a signal to open the circuit breaker and isolate the fault, FPIs can only detect the fault and report the information. As a result, IEDs offer additional features that allow for rapid response to a fault and provide other functions to improve fault protection. These devices possess the ability to detect the type, size, and direction of a fault, as well as continuously monitor these variables as shown in Fig. 6 thereby improving the overall reliability of the electrical distribution system [13]-[15].

DOI: https://doi.org/10.59122/164CFC12







Volume 2, Issue 2, 2024

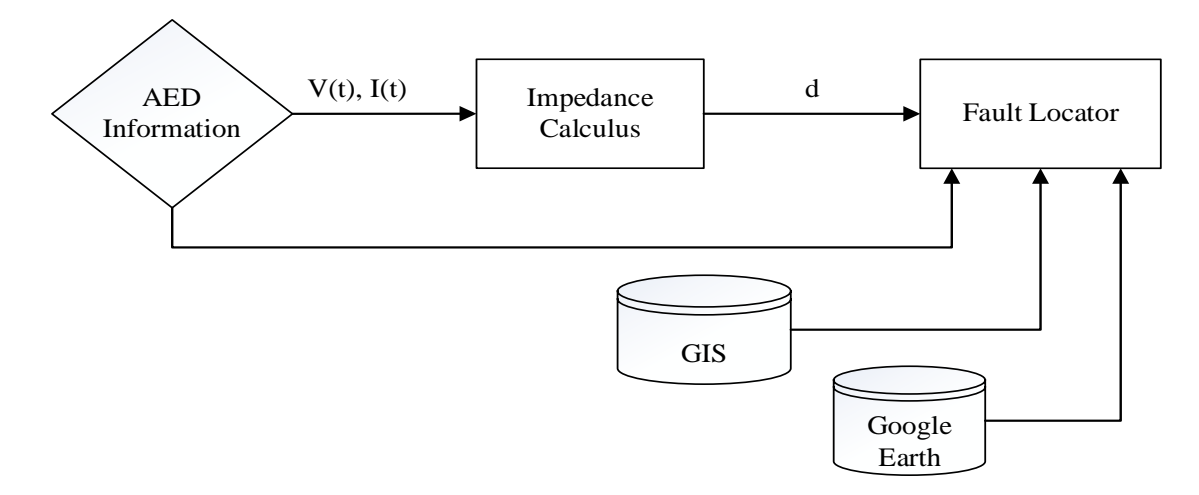


Fig. 6.: Data flow of fault location

When using a fault indicator to collect circuit fault information, the primary method is to determine the type of fault by analyzing the current information in the fault indicator. The fault indicator employs a sensing device to monitor changes in the circuit's current, mainly detecting the conditions when a wire is grounded or short-circuited.

During a ground fault, the voltage of the affected wire relative to the ground will suddenly drop significantly. This rapid decrease in voltage, once it surpasses a predefined threshold, indicates a grounding fault. Similarly, in a short-circuit condition, the fault indicator detects abnormal current flows, which help in identifying the fault type and location [15].

#### **Results and Discussions** III.

# A. Fault detection and its Location Identification in Shecha Feeder

The Logical Single Line Diagram is generated automatically by the ETAP GIS system to simulate balanced load flow, unbalanced load flow, and unbalanced short-circuit analysis. Unbalanced short-circuit analysis is used to introduce faults and compute fault currents in the system, with the fault being applied at any bus. The resulting fault current values can be viewed in ETAP GIS. To locate the fault in the Logical Single Line Diagram within the ETAP GIS system, the presentations must be synced in the window. The fault location's performance is 100%, detecting the fault through the execution of unbalanced short-circuit analysis.

Case 1: Assuming all types of faults occur at bus 28, the simulation for unbalanced short-circuit is displayed in Fig. 7.



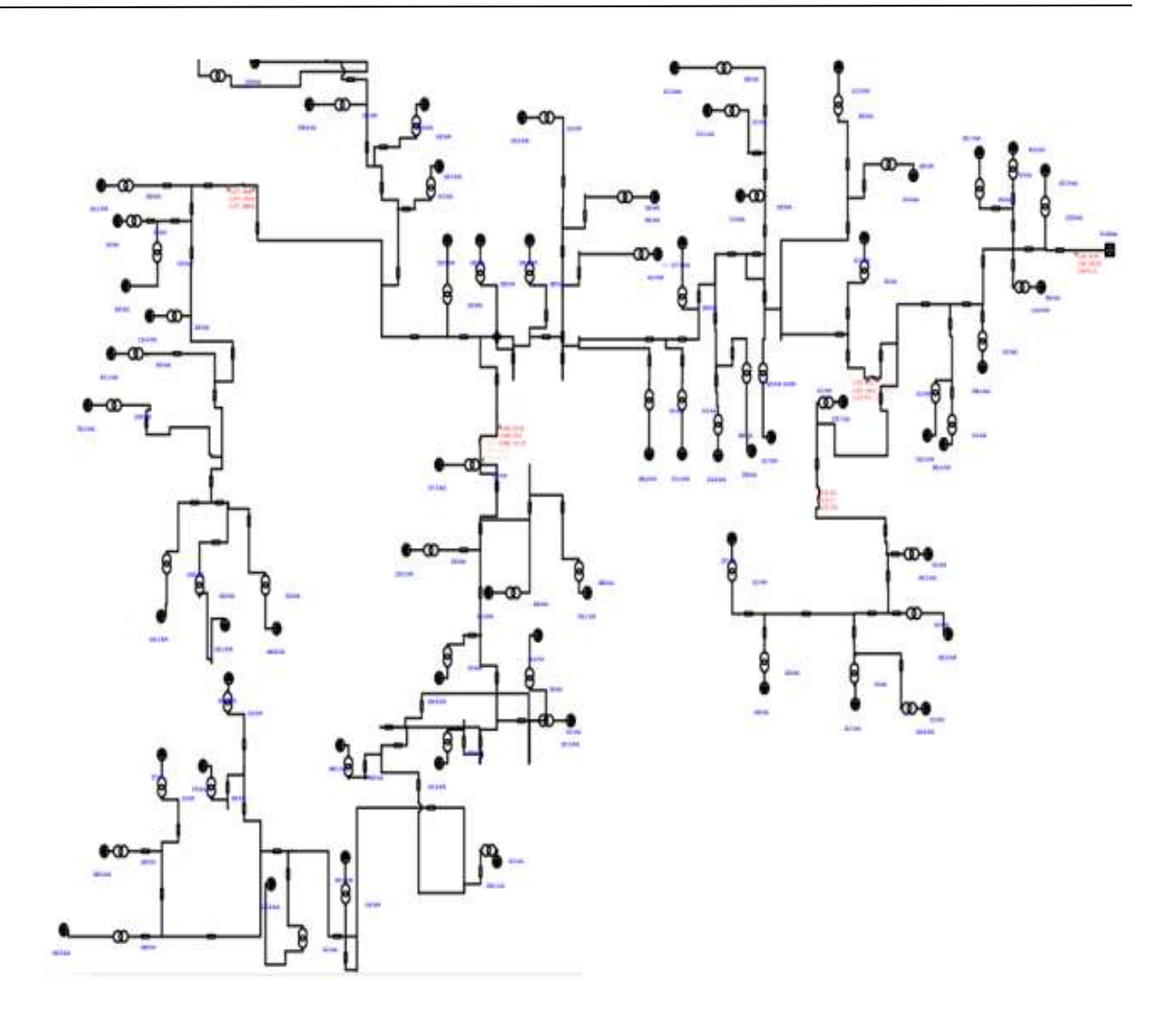


Fig. 7.: Unbalanced short-circuit analysis of Shecha feeder

Fig. 8 illustrates an ETAP GIS network of the Shecha feeder from a geospatial perspective. It identifies the fault and marks its location with a bold red point. The fault location, depicted below, corresponds to Bus number 28, with its GPS point named 336. In terms of geographical location, this fault is situated in front of the Arba Minch Tele office or the Grand Medical Clinic. This fault is also located at Longitude 37°33'4"E and Latitude 06°01'20"N, as shown in Fig. 8.





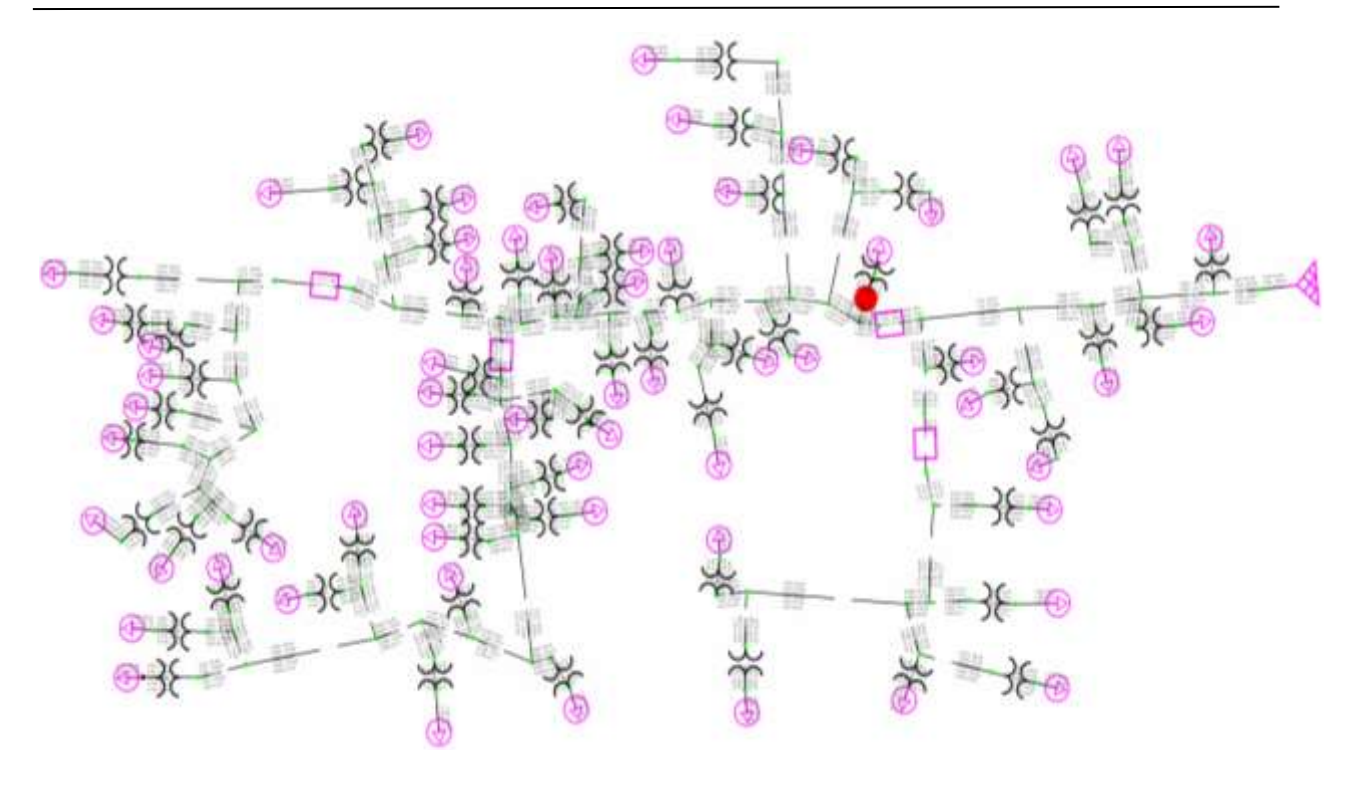


Fig. 8.: Fault location by ETAP GIS system for Case 1

Once the fault is detected and located by using the ETAP GIS system, there are many options to see the location of the fault. It is also possible to find the distance of the fault by adding the distances of the lines.

Fault distance from substation = length of (Line1 + Line2 + Line6 + Line9 + Line10 + Line25 + Line26 + Line 27) = 552m + 380m + 206m + 372m + 650m + 136m + 399m + 2m

= 2,697m





Fig. 9.: Fault location in Google Earth for Case 1

As illustrated in Fig. 9., the faulted area in the electric distribution line has been accurately identified usin g the ETAP GIS software. This precise location is then showcased in Google Earth, providing a clear visu al representation of the fault on the map.

# B. Load Flow Analysis of Shecha Feeder

The total length of this feeder is 18.154 kilometers, with the longest branch measuring 7.155 kilometers and the shortest branch measuring 0.552 kilometers. ETAP software, utilizing precise data, was used to conduct a load flow analysis. The analysis revealed the following:

The shortest branch exhibits a 3.69% voltage drop, resulting in a terminal medium side voltage of 14.4375 kV. The longest branch experiences a more significant 18.34% voltage drop, leading to a terminal medium side voltage of 12.2625 kV. The low side voltage for the shortest branch is 385 V, while the longest branch measures 327 V. The feeder's total active power is 14.776 MW, with a reactive power of 8.082 MVAr. This equates to an apparent power of 16.842 MVA, representing 67.37% of the power transformer's 25 MVA capacity. The load flow analysis identified an overload condition in transformer DT32, operating at 107.2% of its capacity. The feeder experiences significant branching losses, with 2,197.20 kW of active power loss and 1,154.3 kVAr of reactive power loss. Minimizing these losses is crucial. Detailed reports on load flow, branch loading, and branch losses are included in appendices 3, 4, and 5, respectively.

DOI: https://doi.org/10.59122/164CFC12



Copyright and License Grant: CC By 4.0 ( )



# C. The Time Analysis for Fault Finding

To analyze the time aspect, a three-year dataset of faults lasting an hour, or more was collected from the Arba Minch Substation. The time taken to locate the respective faults was obtained from the EEU Arba Minch District Distribution Operation office. The data analysis reveals that the time spent finding faults constitutes 63.23% of the total fault-clearing time, while the remaining 36.77% is dedicated to technical maintenance for service restoration. This indicates that energy losses (Energy Not Supplied and Energy Not Sold) are a result of the traditional fault-finding method.

In the context of the Shecha feeder, the average estimated time to find faults using the conventional method is 63.23% of the total outage time. However, by employing the GIS method, the required time to locate or find faults is reduced to less than or equal to one minute. This translates to less than 0.56% of the total fault duration, resulting in a 99.11% reduction in required time compared to the conventional method.

- The percentage time to find the fault by conventional method =  $\frac{1.864}{2.948}$  x 100 = 63.23 %
- Technical Maintenance time = 100 63.23 = 36.77 %
- The percentage time to find the fault by GIS method =  $\frac{1}{60 \times 2.948} \times 100 = 0.56\%$
- The time reduced by GIS referred to Conventional method =  $\frac{63.23-0.56}{63.23}$  x 100 = 99.11 %
- SAIDI due to fault detection and location by try-and-error approach  $\cong \frac{63.23}{100} \times 271.3 = 171.54$
- ❖ SAIDI value with improved GIS technique  $\cong \frac{100-99.11}{100}$  x 171.54 = 1.53

# D. Economic Loss Analysis

1) Energy not Supplied or Energy Not Sold: In Table I, the average energy loss in terms of real power and reactive power is depicted under the assumption of various load conditions (25%, 50%, 75%, and 100% of the total load) in a conventional method during a single fault. Assuming a 100% load during a single fault, the maximum energy not supplied amounts to 24,784.58 kWh and 13,625.41 kVArh, while the minimum energy not supplied is 6,196.15 kWh and 3,406.35 kVArh, considering the fault load as 25% of the full load.

DOI: https://doi.org/10.59122/164CFC12





Table I: Economic Loss Analysis

No.	Full Load		% of Load Assumption Full Load		sumption	Average Time taken to Single	Energy	Not Sold
	KW	KVAr		KW	KVAr	Fault (Hr.)	KWH	KVArh
1	13,296.45	7,309.77	25	3,324.11	1,827.44	1.86	6,196.15	3,406.35
2	13,296.45	7,309.77	50	6,648.23	3,654.89	1.86	12,392.29	6,812.71
3	13,296.45	7,309.77	75	9,972.34	5,482.33	1.86	18,588.44	10,219.06
4	13,296.45	7,309.77	100	13,296.45	7,309.77	1.86	24,784.58	13,625.41

<sup>2)</sup> Analysis of Loss in Revenue: The Revenue loss can be analyzed in two ways. These are unsold Electricity (Unplanned Outage) of 15/33 KV and according to EEU Tariff.

According to EEU, the unsold electricity (unplanned outage) charge of the 15/33 KV line for two hours is 84,000 ETB. Taking the minimum, average, and maximum duration of finding a fault by a conventional method, the revenue not collected is illustrated in Table II below. The minimum revenue not collected per fault is 42,000 ETB, the average revenue not collected per fault is 78,288 ETB and the maximum revenue not collected per fault is 231,000 ETB.

Table II: Revenue Loss Analysis

No.	Duration of finding a fault	Unplanned Outage for 2 hours	Revenue not collected
1	1	84,000 ETB	42,000 ETB
2	1.864	84,000 ETB	78,288 ETB
3	5.5	84,000 ETB	231,000 ETB

Economic loss analysis shows significant energy not supplied during faults, with revenue losses due to unsold electricity. The GIS method, which only incurs the cost of software and utilizes existing measuring and relay protection devices, significantly reduces the time and economic losses associated with fault detection and location. This makes it a highly scalable and efficient solution for the Shecha feeder and the entire Arba Minch electric distribution system.

#### IV. Conclussion

In this study, the existing fault detection and location identification method for the Arba Minch district's 15 KV Shecha feeder was evaluated. The feeder is 18.154 km long, with branches ranging from 0.552 km to 7.155 km. Currently, fault detection and location identification in the Arba Minch distribution system uses a conventional, manual approach, which is laborious and time-consuming. This method requires more

Received: 25 July 2024; Revised: 9 October 2024; Accepted: 26 October 2024; Published: November 2024.

DOI: https://doi.org/10.59122/164CFC12

Copyright and License Grant: CC By 4.0 (a)



personnel and prolongs outage times. About 63.23% of the total fault duration is spent on detection and location identification, with the remaining 36.77% on technical maintenance. Consequently, energy not supplied per fault is 24,784.58 KWh and 13,625.41 KVArh. Revenue losses range from 42,000 ETB to 231,000 ETB, depending on the fault location time, which can be up to 5.5 hours. The SAIDI value of this feeder is 271.3, with 171.54 due to fault finding, representing significant economic losses.

To address these issues, the GIS technique was implemented for fault detection and location identification. The ETAP GIS system successfully detected and identified the location of the faults with 100% accuracy, reducing outage time by 99.11%. This eliminated economic losses such as unsupplied energy (24,784.58 KWh and 13,625.41 KVArh) and uncollected revenue (42,000 ETB to 231,000 ETB). The SAIDI value due to fault location decreased from 171.54 to 1.53.

# References

- 1. Tefera Derbe, "GIS-Based Modeling and Performance Improvement of Distribution Network (Case Study: Adama Town 15 kV Distribution Network)," MSc. Thesis, Addis Ababa University, Addis Ababa, 2021. Available: <a href="http://etd.aau.edu.et/handle/12345678/31681">http://etd.aau.edu.et/handle/12345678/31681</a>
- 2. Y. Kifle, B. Khan, and P. Singh, "Assessment and Enhancement of Distribution System Reliability by Renewable Energy Sources and Energy Storage," Journal of Green Engineering, vol. 8, no. 3, pp. 219–262, 2018, DOI: https://doi.org/10.13052/jge1904-4720.832.
- 3. Samuel Kefale, "Smart distribution system by using binary particle swarm optimization", International Journal of Engineering and Applied Sciences (IJEAS), vol. 7, no. 1, 2020. DOI: https://dx.doi.org/10.31873/IJEAS.7.01.02.
- 4. Balakumar, Akililu Getahun, Samuel Kefale and K. Ramash Kumar, "Improvement of the voltage profile and loss reduction in distribution network using Moth Flame Algorithm: Wolaita Sodo, Ethiopia", Journal of Electrical and Computer Engineering, vol. 2021, no. 9987304, 2021, pp. 1–10. DOI: https://doi.org/10.1155/2021/9987304
- 5. J. D. Taft, "Fault intelligence: Distribution grid fault detection and classification," Pacific Northwest National Laboratory Richland, U.S. Department of Energy, September, 2017, [Online]. Available: https://gridarchitecture.pnnl.gov/media/white papers/FaultIntelligence\_PNNL.pdf.
- 6. M. A. Ali, "Fault location methods for distribution systems: A review," in Proc. 2020 IEEE Power Energy Soc. Gen. Meeting, 2020, pp. 1-5. [Online]. Available: https://ieeexplore.ieee.org/document/8910314

Copyright and License Grant: CC By 4.0 (a)



Volume 2, Issue 2, 2024

- 7. W. Ren and L. Liu, "Traveling wave fault location methods for power distribution networks," J. Geogr. Energy, vol. 8, no. 3, pp. 32-40, 2020, DOI: https://doi.org/10.13052/jge1904-4720.832.
- 8. F. A. Albasri, Z. Al Zaki, E. Al Nainoon, H. Alawi and R. Ayyad, "A Fault Location System Using GIS and Smart Meters for the LV Distribution System," 2019 International Conference on Innovation and Intelligence for Informatics, Computing, and Technologies (3ICT), 2019, pp. 1-6, DOI: 10.1109/3ICT.2019.8910314. https://ieeexplore.ieee.org/document/8910314
- 9. D. Courtney, T. Littler, J. Livie, and K. Lennon, "Localized fault location on a distribution network - case studies and experience," Journal of Engineering, vol. 2018, no. 15, pp. 885–890, Sep. 2018, DOI: https://doi.org/10.1049/joe.2018.0145.
- 10. A. Abbawi, Ibrahim Ismael Alnaib, O. Sharaf, and Karam Khairullah Mohammed, "Faults detection, location, and classification of the elements in the power system using intelligent algorithm," Bulletin of Electrical Engineering and Informatics, vol. 12, no. 2, pp. 597-607, Apr. 2023, DOI: https://doi.org/10.11591/eei.v12i2.4456.
- 11. R. Vikramsingh, Parihar, S. Jijankar, A. Dhore, A. Sanganwar, and K. Chalkhure, "Automatic Fault Detection in Transmission Lines using GSM Technology," International Journal of Innovative Research in Electrical, Electronics, Instrumentation and Control Engineering ISO, vol. 3297, pp. 2321–5526, 2007, DOI: https://doi.org/10.17148/IJIREEICE.2018.6419.
- 12. Paolo Mercorelli, "Recent advances in intelligent algorithms for fault detection and diagnosis," Sensors, vol. 24. no. 8, pp. 2656–2656, Apr. 2024, DOI: https://doi.org/10.3390/s24082656.
- 13. X. Su, "Engineering fault intelligent monitoring system based on Internet of Things and GIS," Nonlinear Engineering, vol. 12, no. 1, pp. 1–11, Jan. 2023, DOI: https://doi.org/10.1515/nleng-2022-0322.
- 14. C. Wattanasakpubal and T. Bunyagul, "Fault location algorithm and development the automated fault location system," vol. 2, no. 1, pp. 68-78, 2010, Accessed: Jul. 20, 2023. [Online]. Available: https://www.thaiscience.info/Journals/Article/R%26DT/10896985.pdf
- 15. Y. Xie, Y. Zhou, and W. Liu, "Fault diagnosis of power network based on GIS platform and Bayesian networks," TELKOMNIKA (Telecommunication Computing Electronics and Control), vol. 14, no. 2, p. 741-747, Jun. 2016, DOI: https://doi.org/10.12928/telkomnika.v14i2.2750.

**DOI:** https://doi.org/10.59122/164CFC13

Copyright and License Grant: CC By 4.0



# Structural Reliability Studies on Pulverized Glass Powder Concrete Subjected to Bending Forces with Natural Aggregate

Kolo, D. N<sup>1\*</sup>., Aguwa, J. I. <sup>1</sup>, Hadi, A. M<sup>1</sup>., Shehu, M<sup>1</sup>., and Ashraf, M. L.M<sup>2</sup> <sup>1</sup>Department of Civil Engineering, Federal University of Technology, Minna, Nigeria <sup>2</sup>Department of Civil Engineering, University of Bani Walied, Bani Walied City, Libya \*Corresponding Author's Email: daniel.kolo@futminna.edu.ng

### Abstract

Nigeria is a fast-growing country on the African continent. It has diverse cultures and economic diversity in society. The shortage of housing and basic infrastructure in Nigeria is increasing with a continuous rise in the price of construction materials. Cement is a major component in concrete production. Its production, however, is accompanied by huge carbon dioxide emissions. This research presents the results of structural reliability analysis conducted on a reinforced concrete beam produced with pulverized glass powder as partial replacement for cement with Natural aggregate (NA) as coarse aggregate by subjecting it to bending forces. The first order reliability method (FORM) was employed to determine the level of safety of the beam. The result of the sensitivity analysis showed that the pulverized glass powder beam with NA as coarse aggregate is structurally safe at a span of 3000 mm and depth of 600 mm with probabilities of failure of  $1.00 \times 10^{-3}$  and  $1.04 \times 10^{-3}$  respectively.

Keywords: Beam, Bending, Concrete, Natural Aggregate, Pulverized Glass, Structural Reliability

#### T. Introduction

Cement is a vital component of concrete production. The industry is a leading source of carbon dioxide emissions along with the burning of fossil fuels and deforestation. Emission of these gases into the atmosphere results in global warming with CO<sub>2</sub> contributing about 65% to global warming. The cement industry worldwide is believed to be the source of about 7% of the entire greenhouse gas emissions on planet Earth. Sequel to this premise, there exists an urgent need to identify alternative binders to make concrete. The reality of this has resulted in extensive research and analysis into the possibility of using waste materials and industrial by-products as partial cement replacement in concrete production [1]. Several efforts have been made by researchers in the construction industry into the use of waste glass powder as partial replacement of cement [6,8]. In this study finely powdered pulverized waste glass was used as partial replacement of cement in the production of concrete incorporating locally sourced Natural aggregate (NA) as coarse aggregate.

DOI: https://doi.org/10.59122/164CFC13



Copyright and License Grant: CC By 4.0

@ **①** 

Volume 2, Issue 2, 2024

Deposits of the NA used in this research are found in abundance in Bida, Niger state, Nigeria. The use of this naturally occurring aggregate is common among the locals of this area. This is because it is cheaper and involves less energy and resources when compared to the process of producing the conventional crushed granite. [5] performed structural reliability analysis on reinforced concrete beam with washed and unwashed NA, currently no research exists on reliability studies of the NA and Pulverized glass as cement replacement, this research produces timely and justifiable results.

All structural engineers design structures with safety, aesthetics, and economy as factors of paramount importance. Hence the load carrying capacity of such structures must exceed the imposed demand on it. See Eq. 1:

Capacity 
$$>$$
 Demand (1)

As long as the conditions in Eq. (1) are satisfied, structural safety is assured for all reinforced concrete structures [4].

According to Ali Mirza [5], uncertainties in the resistance of reinforced concrete members are as a result of variabilities in reinforced concrete constituent material strength and densities, the member geometry, the errors in calculations for strength, and the imposed loads. These result in difficulties in determining the absolute safety of reinforced concrete structures with deterministic approach. Hence, one of the most reliable approaches in determining the level of safety inherent in such a structure is by utilizing reliability analysis or by computing its probability of failure [6].

### II. Materials and Methods

The fine aggregate (FA) was sourced from a riverbed in Chanchaga, Minna, Niger state. It was clean and free from impurities. It was ensured that the FA met guidelines as enshrined in BS 882 (1992). The water used was sourced from the Civil Engineering departmental laboratory, Federal University of Technology Minna, Niger state. The water was clean and fit for drinking; it met standards stipulated in [8]. The cement was Ordinary Portland cement (OPC) categorized as CEM 1 in [9]. The Natural aggregate (NA) was sourced from the Bida local government in Niger state (Latitude N9°55' E and Longitude N5°52'E). It is a brownish-red aggregate. It conformed to stipulations in [7]. Waste glass from local glass/aluminum retailer in Minna was obtained and transported to the Civil Engineering departmental laboratory where it was further processed to pulverized form. The Natural aggregate and pulverized glass powder are presented in Fig. 1 and 2, respectively.

DOI: https://doi.org/10.59122/164CFC13





Fig. 1.: Natural aggregate



Fig. 2.: Pulverized glass powder

First order reliability method (FORM) was employed as the method of reliability analysis of the reinforced concrete beam. It is a simplifies method in which only the mean and standard deviations for load and resistance values ae used to compute reliability indices. All input variables are taken to be normally distributed [4].

For a simply supported reinforced concrete beam, the performance function is represented by Equation 2:

$$Z = R - I \tag{2}$$

Where R represents the resistance of the beam and I is the imposed load Equation (2) can further be transformed into Equation (3):

$$g_1(x) = 0.156f_{cu}bd^2 - \frac{W}{8}L^2$$
 (3)

Copyright and License Grant: CC By 4.0



The input data for the various parameters used for reliability and sensitivity analysis are presented in Table I. All variables are assumed to be normally distributed.

Table I: Bending failure reliability analysis data

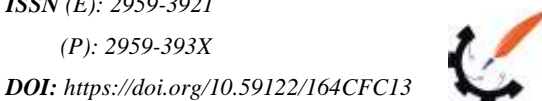
Parameter	Value	COV	STD	
Thickness of slab, h <sub>s</sub> (mm)	150	0.07	10.50	
Height of Beam, h (mm)	400	0.05	20.00	
Beam width, b (mm)	225	0.05	11.25	
Beam effective depth, d (mm)	359	0.05	17.95	
Diameter of tension bar, Φ (mm)	16	0.04	0.64	
Area of tension reinforcement A <sub>s</sub> (mm <sup>2</sup> )	402	0.04	16.08	
Shear reinforcement, A <sub>sv</sub> (mm <sup>2</sup> )	101	0.04	4.04	
Concrete compressive strength f <sub>cu</sub> (N/mm <sup>2</sup> )	16.45	0.25	4.11	
Concrete unit weight	24	0.04	0.64	
Dead load, DL (kN/m)	17.70	0.10	1.77	
Live load, LL (kN/m)	3.33	0.18	0.60	
Yield strength of steel, $f_y$ (N/mm <sup>2</sup> )	460	0.05	23.0	
Span of Beam, L (mm)	4000	0.22	880	

COV: Coefficient of variation

STD: Standard deviation

# III. Results and Discussion

Tables II, III and IV present the results of the specific gravity tests conducted on the fine aggregate, pulverized glass powder and coarse aggregate (NA). The fine and coarse aggregates were found to have specific gravities of 2.60 and 2.68 respectively. These values are in line with BS requirements for 2.60 - 3.0 for fine aggregates and 2.4 - 2.8 for coarse aggregates. The specific gravity of PGP was found to be 2.45. This value is however lower than the specific gravity of 3.15 for cement.



Copyright and License Grant: CC By 4.0



Table II: Specific gravity of Fine aggregate

Trials	1	2
Weight of empty cylinder (g) W <sub>1</sub>	116.50	116.70
Weight of cylinder + water (g) W <sub>4</sub>	436.30	404.00
Weight of cylinder + sample (g) W <sub>2</sub>	204.60	175.30
Weight of cylinder + sample + water (g) W <sub>3</sub>	482.00	430.90
Specific gravity	2.59	2.61
Average Specific Gravity	2	2.60

Table III: Specific gravity of Pulverized Glass (PGP)

Trials	1	2
Weight of empty cylinder (g) W <sub>1</sub>	116.50	116.70
Weight of cylinder + water (g) W <sub>4</sub>	436.30	404.00
Weight of cylinder + sample (g) W <sub>2</sub>	166.40	163.90
Weight of cylinder + sample + water (g) W <sub>3</sub>	445.10	413.90
Specific gravity	2.55	2.35
Average Specific Gravity	2	2.45

Table IV: Specific gravity of Coarse aggregate (NA)

Trials	1	2
Weight of empty cylinder (g) W <sub>1</sub>	116.50	116.70
Weight of cylinder + water (g) W <sub>4</sub>	257.80	231.70
Weight of cylinder + sample (g) W <sub>2</sub>	446.20	430.40
Weight of cylinder + sample + water (g) W <sub>3</sub>	358.00	358.60
Specific gravity	2.67	2.69
Average Specific Gravity	:	2.68

Received: 24 August 2024; Revised: 26 October 2024; Accepted: 28 October 2024; Published: November 2024.



Table V presents the proportions of the various constituent materials used in the production of the PGP concrete.

Table V: Mix proportions for various constituents of PGP Concrete

S/No	Cement	PGP	Cement	PGP	Water	Fine Aggregate	Coarse
	Content (%)	(%)	(kg)	(kg)	(kg)	(kg)	Aggregate (kg)
1	100	0	7.20	0.00	3.96	14.76	31.83
2	95	5	6.84	0.36	3.96	14.76	31.83
3	90	10	6.48	0.72	3.96	14.76	31.83
4	85	15	6.12	1.08	3.96	14.76	31.83
5	80	20	5.76	1.44	3.96	14.76	31.83

Fig. 3 presents the result of sensitivity analysis conducted on the beam span (L) for the Pulverized glass powder concrete beam subjected to bending forces. An increase in the span resulted in lower safety index values, these values were lower than the target reliability ( $\beta_T$ ) value of 3.0. A general decrease in the beam span; however, produced increased safety index values. The beam was found to be safe at a span of 3000 mm with reliability index of 3.09 and Probability of failure ( $P_f$ ) of  $1.00 \times 10^{-3}$ .

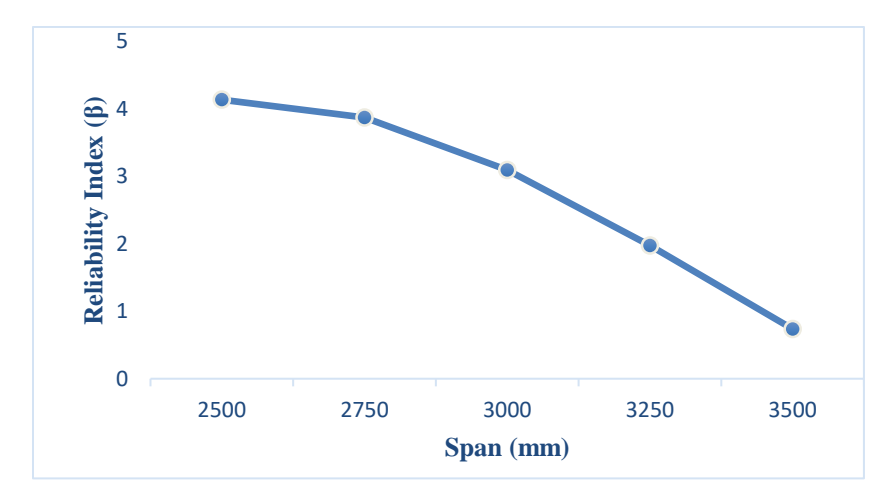


Fig. 3.: Relationship between span and reliability index in bending

Fig. 4 presents the sensitivity analysis conducted on the beam depth. A general increase in safety index (β) was recorded as the depth was increased. The Pulverized concrete beam was adjudged to be structurally safe at a depth of 600 mm with corresponding safety index of 3.08 and probability of failure ( $P_f$ ) of 1.04  $\times$  $10^{-3}$ .

ISSN (E): 2959-3921

DOI: https://doi.org/10.59122/164CFC13

Copyright and License Grant: CC By 4.0



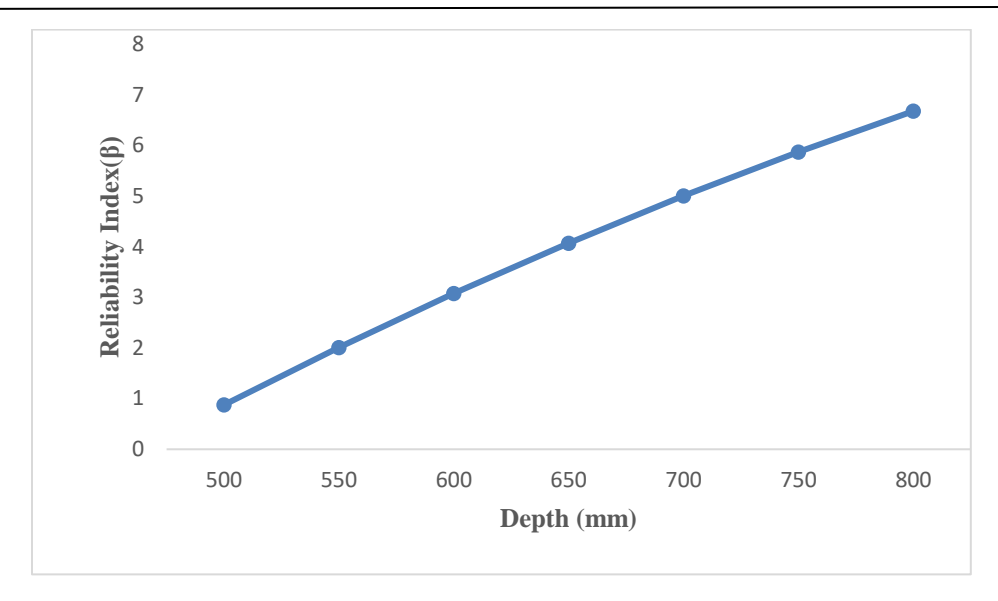


Fig. 4.: Relationship between depth and reliability index in bending

The result of varying the dead load on the beam is presented in Fig. 5. A general increase in safety index was recorded as the design dead load (gk) was reduced. The beam was deemed safe at an applied dead load of 7.70 kN/m with a safety index of 3.37 and corresponding probability of failure ( $P_f$ ) of 3.76  $\times$  10<sup>-4</sup>.

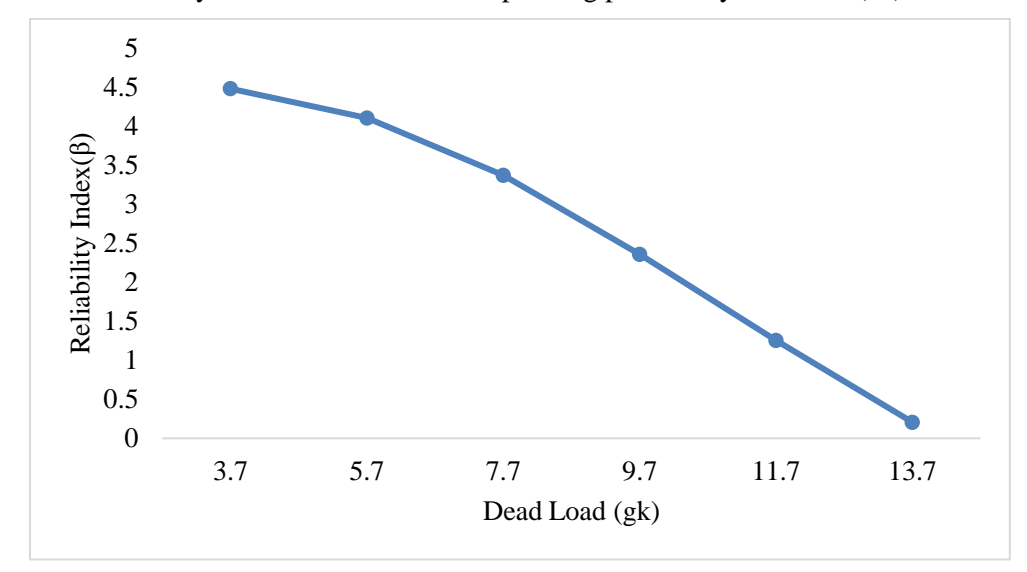


Fig. 5.: Relationship between dead load and reliability index in bending

Fig. 6 presents the result of sensitivity studies conducted by varying the Area of Tension reinforcement (A<sub>s</sub>) of the beam. The safety indices (B) increased with an increase in the area of tension reinforcement and reduced with decreasing  $A_s$ . The beam was adjudged safe with  $A_s$  value of 800 mm<sup>2</sup> and corresponding  $\beta$ of 5.04 and  $P_f 2.20 \times 10^{-4}$ .





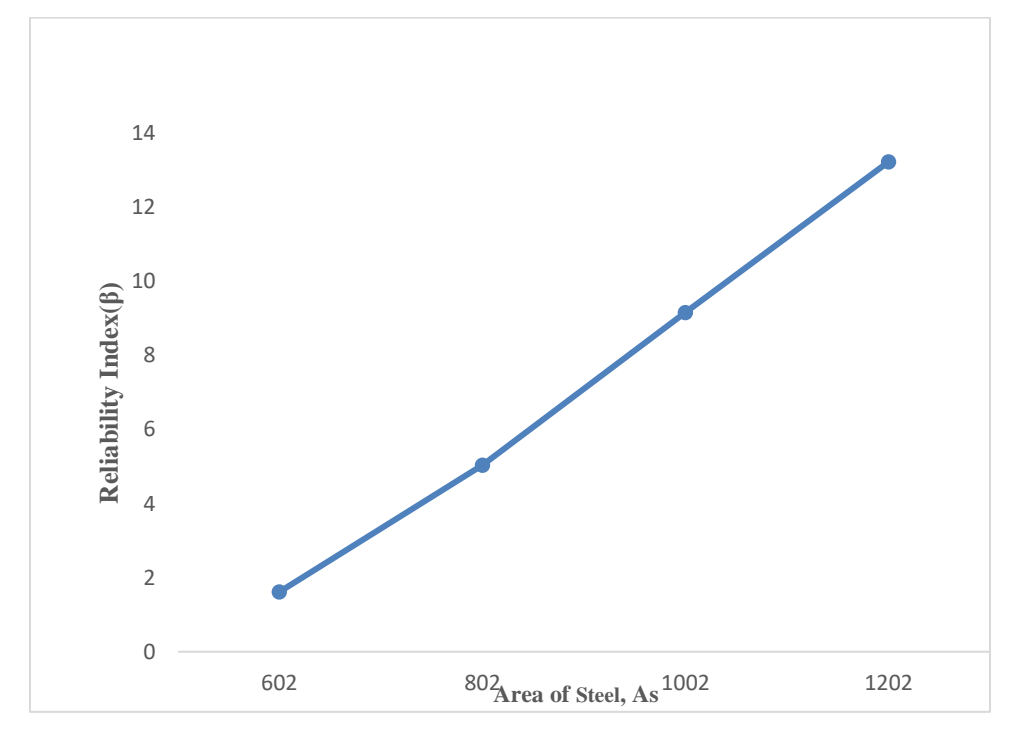


Fig. 6.: Relationship between area of tension reinforcement and reliability index in bending

#### IV. Conclusion

The Pulverized glass powder reinforced concrete beam utilizing the natural aggregate as coarse aggregate is structurally safe at a span of 3000 mm and depth of 600 mm carrying a dead load of 7.70 kN/m with corresponding safety indices of 3.09, 3.08 and 3.37, respectively.

Thus, it was concluded that the incorporation of this waste glass in concrete production has proven to be structurally efficient and should be encouraged as a step towards achieving sustainability in construction.

# References

- 1. I. Ali, "Behavior of Concrete by using Waste Glass Powder and Fly Ash as a Partial Replacement of Cement", International Journal of Engineering Research & Technology (IJERT), vol. 4, no.5, pp 1238-1243, 2015. ISSN: 2278-0181.
- 2. S. M. Auta and A. Abdullahi, "Effect of Pulverized Glass Powder on the Compressive Strength of Revibrated Concrete", Global Virtual Conference in Civil Engineering (GVCCE), 2021.
- 3. D. N. Kolo, J. I. Aguwa, T. Y. Tsado, M. Abdullahi, A. Yusuf, and S. F. Oritola, "Reliability studies on reinforced concrete beam subjected to bending forces with natural stone as coarse aggregate", Asian Journal of Civil Engineering, vol. 22, no. 3, pp 485 – 491, 2020. ISSN: 1563-0854.

DOI: https://doi.org/10.59122/164CFC13



Copyright and License Grant: CC By 4.0



Volume 2, Issue 2, 2024

- 4. A. U. Barambu, O. A. U. Uche, and M. T. Abdulwahab, "Reliability-based code calibration for load and safety factors for the design of a simply supported steel beam", *USEP: Journal of Research Information in Civil Engineering*, vol. 14, no.1, pp 1275 1291, 2017.
- 5. S. Mirza Ali, "Reliability-based design of reinforced concrete columns". *Elsevier (Structural Safety)*. Vol.18, no. 2, pp. 179–197. 1996.
- 6. P. Pandey, V. Shaji, R. R. Prasad, M. Yadav, and K. S. Santhy, "Reliability Analysis of Isolated Column Footings Using Monte Carlo Simulation", *International Journal of Scientific & Engineering Research*, vol. 7, no. 4, pp 62 69, 2016. ISSN: 2229-5518.
- 7. BS 882, "Specification for aggregates from natural sources for concrete". British Standard, 1992. Institute. 2 Park Street, London WIA 2BS.
- 8. BS EN 1008, "Mixing water for concrete: Specification for sampling, testing and assessing the suitability of water, including water recovered from concrete industry as mixing water for concrete", London, British Standards Institution. 2002.
- 9. BE EN 197-1, "Composition, Specifications and conformity criteria for common Cements". London, British Standards Institute. 2000.

Volume 2, Issue 2, 2024

DOI: https://doi.org/10.59122/174CFC16

Copyright and License Grant: CC By 4.0



# Effect of Fine Fractions on Engineering Properties of Sandy Soils in Southern Ethiopia's Gamo Zone

Paulos Sisay Shido<sup>1\*</sup>, Democracy Dilla Dirate<sup>1</sup>, and Dr. Bisrat Gissila<sup>1</sup>

<sup>1</sup> Faculty of Civil Engineering, Arba Mich University, Arba Mich, Ethiopia

\*Corresponding Author's Email: pauloyahoocivil@gmail.com

# Abstract

This study investigates the influence of fine content on the engineering properties of sandy soil. The objective is to determine the effect of fine fractions on the engineering properties of sandy soil. Sand samples were collected from the Kulfo riverside and Hamasa, Mirab Abaya. The sand samples were classified as medium and fine sand in the laboratory, based on sieve sizes of 2 mm to 0.425 mm and 0.425 mm to 0.075 mm, respectively. Fine fractions were obtained by sieving through a 75 µm sieve. Laboratory tests were conducted on reconstituted sandy soil samples with varying fine content (0%, 5%, 12%, 20%, and 30% by weight). The plasticity of the reconstituted sandy soil samples was zero for both medium and fine sand with fine contents up to 12%. Plasticity began to develop at 20% fine content and increased with further increases in fine content. The average plasticity index for medium and fine sand was 5.88% and 8.46%, respectively, as the fine content increased. As the fine fraction increased, the average Maximum Dry Density for medium and fine sand increased from 1.79 g/cm<sup>3</sup> to 1.95 g/cm<sup>3</sup>, and the Optimum Moisture Content increased from 10.64% to 13.9%. The increase in fine fractions led to increased particle interlocking, significantly impacting the Maximum Dry Density. The average California Bearing Ratio (CBR) value for medium sand decreased from 32.60% to 13.14%, and for fine sand decreased from 24.78% to 11.80% with increasing fine content. The results showed that the compression index increased with increasing fine content, reaching 0.03368 for fine sand and 0.03059 for medium sand at Mirab Abaya with a 30% fine content. The maximum permeability value for medium sand at Mirab Abaya was  $2.18 \times 10^{-2}$ cm/sec, while the values for medium and fine sand at the Kulfo riverside were  $1.57 \times 10^{-2}$  cm/sec and 7.22 $\times$  10<sup>-2</sup> cm/sec, respectively. The direct shear test results for medium and fine sand from the Kulfo riverside ranged from 16.6° to 0° and 10.4° to 0°, respectively. For fine sand, the range was 10.4° to 0°. Increasing fine fractions in sandy soil generally affects the engineering characteristics of fine and medium sandy soils.

Keywords: California Bearing Ratio, Fine Fraction Content, Fine Sand, Medium Sand

Volume 2, Issue 2, 2024



DOI: https://doi.org/10.59122/174CFC16



# I. Introduction

As sand is an important construction material, it is always desirable to use good-quality sand. To judge the quality of the available sand, one must know the properties of good sand. Before using sand in a project, these desirable properties must be ensured. Natural sand commonly consists of fines and sand particles with different proportions, and the fines content significantly affects the engineering properties of sandy soil. Sand is known as the main material in land reclamation works to develop and widen an area. The Geotechnical Engineer should ensure that the sand used can withstand the load imposed by the structures that can be built on it [1]. The most common type of soil that influences a sandy soil's engineering properties seems to be fine-grained soil. The fine fraction has a large influence on soil behavior. Sandy soils are typically believed to behave with easily defined physical properties, such as a lack of structure or no structure, poor water retention properties, permeability, and high sensitivity to compaction. The most common types of sand are concrete sand, pit sand, naturally occurring or river sand, manufactured sand, utility sand, and quarry fill sand. These sands have unique engineering characteristics that make them suitable for various engineering applications. With fines contents of 18% in the sand fines mixture, the maximum and minimum void ratios reached minimum values. All parameters of deviator stress, volumetric strain, shear stress, internal friction angle, and cohesion increased as the fines content increased in the consolidated drained shear test. For constant-void-ratio and steady specimens, the critical state parameter (M) decreased and seemed to be stable for same-peak-deviator-stress specimens. Furthermore, as the fines content increased, so did the cohesion, internal friction angle, and critical state in the consolidated undrained test [2].

The impact of fines content and type can be determined using an odometer test and the intergranular void ratio [3]. At a fine content of approximately 30%, the shear strength and stress-strain characteristics of the mixture exhibit significant changes. As fine content increases, the drained angle of friction decreases, leading to a decrease in drained shear strength [4]. The angle of internal friction ( $\emptyset$ ) decreases with the increasing fineness modulus up to 1.50, and the variation can be expressed by the linear equation  $\emptyset^{\circ} = 37 - 0.245$ . The angle of internal friction becomes almost constant for all fine contents as the mm sieve (FM=1.70) of sand increases, with such a value estimated at 35.6° [5].

Up until the critical fine content, the addition of finer particles leads to a decrease in the void ratio. However, after this critical point, the coefficient of volume compressibility increases from 0% to 15% as more fine particles are incorporated into the specimens.

Copyright and License Grant: CC By 4.0

(P): 2959-393X **DOI:** https://doi.org/10.59122/174CFC16



0 📵 0

Increases in dry density are noticed as fine content increases [6]. The angle of internal friction of the examined soil samples decreased with increasing fines content; the polynomial expression: =  $-0.000f^2$  - 0.456f + 47.16; =  $-0.002f^2$  - 0.19f + 43.06; =  $0.001f^2$  - 0.571f + 41.4 provided the best fit between fines content and soil sample cohesiveness, where f is the fines content in percent and  $\Phi$  is the angle of internal friction in degrees [7].

The threshold fine content, t\*1, marks a significant behavioral change as determined by consolidation loading and consistency measurements using a fall cone instrument. This transition corresponds to a shift towards a percolation regime involving both fine and coarse particles.

A second behavioral threshold, t\*2, is evident from hydraulic conductivity measurements using oedometric loading, thermal conductivity measurements using a needle probe, and critical state strength determined by undrained triaxial loading. This threshold coincides with a transition from a state dominated by systemwide coarse particle clusters to a state without such clusters [8].

### II. Materials and Methods

Sandy soil is a granular material made up of finely divided rock and mineral particles that occur naturally. This study will conduct an intensive laboratory study of sandy soil with mixed ratios of investigated fine fractions around study areas to use a series of index and engineering laboratory tests. Sandy soil samples from various locations were designed (separated) in the laboratory based on their grain sizes using sieve sizes, and fine soil samples were collected from different locations and mixed with ratios of fine fractions using a series of index and selected engineering laboratory tests for this study. Soils can be submitted to a variety of laboratory tests to determine a variety of soil characteristics.

Most laboratory testing methods employed in this study followed the standards established by the American Society for Testing and Materials (ASTM). The California Bearing Ratio (CBR) test, specifically, was conducted following the guidelines outlined in both British Standard and American Association of State Highway and Transportation Officials (AASHTO) standards.

The sand and Fine Fraction samples used in the test were collected from the Gamo Zone in Southern Ethiopia and decpicted in Fig. 1. Shear Strength, CBR, Consolidation, Compaction, Permeability, and Plasticity tests were performed on two kinds of sandy materials containing various percentages of fines, i.e. 0, 5, 12, 20, and 30%. In this paper, fines content is stated as a percent of soil mass passing through a 0.075 mm sieve (No. 200 according to ASTM).





#### A. Sandy Soils

To start, Medium Sand samples were sieved through a stack of ASTM Sieve No.10 – No.40 (2mm – 425mic) sieves, and Fine Sand samples were sieved through a stack of ASTM Sieve No.40 – No.200 (425mic – 75mic) sieves. For testing purposes, medium sand samples that passed sieve No.10 were retained on No.40, and fine sand samples that passed sieve No.40 were retained on No.200.



Fig.1.: A), Fine sand of site one, B) fine sand of site two, and C) Medium sand of site three

# III. Results and Discussion

This section contains the results of the many tests carried out in this study. The fluctuation of several test parameters was examined, and conclusions were drawn from the detailed examinations.

# A. Soil Classification as per Unified Soil Classification System and Plasticity Chart

Table I: Soil classification for fine-grained soil as per AASHTO and USCS

Tests	Test Pits	TP-One	TP-Two	TP-Three	TP-Four
	#10	99.9	99.8	99.6	99.4
Percentage Pass	#40	99.5	99.2	98.6	98.4
	#200	97.9	97.4	96.8	96.3
	LL	53.82	55.47	53.92	52.56
Atterberg Limit	PL	37.06	37.84	36.16	37.53
	PI	16.75	17.63	17.76	15.03
Compactions	MDD	1.488	1.51	1.53	1.444
	OMC	29	28	27	31.5



Copyright and License Grant: CC By 4.0



Specific Gravity	Gs	2.65	2.66	2.65	2.67
PI plots	Below A-line	Below A-line	Below A-line	Below A-line	Below A-line
Soil Classification	USCS	MH (elastic silt)	MH (elastic silt)	MH (elastic silt)	MH (elastic silt)
	AASHTO	A-7-5	A-7-5	A-7-5	A-7-5

Test Pit-one was selected as the fine fraction for examination from the four test pits described above in Table I based on their Percentage pass on sieve number 200 as per ASTM standard.

# B. Atterberg Limit

The Atterberg limits of the samples increased significantly as the fines content increased. This trend suggests that as the number of particles increased, the material's specific surface area and activity also increased, leading to higher Atterberg limit values.

As depicted in Table II, the liquid limit and plastic limit are the most useful parameters for identifying and classifying fine-grained cohesive soils. Soils with a high liquid limit often exhibit poor hydraulic conductivity. For applications such as landfill liners, soils with a higher liquid limit are preferred due to their lower hydraulic conductivity.

Table II: Classification of sandy soil for different fine content based on plasticity chart

Q:4		M	edium san	d	F	Fine sand		Soil type
Sites	% Fine	LL	PL	PI	LL	PL	PI	
	0	-	-	NP	-	-	-	NP
Site-1	5	-	-	NP	-	-	-	NP
Site-i	12	-	-	NP	-	-	-	NP
	20	20.49	15.84	4.65	22.25	16.35	5.89	CL (lean clay)
	30	25.40	19.06	6.34	25.17	18.00	7.17	CL (lean clay)
	0	-	-	NP	-	-		NP
Site-2	5	-	-	NP	-	-		NP
S11C-2	12	-	-	NP	-	-		NP
	20	17.98	12.55	5.43	19.36	12.87	6.48	CL (lean clay)
	30 0	23.33	16.01	7.32 NP	24.38	14.79	9.59 -	CL (lean clay) NP
	5	-	-	NP	-	-	-	NP
Site-3	12	-	-	NP	-	-	-	NP
	20	19.50	13.09	6.40	18.26	12.99	5.27	CL (lean clay)
	30	24.06	16.43	7.63	25.49	16.87	8.62	CL (lean clay)

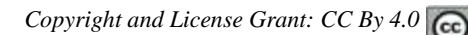




Table II illustrates that the reconstituted sandy soil samples, composed of both medium and fine sand, exhibited non-plastic behavior (plasticity index = 0%) for fine contents up to 12%. However, as the fine content increased beyond 20%, plastic behavior emerged. The average plasticity index for medium and fine sand was found to be 5.88% and 8.46%, respectively, with increasing fine content.

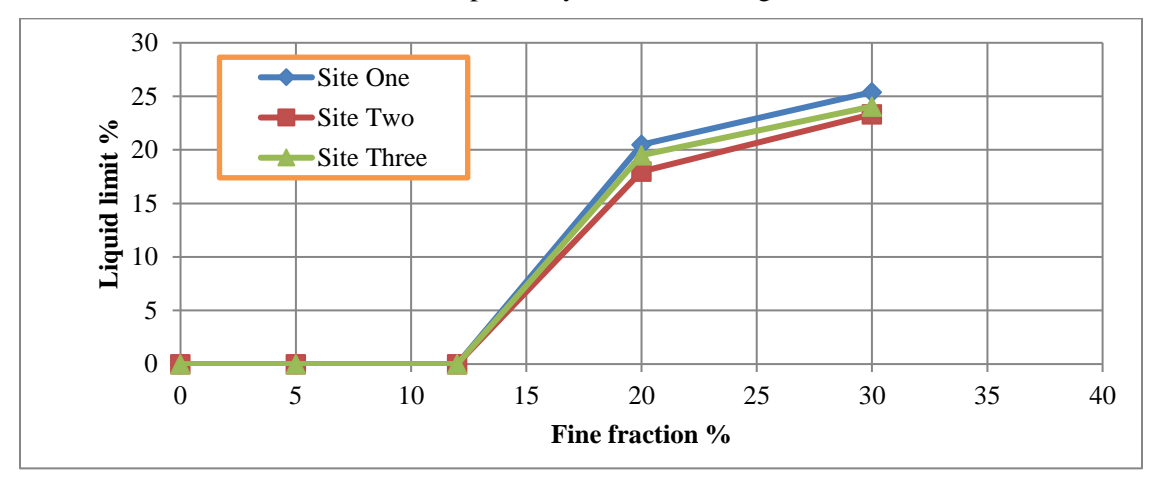


Fig. 2.: Variation in LL, with an increase in fines content of medium sand for all sites The link between fine content and liquid limit, plastic limit, and plastic index is depicted in Fig. 2. The LL, PL, and PI all increase as the fine material increases in this graph.

# C. Compaction Characteristics

Compaction curves can reveal a lot about a material's behavior during a test. It is obvious that as the fine fractions rise, the dry density increases. The finer particles occupy the vacuum spaces between the sand particles, causing an increase in M.D.D. However, particles of more than 30% may have influenced the gradation of sand soil to poor gradation, resulting in a fall in M.D.D. Furthermore, because of cohesion, the relative ease with which particles can move under compaction effort decreases with increased fines content, resulting in a lower maximum dry density.

The increase in fine fractions owing to particle interlocking has a major impact on maximum dry density. Because small particles interlock the spaces between large particles, the M.D.D rises as the percentage of fines increases. As depicted in Table III, the amount of water in M.D.D. is another aspect that influences its worth. In general, the O.M.C of the soil rises as the clay percentage rises, owing to the fine content' increased specific surface area.

Table III: Summary of Modified Compaction Test of Specified Soil Mixtures for All Sites

Sanda	Sands % Fines		MDD (g/cm <sup>3</sup>	()	OMC (%)		
Salius	70 1 11108	Site One	Site Two	Site Three	Site one	Site two	Site three

(P): 2959-393X



Copyright and License Grant: CC By 4.0



	0	1.86	1.81	1.77	8.53	9.80	9.60
M - 1	5	1.89	1.84	1.80	11.19	10.20	10.00
Medium Sand	12	1.94	1.87	1.84	11.48	11.20	11.20
2 11-2	20	1.96	1.92	1.90	11.60	12.00	12.80
	30	1.98	1.94	1.97	12.74	13.52	14.16
	0	1.76	1.77	1.79	11.96	12.00	11.97
Fine Sand	5	1.83	1.78	1.82	12.60	12.82	12.40
Fine Sand	12	1.87	1.88	1.88	12.64	13.08	13.71
	20	1.90	1.93	1.94	12.70	13.90	14.04
	30	1.92	1.97	1.98	13.35	14.64	15.00

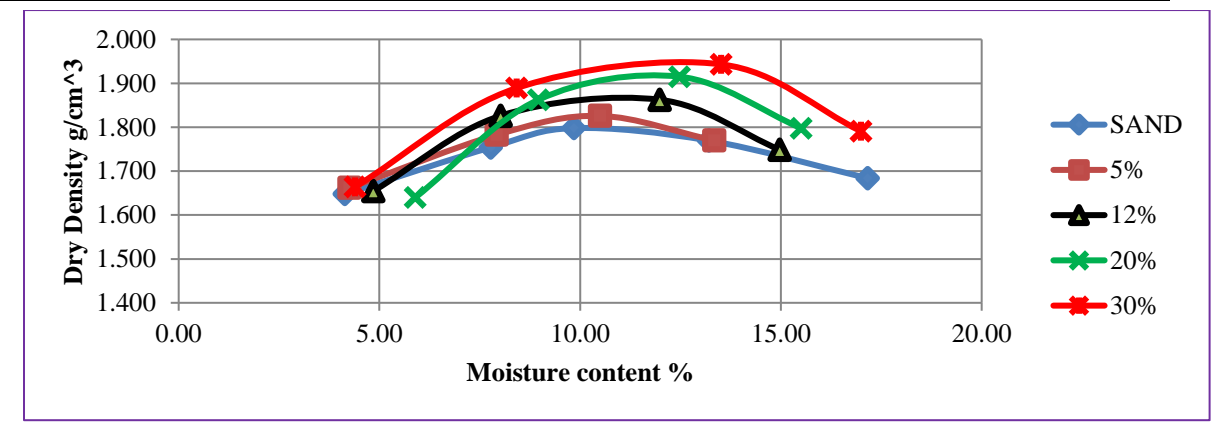


Fig. 3.: Combined compaction curve for medium sand of site one.

The relationship between fine fraction with dry density and OMC of reconstituted soil samples increases in Fig. 3 and the combined compaction curve crosses each other as a result. Several studies indicated that for fine fraction content of 50% and greater in reconstituted sandy soil, the MDD decreases and OMC increases because of the higher water-holding capacity of fine fractions. In addition, MDD and OMC decrease at 40% of fine fractions.

# D. California Bearing Ratio

The CBR of sand falls as the fine content increases until it reaches 30%, indicating that an increase in fines reduces the CBR of sand for both medium and fine sand of all sites. As a result depicted in Table IV, the CBR's optimal fine content value is 30%.

Table IV: Summary of CBR and moisture content test results of specified soil mixtures for all sites of medium and fine sands

	- -		CBR	
Sands	% Fine	Site One	Site Two	Site Three

(P): 2959-393X

DOI: https://doi.org/10.59122/174CFC16



Copyright and License Grant: CC By 4.0



		Moisture	CBR	Moisture	CBR	Moisture	CBR
		Content (%)	(%)	Content (%)	(%)	Content (%)	(%)
	0	12.82	26.91	11.04	30.75	10.21	40.09
	5	13.70	25.15	12.87	29.76	11.52	38.22
Medium	12	15.51	23.61	14.77	26.69	13.30	34.05
Sand	20	17.14	10.54	16.72	20.87	15.76	29.12
	30	18.82	4.94	18.07	16.26	17.93	18.23
	0	14.65	18.12	13.09	23.72	12.06	32.51
	5	15.78	17.13	14.35	22.63	13.23	31.63
Fine	12	17.34	14.17	16.31	20.87	15.47	28.12
Sand	20	19.03	8.35	18.56	18.45	17.02	20.87
	30	21.91	4.61	20.02	14.94	19.25	15.87

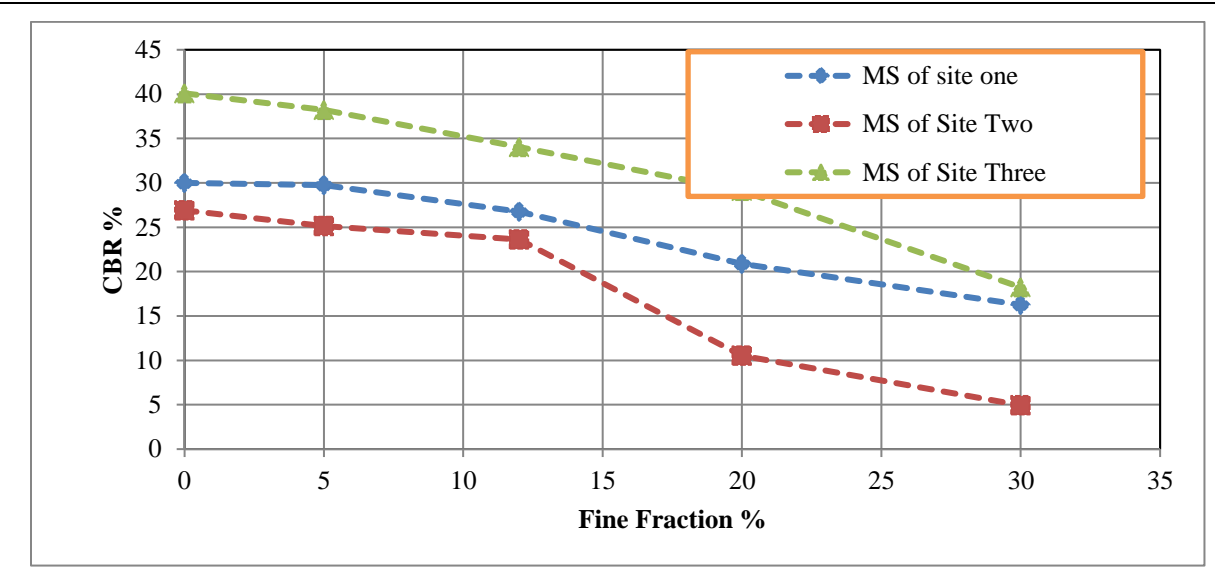


Fig. 4.: Combined Effect of fine fraction on CBR for medium sands of all sites.

The CBR of reconstituted sandy soil reduces steadily up to 12% and then drops significantly from 12% to 30% as fine fraction content increases for both medium and fine sands. For all sites of medium and fine sands, the fine content of the reconstituted sandy soil increases while the strength of the subgrade material decreases, as shown in Fig. 4.



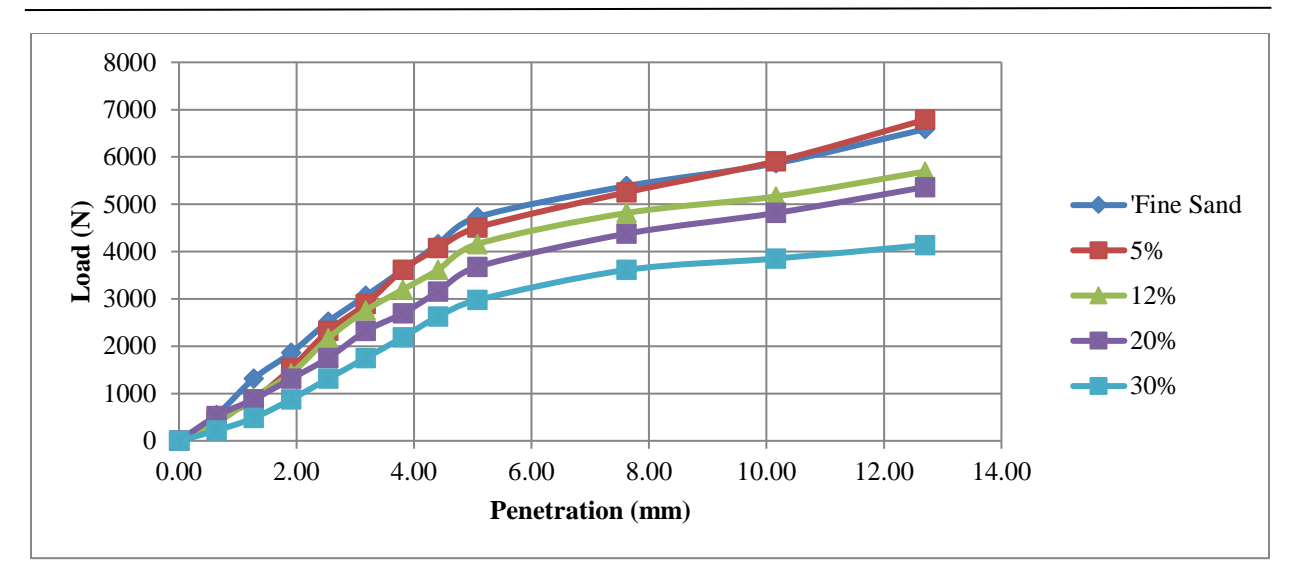


Fig. 5.: Combined CBR Curve for Fine Sand of Site One.

Penetration versus load graph shows above in Fig. 5 that the California bearing ratio for both medium and fine sand decreases as fine fraction content increases from 0% to 30% of all sites. The average CBR value for medium sand decreases from 32.60% to 13.14% and fine sand decreases from 24.785 to 11.80% as fine content increases.

#### E. Permeability

The soil permeability determines the amount of extra pore water pressure generated in the embankment or cuttings during the consolidation process when the embankment is pounded by water. The increased pore water pressure affects embankment stability significantly.

The image Fig. 5 and Table V depicts how the permeability of all three sand locations diminishes as the fine content increases. The maximum permeability value for medium sand at site three was  $2.18*10^{-2}$  cm/sec, while the values for medium sand and fine sand at site three were  $1.57 \times 10^{-2}$  cm/sec and  $7.22*10^{-3}$  cm/sec, respectively.

Table V: Summary of permeability test results of specified soil mixtures for site one

	-	Coefficient of Permeability					
Sands	% Fine	Site One	Site Two	Site Three			
	·	K <sub>T</sub> (cm/sec)	K <sub>T</sub> (cm/sec)	K <sub>T</sub> (cm/sec)			
	0	$1.6 \times 10^{-2}$	$1.96 \times 10^{-2}$	$2.18 \times 10^{-2}$			
	5	$9.5 \times 10^{-3}$	$1.01 \times 10^{-2}$	$1.21 \times 10^{-2}$			

(P): 2959-393X **DOI:** https://doi.org/10.59122/174CFC16



Copyright and License Grant: CC By 4.0



Medium	12	$7.9 \times 10^{-3}$	$8.25 \times 10^{-3}$	8.99× 10 <sup>-3</sup>
Sand	20	$6.13 \times 10^{-3}$	$5.93 \times 10^{-3}$	$6.11 \times 10^{-3}$
	30	$2.24 \times 10^{-3}$	$1.63 \times 10^{-3}$	$2.17 \times 10^{-3}$
	0	$7.22 \times 10^{-3}$	$9.39 \times 10^{-3}$	$1.57 \times 10^{-2}$
T' G 1	5	$5.82 \times 10^{-3}$	$6.68 \times 10^{-3}$	$1.05 \times 10^{-2}$
Fine Sand	12	$4.12 \times 10^{-3}$	$4.64 \times 10^{-3}$	$6.81 \times 10^{-3}$
	20	$3.266 \times 10^{-3}$	$3.2 \times 10^{-3}$	$5.21 \times 10^{-3}$
	30	$9.05 \times 10^{-4}$	$1.28 \times 10^{-3}$	$1.28 \times 10^{-3}$

The hydraulic conductivity of sandy soil at specific time intervals for both medium and fine sand soil decreases as fine fraction content increases, as shown in Table VI. The coefficient of hydraulic conductivity of reconstituted sandy soil was extremely high from 0% to 5%, and it decreased dramatically from 20% to 30%.

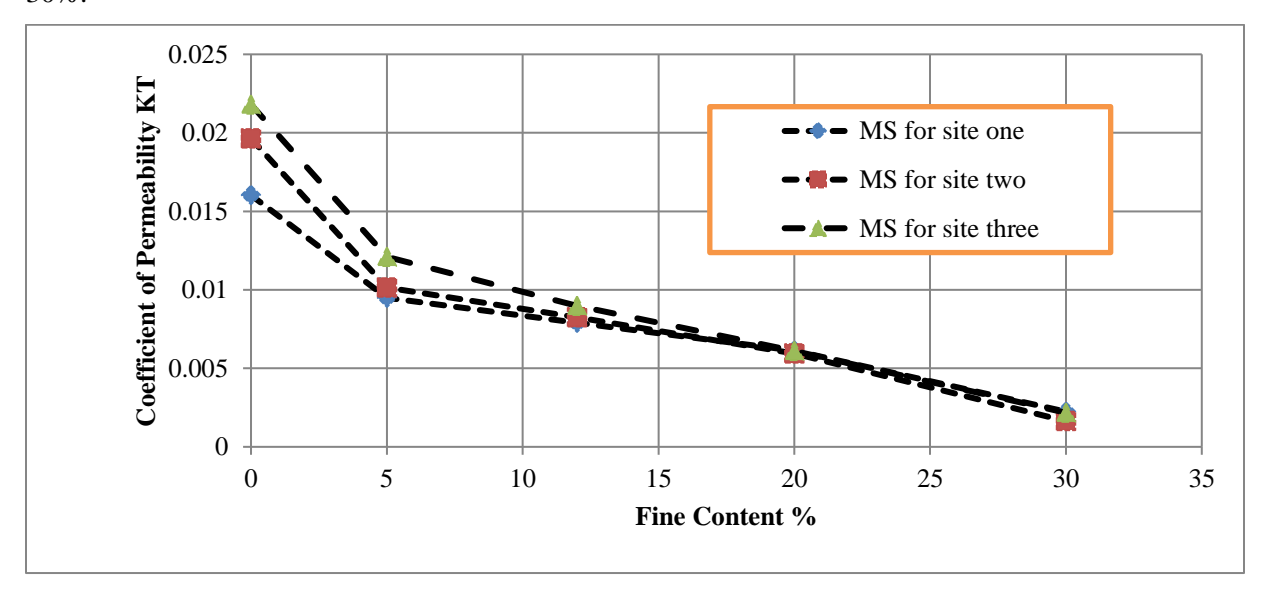
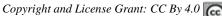


Fig. 6.: Effect of fine content on combined hydraulic conductivity of medium sand for all sites

The coefficient of hydraulic conductivity of medium sands of all sites of sandy soil drops at 5% of fine fraction and goes smoothly up to 30% while fine sands decrease smoothly from the start to 30% of fine fraction. The combined graphs show that the permeable capacity of soil is nearly the same after 20% to 30%, as shown in Fig. 6.





#### F. Consolidation

Consolidation curves for dense and very loose material were examined to highlight the influence of fines content on the initial void ratio & final void ratio. The curves of consolidation for each loading phase are displayed below.

Table VI: Initial and final void ratio of all sites for medium sands

			Void Ratio	e <sub>°</sub>		
Fine Content			Medium Sa	nd		
(%)	Site One		Site Two		Site T	hree
	Initial e <sub>。</sub>	Final e <sub>。</sub>	Initial e <sub>。</sub>	Final e <sub>。</sub>	Initial e <sub>。</sub>	Final e <sub>o</sub>
0% Fines	0.82	0.71	0.8	0.7	0.71	0.65
5% Fines	0.62	0.54	0.76	0.69	0.7	0.61
12% Fines	0.56	0.49	0.66	0.59	0.63	0.54
20% Fines	0.50	0.41	0.58	0.52	0.61	0.53
30% Fines	0.46	0.39	0.53	0.47	0.57	0.51

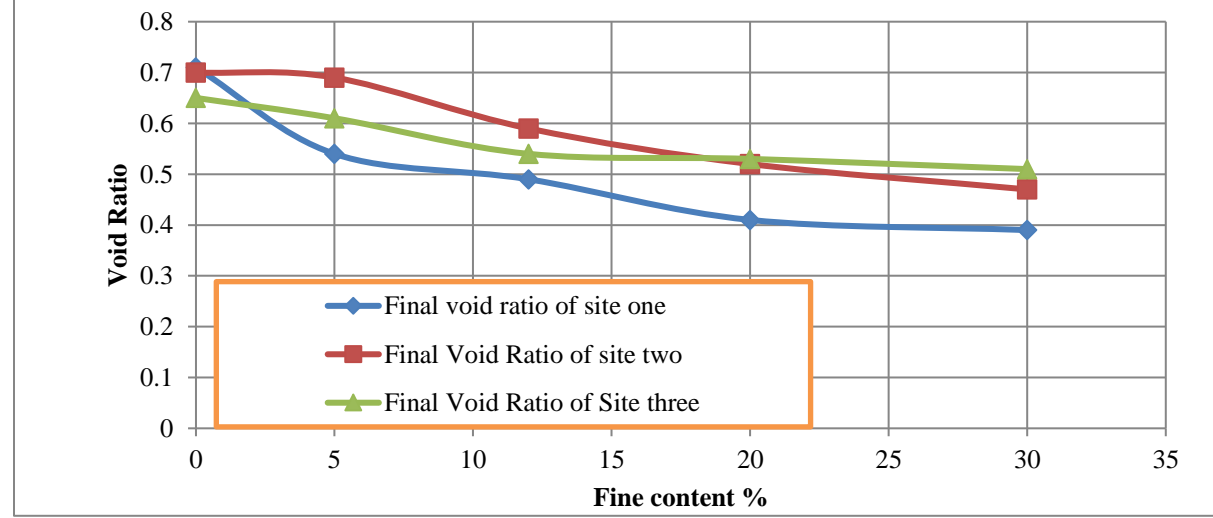
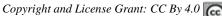


Fig. 7.: Final void ratio versus fine content relationship for medium sands of all sites

Fig. 7 shows that for medium and fine sand materials of reconstituted soil samples of all sites, the value of the initial and final void ratio decreases as fine content increases.

# G. Compressibility Characteristics

To obtain the compressibility of the reconstituted soil sample and its variation with different fines content, a series of 1D – compression tests were preferred on both the fine and medium sands of all sites.







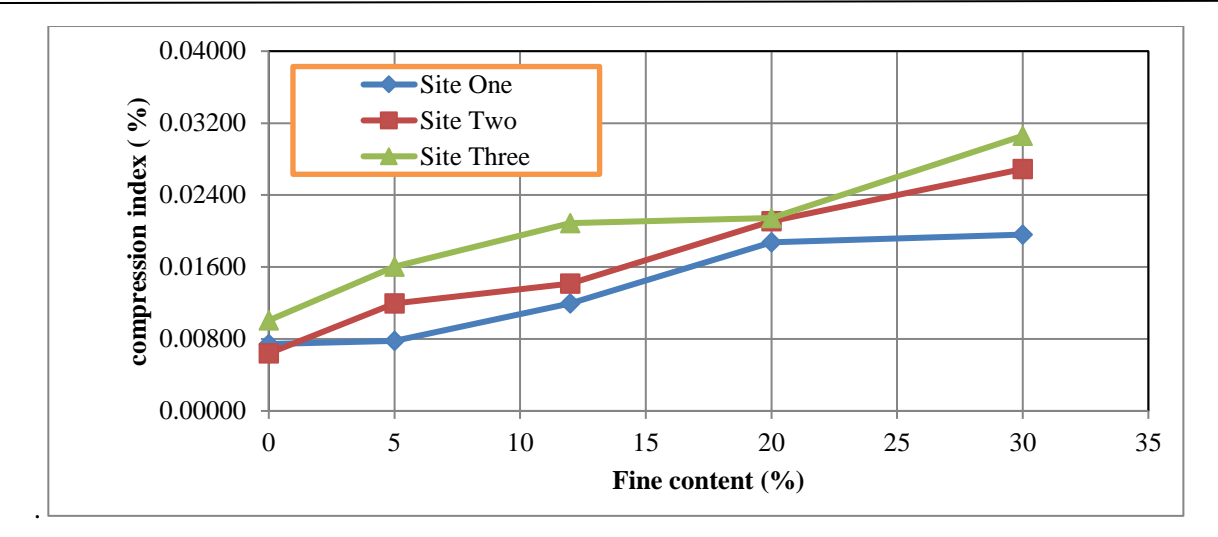


Fig. 8.: Compressibility curves with various fines content for medium sand of all sites

Fig. 8 indicates that the compression index of the sand increases as the fine contents are raised to 30 percent and the increment in fines increases the compression index of reconstituted sand soil. The result in Fig. 8 showed that when the fines content grows, Cc rises to a compression index of 0.03368 of fine sand and 0.03059 of medium sand for site three linked with a fines content of 30%.

#### H. Direct Shear Tests

Sand samples with various fine contents were subjected to direct shear tests (0%, 5%, 12%, 20%, and 30%). As a result, 30 direct shear tests were carried out, each with three normal loads. Table VII shows the maximum shear stresses obtained against each normal load (stress).

Table VII: Direct shear data obtained for medium sand samples of all sites

Fine Content (%)	Applied normal load, kPa	Site One	Site Two	Site Three
		The angle of	of internal fri	ction, φ°
0	9.6			
0	19.2	14.8	16.6	15.4
	28.8			
	9.6			
5	19.2	13.6	15.7	13.9
	28.8			
	9.6			
12	19.2	12.3	11.3	11.4
	28.8			

DOI: https://doi.org/10.59122/174CFC16



Copyright and License Grant: CC By 4.0



	9.6			
20	19.2	9.7	9.3	9.4
	28.8			
	9.6			
30	19.2	7.8	5.78	7.4
	28.8			

The angle of internal friction of medium and fine sand decreased by 17.73% and 11.41% respectively, as shown in Table VII. In comparison to the prior study [5], the present study's angle of internal friction was reduced by 57.37% because the prior study's normal load was 77.4kPa, 154.8kPa and 309.6kPa while the current study's normal load is 9.6kPa, 19.2kPa and 28.8kPa. Also angle of internal friction results are compared in the above Table VII.

When the fines content increases, the angle of internal friction ( $\emptyset$ ) decreases. The values of shear strength parameters (c and  $\emptyset$ ) at varying fines content of the soil samples are summarized in Table VII. The angle of internal friction value for medium sand from Site One ranges from  $16.6^{\circ}$  to  $0^{\circ}$ . This is a decrease of  $16.6^{\circ}$  %. The angle of internal friction values for fine sand ranges from  $10.4^{\circ}$  to  $0^{\circ}$ . This equates to a  $10.4^{\circ}$ . As the fine content of the samples increases, the angle of internal values decreases.

#### IV. Conclusion

The findings of this study indicate that the fine fraction of sandy soil affects the CBR, Permeability, Shear Strength, Plasticity, Compressibility, and MDD values of sandy soils Permeability and CBR values of the soil decrease as the fine fractions increase, and also the angle of internal friction ( $\emptyset$ ) of the soil decreases. Furthermore, as the fine fraction of the material rises, the optimum moisture content, MDD, and plasticity increase.

- Plasticity has a stronger influence on fine fractions. As the fines content increases, the Plasticity
  Index rises, while the Shear Strength at Maximum Dry Density (MDD) and Optimum Moisture
  Content (OMC) continue to decrease.
- Due to particle interlocking, an increase in dry density significantly impacts the California Bearing Ratio (CBR). The highest CBR value is achieved at the optimum water content.
- Mixtures with fines content ranging from 5% to 30% exhibit a lower ultimate void ratio as the fines content increases.
- Permeability parameters are closely linked to consolidation characteristics. As the fine content increases, the final void ratio and permeability of sandy soil decrease.





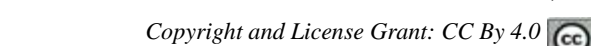
- The coefficient of compressibility, obtained from the 1D Consolidation test, decreases for each specimen as the fines content increases from 0% to 30%.
- The internal friction angle  $(\varphi)$  of sandy soil steadily decreases as the fines content increases from 0% to 30%. Further increases in fines content can lead to a reduction of  $\varphi$  to zero.

### References

- 1. S. Pathariya, "An Experimental Study on Effects of Non-plastic Fines on Engineering Properties of Sand-Silt Mixture," in Proceedings of the Indian Geotechnical Conference 2019, S. Patel, C.H. Solanki, K.R. Reddy, and S.K. Shukla, Eds., Lecture Notes in Civil Engineering, vol. 136, Singapore: Springer, 2021, pp. 1-10. doi: 10.1007/978-981-33-6444-8\_37.
- 2. B. A. Othman, A. Marto, F. Pakir, and A.Z. Salikin, "Influence of Grain Sizes on Undrained Strength of Sand Mixtures," International Journal of Innovative Technology and Exploring Engineering, vol. 8, no. 9, pp. 3154–3159, 2019. doi: 10.35940/ijitee.h7457.078919.
- 3. V.T. Phan, D. Hsiao, and P.T. Nguyen, "Effects of Fines Contents on Engineering Properties of Sand-Fines Mixtures," Procedia Engineering, vol. 142, pp. 213-220, 2016.
- 4. K. Lupogo, "Effect of fines mineralogy on the oedometric compressional behavior of sandy soils," Journal of Civil Engineering and Construction Technology, vol. 4, no. 7, pp. 232-238, 2013.
- 5. M.S. Pakbaz and A.S. Moqaddam, "Effect of Sand Gradation on The Behavior of Sand-Clay Mixtures," Journal of Civil Engineering and Construction Technology, vol. 3, no. 7, pp. 325-331, 2012.
- 6. M.S.I and T. Islam, "Effect of Fine Content on Shear Strength Behavior of Sandy Soil," B.S. thesis, Dept. Civ. Eng., Bangladesh University of Engineering and Technology, Dhaka, Bangladesh, 2017. doi: 10.13140/RG.2.2.32455.39843.
- 7. G. Adunoye, "Fines Content and Angle of Internal Friction of a Lateritic Soil," American Journal of Engineering Research, vol. 3, pp. 16-21, 2014.
- 8. D. Simpson and T.M.A. Evans, "On behavioral thresholds in mixtures of sand and kaolinite clay," Journal of Geotechnical and Geoenvironmental Engineering, vol. 142, no. 2, pp. 17–18, 2014.
- 9. A.F. Cabalar, "The Effects of Fines on the Behaviour of a Sand Mixture," Geotechnical and Geological Engineering, vol. 29, no. 1, pp. 90-100, 2010. doi: 10.1007/s10706-010-9355-z.
- 10. N. Daud, N. Norsyahariati, K.R. Hui, A. Ghafar, and A. Juliana, "The Effect of Soil Particle Arrangement on Shear Strength Behavior of Silty Sand," in 3rd International Conference on Civil

(P): 2959-393X

DOI: https://doi.org/10.59122/174CFC16



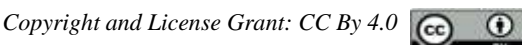


- and Environmental Engineering for Sustainability (IConCEES 2015), MATEC Web of Conferences, vol. 47, Article Number 03022, 2016. doi: 10.1051/matecconf/20164703022.
- 11. K. Yin, "Influence of clay fraction on the mechanical behavior of a soil-concrete interface," Ph.D. dissertation, Dept. Civ. Eng., École centrale de Nantes, Nantes, France, 2021.
- 12. I.I.I. Inan, W.K. Mampearachchi, and P.A.S. Udayanga, "Effect of Fine Percentage on the Properties of Sub-base Material," Engineer: Journal of the Institution of Engineers, Sri Lanka, vol. XLIX, no. 4, pp. 15–25, 2016.
- 13. S.Y. Mehdi Abedi, "Effects of plastic fines on the instability of sand," Soil Dynamics and Earthquake Engineering, vol. 30, no. 3, pp. 61-67, 2010.
- 14. M. Monkul and G.O. Compressional, "Behavior of clayey sand and transition fines content," Engineering Geology, vol. 89, no. 3-4, pp. 195-205, 2007.
- 15. M.Y. Fattah, M.M. Hilal, and H.B. Flyeh, "Effect of fine material on compaction characteristics of subbase material using Superpave gyratory compactor," International Journal of Civil Engineering and Technology, vol. 7, no. 5, pp. 466-476, 2016.
- 16. S.A. Naeini and M.H. Baziar, "Effect of fines content on steady-state strength of mixed and layered samples of a sand," Soil Dynamics and Earthquake Engineering, vol. 24, no. 3, pp. 181-187, 2004

DOI: https://doi.org/10.59122/174CFC14 C

(P): 2959-393X





# Synthesis of Nano-Biocomposite for Light-Weight Structural Applications

Nehemiah Mengistu Zeleke\*<sup>1</sup>, Devendra Kumar Sinha<sup>1</sup>, Santosh Kumar<sup>2</sup>

<sup>1</sup>Department of Mechanical Engineering, Adama Science and Technology University,

Adama, Ethiopia

<sup>2</sup> School of Mechanical Engineering, Indian Institute of Technology, Varanasi, India \*Corresponding Author's Email: Nehemiah.mengistu@gmail.com

### **Abstract**

Biocomposite materials have brought additional possibilities to the manufacturing industry rather than synthetic materials. Biodegradable polymer materials such as Polylactide Acid (PLA) have attracted various industries for numerous applications due to their excellent properties such as tensile strength despite some weaknesses. However, their combination with varying weight percentages of Microcrystalline Cellulose (MCC) (0%, 3%, 6%, and 9%), Montmorillonite (MMT) nano clay (0%, 3%, 6%, and 9%) as reinforcing agents, and Sorbitol (S) (10%, 20%, 30%, and 40%) as plasticizers to enhance properties, fabricated at various temperatures (100°C, 125°C, 150°C, and 175°C) using the melt-mixing method, can be evaluated under different testing standards and optimized to achieve an optimal experimental setup. This study prepared 16 biocomposite samples through Taguchi's Orthogonal Array experimental design. The optimal factor level combination was investigated for Flexural Strength (FS) at 3% MCC and 9% MTT fillers, and 20% S plasticizer and at 175-degree centigrade, 3%MCC, 9%MTT, 20%S and 175-degree centigrade, at these levels, FS (Flexural Strength) is 96.5 MPa, Flexural Modulus (FM) (6%MCC, 9%MTT, 20%S, and 175-degree centigrade), at these control factors FM is 9.8 GPa, Tensile Strength (TS) (9%MCC, 9%MTT, 10%S, and 175-degree centigrade), at these levels, TS is 85.2 MPa, Young's Modulus (YM) (6%MCC, 9% MTT, 0%S, and 150-degree centigrade), at these experimental run YM is 4.22 GPa, Water Absorption (WA) (0% MCC, 0% MTT, 0% S and 150 degree centigrade), WA is 2.42% and Density (D) (9%MCC, 9%MTT, 30%S and 175 degree centigrade) at this experimental setup D is 0.0427g/mm3. A general multiple linear model was established for each result prediction. Analysis of variance (ANOVA) for the regression model shows the statistical significance of the regression model and the significance of the factors that affect each response. The addition of fillers and plasticizers significantly improves the properties of PLA material and the developed biocomposite material is expected to be utilized for lightweight load-carrying applications in structural and biomedical areas.

**Keywords:** Biocomposite, Micro Crystalline Cellulose, Montmorillonite, Polylactide Acid, Sorbitol, Multiple Linear Model

Ethiopian International Journal of Engineering and Technology (EIJET)

Volume 2, Issue 2, 2024

Copyright and License Grant: CC By 4.0



#### I. Introduction

Material designers and processing firms are in unwavering investigation for novel and enhanced materials and fabrication methods to make materials that have enhanced mechanical properties, that are renewable, eco-friendly, and of low cost. One of the areas that gained the most attention in this regard is the field of biocomposite also alternatively referred to as natural fiber composite [1]. Biocomposite is a combined constituent made from natural resources as a strengthening and the matrix is produced by a polymer from synthetic or natural materials [2]. This biocomposite material has numerous advantages in terms of its ecofriendliness, recyclability, biodegradability, low density, carbon dioxide neutrality (non-toxic), good insulating and acoustic properties, good thermal properties, and non-abrasiveness [3-5]. As a result, it has many industrial applications in the fields of automotive, building, packaging, and furniture [6]. Natural fibers contain three main essential polymers: hemicellulose and cellulose are the polysaccharides and those called holocellulose and lignin are the aromatic polymers. The lignin and hemicellulose content in fibers influences the end characteristics of biocomposites as they have a higher attraction for moisture and are hydrophilic. Researchers and material engineers have devoted themselves to the elimination of these (hemicellulose and lignin) contents in cellulose applications and their derivatives microcrystalline cellulose (MCC) and Nano-cellulose (NC) as fillers in different polymers. Additionally, they are in continuous search for new and higher sources of cellulose material and high amounts of cellulose-based biocomposite materials [7]. Cellulose is the abundant and most essential polymer in nature, which can be derived from renewable resources. Its presence as the common constituent on the cell wall of plants was first observed by Braconnot in 1819 [8]. It has a dense microfibril structure with a linear chain of β-1,4-glycosidic-linked D-glucose units as the main building blocks having crystallinity and strong hydrogen bonds that offer excellent mechanical strength, nontoxic, and biodegradability properties [9]. It is a promising renewable and biodegradable resource that could potentially substitute man-made fibers in industrial applications [10]. It is extensively utilized in numerous areas, such as water treatment, food industry packaging, biomaterial composites, textile and paper manufacturing, and the pharmaceutical industry as a raw material [11]. Numerous plants such as jute, flax, hemp, bamboo, wood, and cotton have abundant cellulose content [12]. Furthermore, cellulose has been isolated from different resources, i.e. hop stems [13], milkweed stems [14], coffee husks [15], rice husks [16], Cissus quadrangularis root [17], etc.Its derivative, microcrystalline cellulose, is a tasteless and micro-sized naturally available constituent investigated from partially depolymerized and purified cellulose. Cellulose chains are combined to make microfibrils and these microfibrils are additionally combined to make "cellulose macro fibers". Therefore, natural fibers that hold cellulose structure are considered "cellulose microfibers", which contain both "amorphous" and

Copyright and License Grant: CC By 4.0



(P): 2959-393X

DOI: https://doi.org/10.59122/174CFC14





"crystalline" cellulose regions [18]. Acidic attack treatment is used to reduce cellulose macro fibers properties by removing the amorphous region for the intention of crystalline region separation. Then, these crystallites can move without restrictions due to an increase in size. In research works, this structure is generally named "microcrystalline cellulose". Its extraction techniques are various containing biological, chemical, and mechanical treatment. Chemical treatment, predominantly acid hydrolysis, is the common technique used for the isolation of MCC [19]. Polylactic acid is a bio-degradable and eco-friendly polymer made up of lactic acid by-products such as starch sugar cane, potatoes, corn grain, etc., and renewable agricultural products [20, 21]. It is considered a leading candidate thermoplastic polymer that yields different components for structural, packaging, and biocompatibility applications. Currently, different biobased polymer materials are used for binding natural fibers. Among these polymers, PLA is the dominant one that is being studied intensively [22]. However, it has low performance on mechanical and thermal properties as well as high cost. These pose great scientific challenges and limit their large-scale applications to outdoor environments [23, 24]. Recently, several studies that used plasticization [25], copolymerization [26], blending [27], fiber-reinforced composite [28], and nano-based composite [29] fabrication have been done to enhance the PLA bioplastic properties. Plasticizers are commonly used materials to modify polymers and are considered the most common plastic material additive. They are a type of non-volatile and low molecular weight organic compounds that improve the processability and flexibility of the polymer by decreasing the glass transition temperature. The plasticizing theory assumes that the low molecular weight of a plasticizer permits decreasing connecting forces such as Vander Waals forces, hydrogen bonding, etc. between the polymer chains by penetrating the intermolecular spaces and reducing the intermolecular frictions [30]. The inclusion of these materials in polymers influences the viscosity, density, elastic modulus, hardness, impact resistance, water absorption, crystallization, melting temperatures, permeability, and degradation rate [31]. Plasticizers can be differentiated into petro-based or bio-based. Bio-based plasticizers are assumed as ideal green plasticizers and non-toxic, have good miscibility, are efficient, low cost, high resistance to leach from polymer. The most common bio-based plasticizers are polyols such as glycerol, diethylene glycol, ethylene glycol, tri ethylene glycol, tetra ethylene glycol propylene glycol, polyethylene glycol, xylitol, mannitol and sorbitol, monosaccharides (glucose, fructose, mannose, sucrose), fatty acids, vegetable oils, ethanolamine, urea, triethanolamine, lecithin, waxes, surfactants, amino acids, and water [32]. The inclusion of a plasticizer in biodegradable composites reduces the composite fragility behavior noticeably [33]. As a plasticizer, sorbitol has superior mechanical and physicochemical properties than other polyols [34]. As the study reports, the incorporation of sorbitol plasticizer amounts up to 30 wt.%, simplifies the creation of crystalline areas in chitosan films. These crystalline areas act as cross-links limiting the movement of amorphous chemical chains and lead to

DOI: https://doi.org/10.59122/174CFC14

ISSN (E): 2959-3921

(P): 2959-393X

6

Copyright and License Grant: CC By 4.0



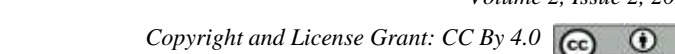
improvement in thermo gravimetric results. Furthermore, the inclusion of sorbitol was capable to increase the physicochemical and thermal characteristics of chitosan films [35].

Clay is a material class having layered clay minerals or silicates with traces of organic matter and metal oxides. The classes of clays are classified in terms of their crystal structure and chemical compositions. Based on the ratios of its building block (silica tetrahedron and aluminum (or other) octahedron) natural clay is categorized into three groups kaolinite (1:1), montmorillonite, and vermiculite (2:1) and chlorite (2:2), related with constitutive interchanging layers of "SiO2" and "AlO6" units. Montmorillonite (MMT) is the frequently used Nano clay because of its availability, eco-friendliness, high aspect ratio, high swelling property in polar spaces, and well-analyzed chemistry [36, 37]. The incorporation of Nano clay into polymers and natural fiber-reinforced polymers improves the performance (physical, mechanical, thermal, ultraviolet, diffusional barrier, etc.) of Nanocomposites [38]. The mechanical property of polymer matrix composite is greatly enhanced due to the interfacial level interaction between the constituent and better dispersion of the Nano clay in the polymer matrix. This ensures better load transfer between them and highly uniform stress distribution for better properties [39]. Previously, conducted research work has shown Nano clay's usefulness to make excellent properties of biocomposites. Nano clay content addition is considered a basic constituent. The inclusion of Nano clay into a polyester matrix improves the mechanical performance and decreases the shrinkage of the composite material [40]. On the same matrix material incorporation of graded Nano clay, the flexural and tensile strength with modulus improves [41]. Additionally, the loading of Nano clay, Nanomer I30 E, into epoxy resin enhanced the tensile strength with a reduction in strain at failure [42]. The addition of Cloisite 20A Nano clay enhanced the mechanical properties of vinyl ester composites, specifically fracture toughness with an insignificant reduction in flexural strength [43]. Moreover, it has been verified that the flammability behavior of polymer composite is improved with a charging of 2 % of Nano clay [44].

Optimization is an important method used to determine the well-known design factors that can provide the optimal (maximum or minimum) result for a given problem. Problems of optimization are figured out through non-conventional and conventional techniques [45]. Non-conventional optimization techniques were used for the optimization of multi-response characteristics. Conventional techniques are statistical designs of experiments that consist of response surface methodology and Taguchi's method. These methods were used to find the optimal factors of single-quality characteristics. Taguchi's method has a special design method called an orthogonal array used to analyze a large number of factors with a lesser number of experiments. The results drawn from these small experiments are acceptable over the whole experimental domain varied by the control factor and its levels. The result of experiments is converted into a signal-to-noise (S/N) ratio. It is used to measure the deviation of the response from the desired value.

ISSN (E): 2959-3921

(P): 2959-393X DOI: https://doi.org/10.59122/174CFC14





Based on this background, in the present study, the flexural strength, flexural modulus, tensile strength, Young modulus, hardness, water absorption, and density properties of PLA-based biocomposite at different filler (MCC and MTT) and plasticizing (sorbitol) content with operating parameter (temperature) are determined. Fillers and plasticizer content with operating parameters are considered as process parameters to determine how they behave for flexural stress, tensile stress, and indentation. Taguchi's orthogonal array is used to optimize the responses of PLA-based developed biocomposite. Regression model analysis of variance is executed to expose the statistical significance of the regression model and the significance factor level of influence on the responses of developed biocomposite.

#### II. **Materials and Methods**

# A. Description of Materials and Bio-composite Preparation

In this study, the biocomposite sample material used is made from coffee husk-derived MCC and MMT Nano clay powder as a reinforcing agent, and PLA as a matrix material. Additionally, sorbitol powder was used as a plasticizer. The PLA grade NCZ-NP-381/22, MMT Nano clay grade NCZ-MN-118/20, and D sorbitol were supplied from India, Aritech Chemazone Pvt. Ltd. The reinforcing material, MCC was extracted from the outer skin of isolated coffee husk according to the procedure reported in Nehemiah M.Z. et.al [15]. All samples of MCC/MMT/S/PLA biocomposite were fabricated using the melt-mixing method. Initially, the designated weight percentage of PLA and sorbitol were mixed and heated at the required temperature on the heating plate. Then, pre-calculated amounts of MCC and MMT were added to the heated blend of PLA and sorbitol and stirred properly to make uniform distributions of reinforcing agent. After that, the material was poured into the mold size of 100x50x4mm with a constant pressure of 2 MPa for 24 hrs. It was then cut into the specimens using a hacksaw according to ASTM standards and sanded using sandpaper. Finally, the post-curing of specimens was carried out at 40 °C temperature in an oven for 3 hours to remove the existence of moisture that may affect the final results.

# B. Experimental Design and Plan of Investigation

In the present research investigation, biocomposite material based on Polylactide acid with coffee huskderived MCC and MTT particles, and an S plasticizer at different T was prepared using a melt mixing setup. The intended amount of MCC and MMT particles were mixed properly to make homogeneous distributions. For the preparation of biocomposite material, four effective parameters (MCC, MTT, S, and T) with four levels for each parameter were used to investigate responses. The control factors and their levels are exhibited in Table I below. The response factors tensile strength and modulus, flexural strength and modulus, hardness value, water absorption, and density values were measured according to their respective ASTM standards.

ISSN (E): 2959-3921

DOI: https://doi.org/10.59122/174CFC14



Copyright and License Grant: CC By 4.0



Table I: Control factors and their values at four levels

Factors	Unit	Levels				
ractors	UIIIt	1	2	3	4	
A – MCC	Wt. %	0	3	6	9	
B – MMT Nano clay	Wt. %	0	3	6	9	
C-Sorbitol	Wt. %	0	10	20	30	
D-Temperature	°C	100	125	150	175	

Taguchi's method has a special design method called orthogonal array used to analyze a large number of factors with a lesser number of experiments. The results drawn from these small experiments are acceptable over the whole experimental domain varied by the control factor and its levels. The result of experiments is changed into a signal-to-noise ratio. It helps to evaluate the variation of the response from the preferred value. Based on the type of desired response, S/N ratio analysis is categorized into three, i.e. the higher the better, the lower the better, and the nominal the better. For developed biocomposite, flexural strength, tensile strength, hardness value, and density have been thought of as the larger-the-better; and for water absorption, it is the smaller-the-better. The S/N ratio for the corresponding responses was calculated using the following cases.

Case 1: The larger-the-better performance characteristics are utilized for a problem when maximization of interest is required.

$$S/N \ ratio = -10 \ log_{10} \left(\frac{1}{n}\right) \sum_{i=1}^{n} \frac{1}{y_{ii}^2}$$
 (1)

Where:  $y_{ij}$  - observed response value, n - Number of replications, i=1, 2, ...n; j=1, 2, ...k

Case 2: The smaller-the-better performance characteristics are used for a problem where minimization of interest is required.

$$S/N \ ratio = -10 \ log_{10} \left(\frac{1}{n}\right) \sum_{i=1}^{n} y_{ij}^{2}$$
 (2)

Taguchi's orthogonal array (L16) experimental design made by "Minitab" software is shown in Table II.

Table II: L16-OA design matrix for biocomposite development

Sample		Coded	Facto	r	Uncoded Factor				
No.	A	В	C	D	MCC (Wt. %)	MMT (Wt. %)	S (Wt. %)	T (°C)	
1	1	1	1	1	0	0	10	100	
2	1	2	2	2	0	3	20	125	
3	1	3	3	3	0	6	30	150	
4	1	4	4	4	0	9	40	175	

Received: July 2024; Revised: 29 November 2024; Accepted: 15 December 2024; Published: 23 December 2024

ISSN (E): 2959-3921 (P): 2959-393X DOI: https://doi.org/10.59122/174CFC14



Copyright and License Grant: CC By 4.0

								_ av
5	2	1	2	3	3	0	20	150
6	2	2	1	4	3	3	10	175
7	2	3	4	1	3	6	40	100
8	2	4	3	2	3	9	30	125
9	3	1	3	4	6	0	30	175
10	3	2	4	3	6	3	40	150
11	3	3	1	2	6	6	10	125
12	3	4	2	1	6	9	20	100
13	4	1	4	2	9	0	40	125
14	4	2	3	1	9	3	30	100
15	4	3	2	4	9	6	20	175
16	4	4	1	3	9	9	10	150

### C. Regression analysis

The factors (MCC, MTT, S, and T) were considered in the development of mathematical models for the response value (TS, YM, FS, FM, HV, WA, and D) accuracy. The correlation between factors (MCC, MTT, S, and T) and response values (TS, YM, FS, FM, HV, WA, and D) accuracy of developed biocomposite was obtained by multiple linear regression, which is a technique that analyzes numerous explanatory factors to forecast the result of performance characteristics [46]. A linear model is developed to control the response (TS, YM, FS, FM, HV, WA, and D) data fitness to represent a characteristic in the form as follows:

$$Y = b_0 + b_1 MCC + b_2 MTT + b_3 S + b_4 T + \varepsilon$$
 (3)

Where Y is the response,  $b_1$ ,  $b_2$ ,  $b_3$ , and  $b_4$  are estimates of the factors and  $\varepsilon$  is the error. The statistical software package MINITAB was applied to develop the models.

#### D. Characterization Techniques of Developed Biocomposite

1) *Flexural:* The flexural strength of the samples was determined as per ASTM D790 through-point bend testing method by UTM machine, i.e. Bongshin Model DSCK machine [47, 48]. The flexural strength and modulus were determined with the given equations;

Flexural strength, 
$$FS = \frac{3FL}{2wt^2}$$
 (4)

Flexural modulus, FM = 
$$\frac{L^3 F}{4wt^3 \delta}$$
 (5)

Where F - is the applied load, L - is the length of the specimen, w - is the width of the specimen, t - is the thickness of the specimen and  $\delta$  - is the deflection.

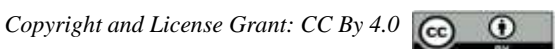
2) *Tensile:* tensile was performed based on ASTM D638 to measure the tensile strength of the samples [49][50].

(P): 2959-393X

Volume 2, Issue 2, 2024

DOI: https://doi.org/10.59122/174CFC14





3) Water absorption: the material's water absorption is important to study in case the developed materials are used in contact with water for determining water uptake in contact with water. This can adversely affect mechanical and ageing properties. The investigation was conducted according to ASTM D570-98, sample size of 20x20x3mm to find out the water absorption of specimens [51]. The water absorption of the specimens was determined as an increase in weight % with the following equation [52].

Increase in weight % = (wet weight – dry weight)/dry weight x 100 (6)

**4)** *Density:* the density of developed biocomposite specimens was carried out according to ASTMD792-98, sample size of 20x20x3mm. Then, the density was determined through the given equation [53].

Density = Mass (g)/Volume (mm
$$^3$$
) (7)

### III. Results and Discussion

# A. Flexural Strength and Modulus of Biocomposite

The flexural strength and modulus of biocomposite samples at different weight percentage of MCC, MTT, and S in PLA at various temperature levels are shown in Table III with their S/N ratio and Fig. 2. Under flexural loading, Table II and Fig. 2 exhibit that the addition of MCC, MTT and S improved the flexural strength and modulus of neat PLA. The flexural strength values of the MCC and MTT reinforced and S plasticized PLA (MCC/MTT/S/PLA) biocomposites could be higher than the neat PLA except for 9MCC/0MTT/30S/125T values at experiment 13. This is probably due to the establishment of agglomeration at higher content of MCC and because increasing S content at higher levels leads to low flexural strength due to its low flexural strength [54]. The experimental setup 3MCC/9MTT/20S/125T combination shows the highest flexural strength with the value of 93.75 MPa as shown in experiment 8, which is 78.5 % greater than that of the neat PLA experiment 1. It is easily assumed that at these contents the fillers are dispersed uniformly within the PLA material. It is clearly shown in Table III that the flexural modulus of each MCC/MTT/S bio-composite sample is greater than that of the neat PLA. This is mainly caused due to flexural 3-point bending tests in which the upper half part of the cross-section of the sample is in compression, whereas the lower half part of the cross-section is subjected to tensile loads. Therefore, the parting boundary would be hindered in the sample on the side compressive, resulting in an improved load transfer mechanism from the matrix material to the fillers [55].



Copyright and License Grant: CC By 4.0



Table III: Flexural strength and modulus of biocomposite with s/n ratios

S. N		Facto	ors			Resp	onses	
<b>5.</b> IN	MCC	MMT	S	T	FS (MPa)	S/N Ratio	FM (GPa)	S/N Ratio
1	0	0	0	100	52.50	34.40	4.1	72.19
2	0	3	10	125	60.00	35.56	5.3	74.53
3	0	6	20	150	75.00	37.50	6.7	76.59
4	0	9	30	175	82.50	38.32	7.5	77.54
5	3	0	10	150	60.00	35.56	5.5	74.89
6	3	3	0	175	71.25	37.05	7.1	77.01
7	3	6	30	100	75.00	37.50	7.5	77.58
8	3	9	20	125	93.75	39.43	9.7	79.79
9	6	0	20	175	63.75	36.08	6.7	76.58
10	6	3	30	150	63.75	36.08	7.1	77.00
11	6	6	0	125	67.50	36.58	7.7	77.79
12	6	9	10	100	71.25	37.05	8.4	78.57
13	9	0	30	125	45.00	33.06	5.0	73.97
14	9	3	20	100	56.25	35.00	8.1	78.22
15	9	6	10	175	56.25	35.00	7.8	77.85
16	9	9	0	150	60.00	35.56	8.6	78.78

The best S/N ratio shown in Table III for FS is 39.43 at experiment number 8 and also offers a higher FS value of 93.75. The weakest S/N ratio is 33.06 observed in experiment 13. The best S/N ratio of FM is observed in the same experimental setup, experiment 8 with a value of 79.79, and the weakest S/N ratio is observed in experiment 1 with a value of 72.19.

### B. Probability Plot

Fig. 1 presents the probability plot of flexural strength and modulus of all samples. As exhibited in Fig. 1 (a) and (b) all data are under normal distribution at the confidence level of 95%. The two lines beside the center line on the left and right show the upper and lower limits of the confidence interval. No sample value is out of the confidence interval. Additionally, the p-values 0.657 and 0.544, which are higher than the significance level of 0.05 show that the data follows a normal distribution.

ISSN (E): 2959-3921

(P): 2959-393X

DOI: https://doi.org/10.59122/174CFC14



Volume 2, Issue 2, 2024

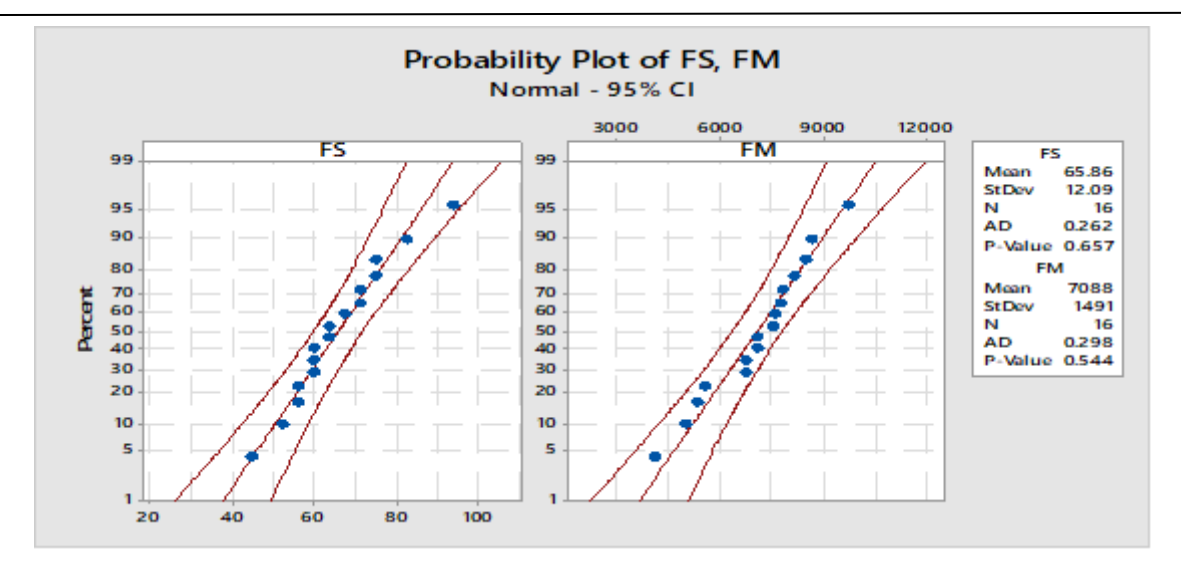


Fig. 1.: Probability plot for flexural strength (a) and flexural modulus (b) of samples

# C. S/N Ratio Analysis of FS and FM

Tables IV and V present responses for the S/N ratio of flexural strength and flexural modulus, respectively. The delta value shows the significance of the control variables and helps to identify the optimal setting that generates higher flexural strength and modulus. The higher values of delta show the more significant variable, and based on values of delta, the whole significant variables are ranked properly. The value of delta ranking in Table IV indicates the MTT content as the most significant parameter in influencing the flexural strength of the biocomposite, followed by MCC content, and then S and T, respectively. The value of delta ranking in Table V indicates that the MTT is the highest significant factor in influencing the flexural modulus of the biocomposite, followed by MCC content, and then S and T, respectively.

Table IV: Response table for s/n ratios of fs (the larger the better)

Level	MCC	MTT	S	T
1	36.45	34.78	35.90	35.99
2	37.39	35.93	35.80	36.16
3	36.46	36.65	37.01	36.18
4	34.66	37.60	36.25	36.62
Delta	2.73	2.82	1.21	0.63
Rank	2	1	3	4



Copyright and License Grant: CC By 4.0



Table V: Response table for s/n ratios of FM (the larger the better)

Level	MCC	MTT	S	T
1	75.22	74.41	76.45	76.64
2	77.32	76.70	76.47	76.53
3	77.49	77.46	77.80	76.82
4	77.21	78.67	76.53	77.25
Delta	2.27	4.26	1.35	0.72
Rank	2	1	3	4

The S/N Ratio graphs are plotted for flexural strength and flexural modulus responses in Fig. 2. (a) and (b). The graph is drawn using the optimal control factors, and the optimal value is the one with the highest value of mean SNR. It has been found that the maximum flexural strength was obtained for developed biocomposite at 3%MCC, 9%MTT, 20%S, and 175°C T as shown in Fig. 2. (a). At this level, FS is 96.5 MPa. For flexural modulus, 6%MCC, 9%MTT, the 20S, and 175°C showed the maximum S/N ratio as shown in Fig. 2. (b), and at this level FM is 9.8 GPa.

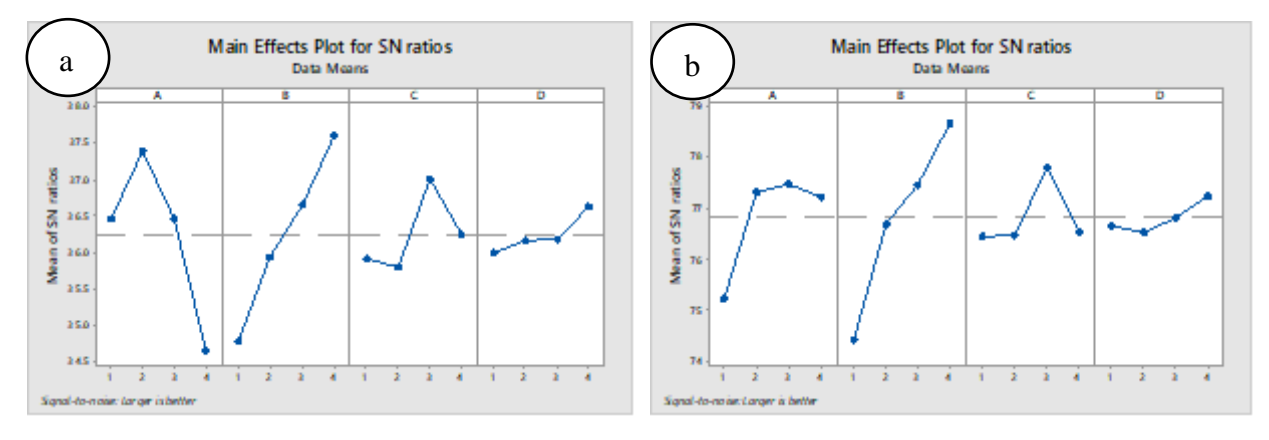


Fig. 2.: Main effect plot for S/N ratios of FS (a) and FM (b)

#### D. Regression Analysis

The relationship between factors that affect the flexural responses and outcomes is expressed by using the regression equation as follows:-

$$FS = 51.80 - 4.78 MCC + 7.03 MTT + 2.16 S + 1.22 T$$
 (8)

$$FM = 2.997 + 0.450 MCC + 1.039 MTT + 0.074 S + 0.074 T$$
 (9)

Table VI presents the significance of factors incorporated in the regression equation of flexural strength. Table VI clearly shows that the regression P-value 0.005 suggests that the factors incorporated in the



Copyright and License Grant: CC By 4.0



experimental setup are statistically highly significant for the linear model, and factors with a P-value less than 0.05 show the most significant parameter that influences the regression equation. Additionally, the larger F-value shows the more significant factor that influences the regression response. Table VI exhibits that MTT and MCC P-values are 0.002 and 0.016, respectively. This indicates that they are the most significant factors that affect the regression model of biocomposite flexural strength, and factors T and S have less significance, respectively.

Table VI: ANOVA for regression model of FS

4	1560 67				
	1568.67	1568.67	392.17	6.91	0.005
1	457.21	457.21	457.21	8.06	0.016
1	988.77	988.77	988.77	17.42	0.002
1	92.99	92.99	92.99	1.64	0.227
1	29.71	29.71	29.71	0.52	0.484
11	624.20	624.20	56.75		
15	2192.87				
	1 1 1 11	1 988.77 1 92.99 1 29.71 11 624.20	1       988.77       988.77         1       92.99       92.99         1       29.71       29.71         11       624.20       624.20	1       988.77       988.77       988.77         1       92.99       92.99       92.99         1       29.71       29.71       29.71         11       624.20       624.20       56.75	1       988.77       988.77       17.42         1       92.99       92.99       1.64         1       29.71       29.71       29.71       0.52         11       624.20       624.20       56.75

Table VII presents the significance of factors incorporated in the regression equation of flexural modulus. Table VII indicates that regression P-value 0.001 suggests that the factors incorporated in the model are statistically highly significant and factors MTT and MCC with P-value s of 0.000 and 0.033, respectively are the most significant factors that affect the regression model of biocomposite flexural modulus, and factor S and T have less significances, respectively.

Table VII: ANOVA for regression model of FM

Source	DF	Seq SS	Adj SS	Adj MS	F-Value	P-Value
Regression	4	25.855	25.855	6.463	9.47	0.001
MCC	1	4.042	4.042	4.042	5.92	0.033
MTT	1	21.594	21.594	21.594	31.63	0.000
S	1	0.110	0.110	0.110	0.16	0.695
T	1	0.108	0.108	0.108	0.16	0.698
Error	11	7.509	7.509	0.682		
Total	15	33.365				



Copyright and License Grant: CC By 4.0 (a)



# E. Tensile Strength and Young Modulus of Biocomposite

Table VIII presents different specimen configurations of PLA-based biocomposites with various loadings of plasticizer, MCC and MTT contents, and temperature to analyze tensile strength and young modulus properties as responses and all data converted to S/N ratio also shown in Table VIII. From Table VIII, it is observed that the loading of S, MCC, and MTT improves the tensile strength of PLA. The experimental setup 6MCC/9MTT/10S/100T combination shows the highest tensile strength followed by 9MCC/6MTT/10S/175T, and experimental combination 6MCC/0MTT/20S/175T shows the lowest tensile strength following the neat PLA. The highest tensile strength experimental setup 6MCC/9MTT/10S/100T biocomposite has 83.3 MPa, which is 50 % greater than that of the neat PLA. It is easily assumed that in these contents, the fillers are dispersed uniformly within the PLA material [56]. The lowest biocomposite combination improves by 5% greater than that of the neat PLA. This is probably because the absence of MTT and increment of S reduces the tensile strength relative to the rest of the experimental setup [57]. As presented in Table VIII, the addition of fillers improves the modulus of elasticity of the neat PLA and plasticizer reduces the modulus of elasticity of neat PLA [58]. Therefore, the tradeoff is conducted to gain the optimal level of parameters. The minor inclusion of fillers without plasticizer at higher temperatures shows the highest young modulus at experiment 6 (3MCC/3MTT/0S/175T) with the value of 4.28 GPa. In this experimental combination, the Young's modulus is increased by 23% more than the neat PLA. This improvement is caused by the presence of MCC and MTT contents which restrict the molecular chain movement in the PLA and form physical and chemical interlocks with the PLA matrix.

Table VIII: Experimental setup and results of TS and YM with S/N ratio

		Fact	tors		Responses				
S. N	MCC	MMT	S	T	TS (MPa)	S/N Ratio	YS (GPa)	S/N Ratio	
1	0	0	0	100	55.5	34.8945	3.28	10.3175	
2	0	3	10	125	68.8	36.7630	3.60	11.1261	
3	0	6	20	150	72.2	37.1734	3.93	11.8879	
4	0	9	30	175	77.7	37.8171	3.70	11.364	
5	3	0	10	150	66.6	36.4782	3.38	10.5783	
6	3	3	0	175	77.7	37.8171	4.26	12.5882	
7	3	6	30	100	67.7	36.6217	3.44	10.7312	
8	3	9	20	125	75.5	37.5653	3.53	10.9555	
9	6	0	20	175	58.3	35.3178	3.12	9.8831	
10	6	3	30	150	72.2	37.1734	3.75	11.4806	
11	6	6	0	125	78.8	37.9403	4.13	12.319	

ISSN (E): 2959-3921

(P): 2959-393X

**DOI:** https://doi.org/10.59122/174CFC14



Copyright and License Grant: CC By 4.0



Volume 2, Issue 2, 2024

12	6	9	10	100	83.3	38.4164	3.95	11.9319
13	9	0	30	125	66.6	36.4773	2.55	8.1308
14	9	3	20	100	70.5	36.9706	2.63	8.3991
15	9	6	10	175	81.6	38.2409	2.89	9.218
16	9	9	0	150	78.8	37.9403	3.21	10.1301

The best S/N ratio shown in Table VIII for TS is 38.41 at experiment number 12 and also offers the highest TS value of 83.3 MPa. The weakest S/N ratio is 34.89 observed in experiment 1. The best S/N ratio of YM is observed in experiment 6 with a value of 12.58 and the weakest S/N ratio is observed in experiment 13 with a value of 8.13.

# F. Probability Plot

The probability plot shows each value of the experimental setup against the percentage of values in the specimen that are less than or equal to it, along a fitted distribution line. Fig. 3 exhibits that all sample values are under normal distribution at the confidence level of 95%. The two lines beside the center line on the left and right show the upper and lower limits of the confidence interval. No sample value is out of the confidence interval. This tendency offers improved outcomes for future estimation of process characteristics.

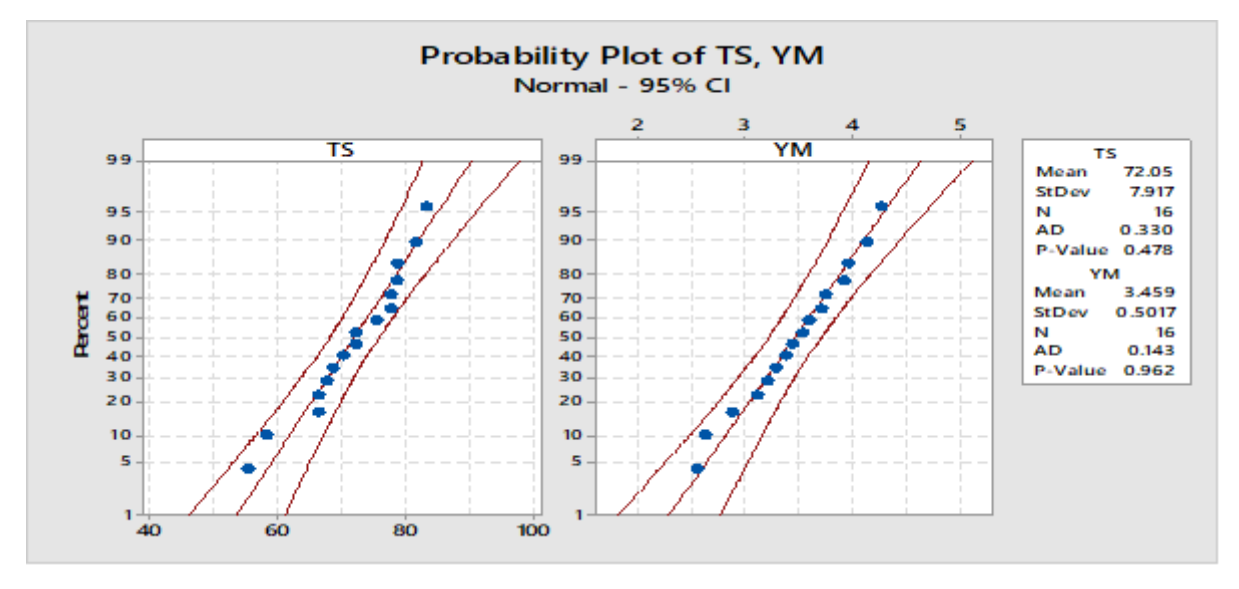


Fig. 3.: Probability plot of FS and YM

# G. Signal to Noise Ratio Analysis of Tensile strength and Young modulus

Table VIII shows the S/N ratios of TS for the greater the better characteristic to maximize the tensile strength of biocomposite material. The optimal experimental setup for the larger the better tensile strength characteristics is 9%MCC, 9%MTT, 10%S, and 175°C. At this level, the TS is 85.2 MPa and MTT primarily

**DOI:** <u>https://doi.org/10.59122/174CFC14</u>



Copyright and License Grant: CC By 4.0



affects the tensile strength followed by MCC, S, and T, respectively. The main effects plot for S/N ratios of TS is presented in Fig. 4 (a).

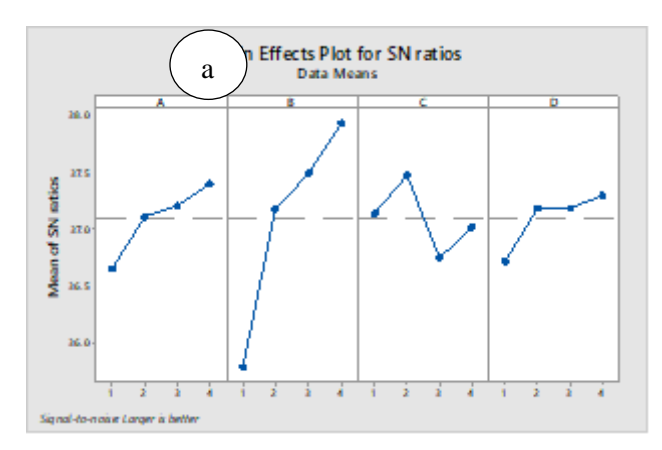
Table IX: Response table for S/noise ratios of TS (the larger the better)

Level	MCC	MTT	S	T
1	36.66	35.79	37.15	36.73
2	37.12	37.18	37.47	37.19
3	37.21	37.49	36.76	37.19
4	37.41	37.93	37.02	37.30
Delta	0.75	2.14	0.72	0.57
Rank	2	1	3	4

Table X presents the S/N ratios of the Young modulus of biocomposites. The optimal experimental setup for the larger the better characteristics of young modulus is 6%MCC, 9%MTT, 0%S, and 150°C. At this level, the YM is 4.28 GPa and is primarily affected by MCC followed by MTT, S, and T, respectively. The main effects plot for S/N ratios of Young modulus is presented in Fig. 4 (b).

Table X: Response table for S/N ratios of Young's modulus (the larger the better)

Level	MCC	MTT	S	T
1	11.174	9.727	11.339	10.345
2	11.213	10.898	10.714	10.633
3	11.404	11.039	10.281	11.019
4	8.969	11.095	10.427	10.763
Delta	2.434	1.368	1.057	0.674
Rank	1	2	3	4



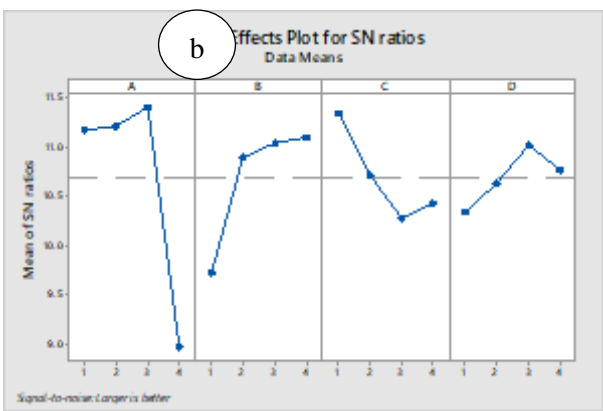


Fig. 4: Main effects plot for S/N ratios of tensile strength (a) and young modulus (b)



Copyright and License Grant: CC By 4.0 

(G)



#### H. Regression Analysis

The regression analysis is a statistical technique that explains the correlation between factors and one or more responses. The relations tensile strength and young modulus have with the input parameters, i.e. MCC content, MTT content, S content, and temperature are given by regression equation as follows;

$$TS = 53.16 + 1.87 MCC + 5.40 MTT - 1.10 S + 1.37 T$$
 (10)  
 $YM = 3.802 - 0.2338 MCC + 0.1583 MTT - 0.1232 S + 0.0618 T$  (11)

ANOVA for regression model of TS and YM of biocomposite

The significance of factors incorporated in the regression equation of tensile strength is given in ANOVA Table XI. The regression P-value (0.002) lesser than 0.05 suggests that a statistically significant relationship occurs between factors and responses in the experimental design. And factors' P-value lesser than 0.05 shows the most significant parameter that influences the regression equation. Additionally, the larger F-value shows the more significant factor that influences the response. Table XI presents that MTT P-value 0.000 and F-value 28.68 indicate that MTT is the most significant factor for the regression model of tensile strength, and factors MCC, T, and S have less and less significance, respectively.

Table XI: ANOVA for regression equation of TS

Source	DF	Adj SS	Adj MS	F-Value	P-Value
Regression	4	716.14	179.04	8.79	0.002
MCC	1	70.27	70.27	3.45	0.090
MTT	1	583.96	583.96	28.68	0.000
S	1	24.10	24.10	1.18	0.300
T	1	37.81	37.81	1.86	0.200
Error	11	223.97	20.36		
Total	15	940.11			

Table XII presents the significance of factors incorporated in the regression equation of the Young's modulus. Table XII clearly shows that regression P-value 0.066 suggests that the factors incorporated in the experimental setup are satisfactory for the linear model because factors with a P-value lesser than 0.05 show the most significant parameter that influences the regression equation. Additionally, the larger F-value shows the more significant factor that influences the regression response. Table XII exhibits that MCC P-value 0.025 and F-value 6.67 indicate that MCC is the most significant factor that affects the regression model of biocomposite young modulus, and factors MTT, S, and T have less and less significance, respectively.



Copyright and License Grant: CC By 4.0



Table XII: ANOVA for regression model of YM

Source	DF	Seq SS	Adj SS	Adj MS	F-Value	P-Value
Regression	4	1.97372	1.97372	0.49343	3.01	0.066
MCC	1	1.09278	1.09278	1.09278	6.67	0.025
MTT	1	0.50086	0.50086	0.50086	3.06	0.108
S	1	0.30381	0.30381	0.30381	1.85	0.200
T	1	0.07626	0.07626	0.07626	0.47	0.509
Error	11	1.80158	1.80158	0.16378		
Total	15	3.77529				

# I. Water Absorption and Density

Table XIII displays the water absorption and density of the developed biocomposite. Underwater absorption, as observed in Table XIII, the combination of MCC, MTT, and S addition highly influences the water absorption of PLA. The experimental setup of higher levels of MCC and S such as 6MCC/3MTT/30S/150T and 9MCC/0MTT/30S/125T, indicated higher water absorptions of 15.17 and 16.22 %, respectively. This is caused mainly because MCC and S have high water absorption trends [59]. Additionally, the water absorption rises with temperature due to the molecular processes. An increase in non-equilibrium vapor pressure at the interface leads to greater absorption of water molecules by the fiber. This phenomenon, associated with a reduction in solid-gas interfacial tension, enhances water absorption [60]. Under the density, the addition of MCC, MTT, and S slightly increases the density of PLA. In related studies, the addition of natural fiber (MTT and MCC) in PLA increases the density of PLA, this is probably due to the high densities of fillers [61].

Table XIII: Water absorption and density of biocomposite with S/N ratios

		Fact	ors			Responses				
S. N	MCC	MMT	S	Т	Water absorption (%)	S/N Ratio	Density (g/mm <sup>3</sup> )	S/N Ratio		
1	0	0	0	100	2.48	-7.91	0.0303	-30.371		
2	0	3	10	125	6.03	-15.60	0.0331	-29.617		
3	0	6	20	150	8.78	-18.87	0.0348	-29.164		
4	0	9	30	175	10.63	-20.53	0.0384	-28.311		

Received: July 2024; Revised: 29 November 2024; Accepted: 15 December 2024; Published: 23 December 2024

ISSN (E): 2959-3921 (P): 2959-393X

3

3

3

3

6

6

6

6

9

9

9

5

6

7

8

9

10

11

12

13

14

15

16



0

3

6

9

0

3

6

9

0

3

6

9

10

0

30

20

20

30

0

10

30

20

10

0



5.54

4.19

12.32

7.81

9.73

15.22

5.11

6.94

16.17

10.02

7.28

6.86

150

175

100

125

175

150

125

100

125

100

175

150

Copyright	and License	Grant:	CC By 4.0	6	•	

-14.87

-12.46

-21.81

-17.86

-19.76

-23.65

-14.17

-16.83

-24.17

-20.02

-17.24

-16.73

0.0371

0.0393

0.0415

Frant: CC By 4.0	@_ <b>①</b>
0.0331	-29.608
0.0342	-29.327
0.0332	-29.569
0.0362	-28.838
0.0364	-28.771
0.0376	-28.508
0.0353	-29.038
0.0381	-28.378
0.0362	-28.826

-28.609

-28.123

-27.639

# J. Probability Plot

The normal probability plot shown in Fig. 5 represents the comparison between the actual experimental results and the predicted values of water absorption and density. As clearly shown in Fig. 5 all the experimental data are under the interval of 95% confidence level.

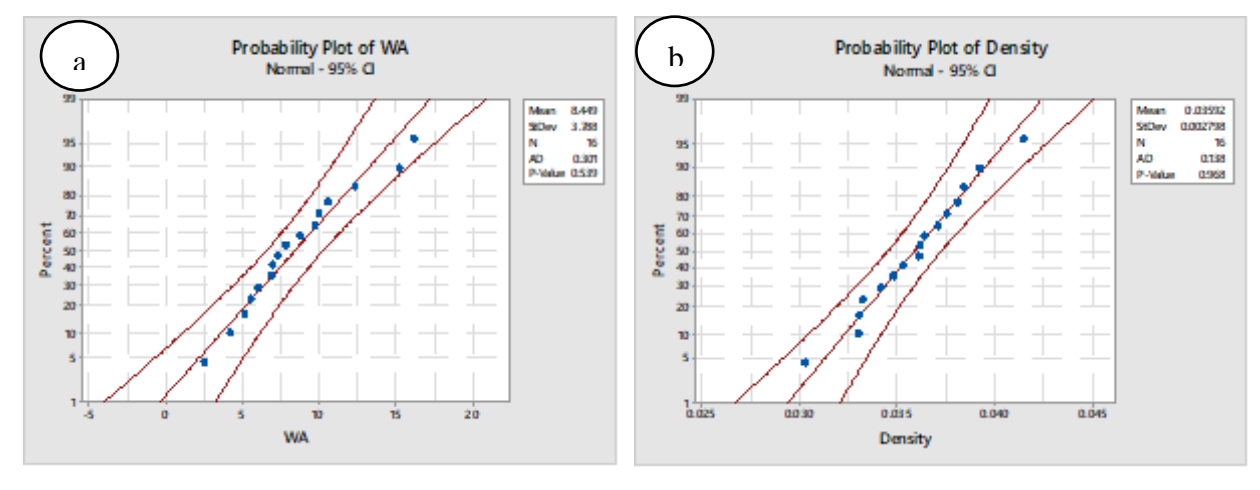


Fig. 5.: Probability plot for water absorption (a) and density (b) of developed biocomposite

As Table XIV and Table XV show, based on the S/N ratio result, it can be examined which factor has the highest influence on water absorption and density, respectively. The optimal water absorption factor of these controlled variables is investigated based on S/N ratios shown in Table XIV and Fig. 6 (a). The optimal factor for WA is at the combination of 0%MCC, 0%MTT, 0%S, and 150°C, and at this level, the WA is 2.42 %. The factors that highly affect water absorption are S and MCC, respectively. This is mainly due to a lot of hydroxyl (-OH) groups in these constituents [62]. The optimization of water absorption factors, based on the criterion that 'smaller is better,' indicates that lower levels of fillers and plasticizers



Copyright and License Grant: CC By 4.0



are most effective, as shown in Fig. 6(a). Table XV and Fig. 6(b) reveal the optimal factors for density, identified at 9MCC/9MTT/30S/175T. At this level, the density is determined to be 0.0427 g/mm<sup>3</sup>.

Table XIV: Response table for S/N ratios of water absorption (the smaller the better)

Level	MCC	MTT	S	T
1	-15.73	-16.68	-12.82	-16.65
2	-16.75	-17.94	-16.14	-17.96
3	-18.61	-18.03	-19.13	-18.53
4	-19.55	-17.99	-22.54	-17.50
Delta	3.81	1.35	9.72	1.89
Rank	2	4	1	3

Table XV: Response table for S/N ratios of density (the larger the better)

Level	MCC	MTT	S	T
1	-29.37	-29.39	-29.09	-29.23
2	-29.34	-29.02	-28.93	-29.08
3	-28.67	-28.97	-28.85	-28.73
4	-28.30	-28.29	-28.80	-28.63
Delta	1.07	1.10	0.29	0.60
Rank	2	1	4	3

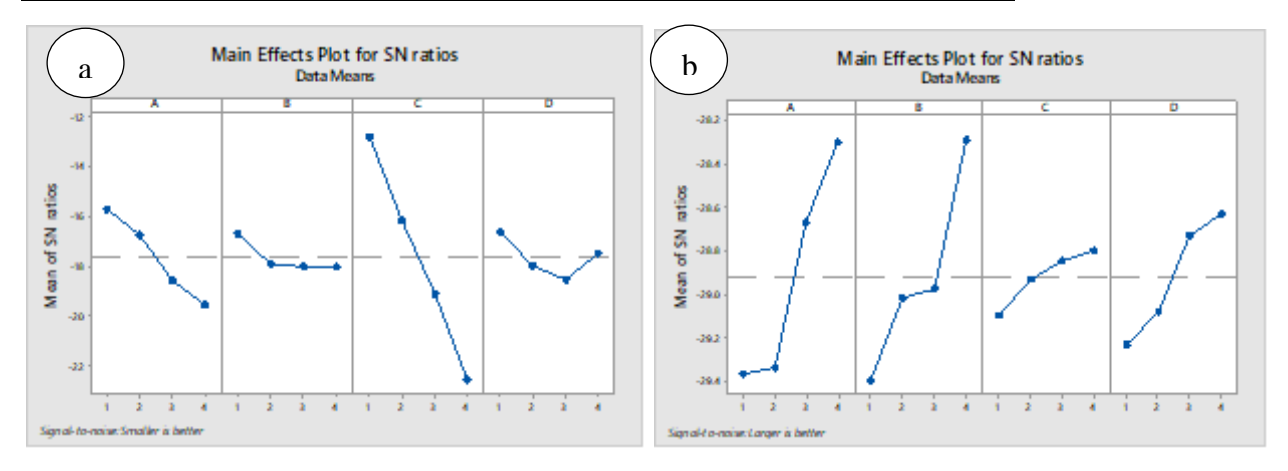
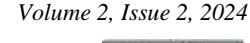


Fig. 6.: Main effect plot for S/N ratios of water absorption (a) and density (b)





# K. Regression Analysis of Correlation between Significant Factors and Water Absorption

The correlation between significant factors and the water absorption of developed biocomposite is established through linear regression. The regression equation for the water absorption is shown as follows;

$$WA = -1.33 + 1.110 MCC - 0.175 MTT + 2.941 S + 0.037 T$$
 (12)

Density = 
$$0.02551 + 0.001581 \text{ MCC} + 0.001381 \text{ MTT} + 0.000332 \text{ S} + 0.000868 \text{ T}$$
 (13)

ANOVA for regression model of water absorption and density of developed biocomposite

The significance of factors incorporated in the regression equation of water absorption and density is given in ANOVA Tables XVI and XVII, respectively. The regression P-value (0.000) suggests that a statistically significant relationship occurs between factors and responses in the experimental design, and factors with a P-value lesser than 0.05 show the most significant element that influences the regression equation. Table 16 presents that S and MCC are the most significant factors for the regression model of water absorption. Table XVII presents that MCC, MTT, and T are the most significant factors for the regression model of density.

Table XVI: ANOVA for regression model of water absorption

Source	DF	Seq SS	Adj SS	Adj MS	F-Value	P-Value
Regression	4	198.222	198.222	49.555	32.11	0.000
MCC	1	24.635	24.635	24.635	15.96	0.002
MTT	1	0.611	0.611	0.611	0.40	0.542
S	1	172.948	172.948	172.948	112.06	0.000
T	1	0.027	0.027	0.027	0.02	0.897
Error	11	16.977	16.977	1.543		
Total	15	215.199				

Table XVII: Analysis of variance for regression model of density

Source	DF	Seq SS	Adj SS	Adj MS	F-Value	P-Value
Regression	4	0.000105	0.000105	0.000026	24.09	0.000
MCC	1	0.000050	0.000050	0.000050	45.73	0.000
MTT	1	0.000038	0.000038	0.000038	34.86	0.000
S	1	0.000002	0.000002	0.000002	2.02	0.183
T	1	0.000015	0.000015	0.000015	13.76	0.003
Error	11	0.000012	0.000012	0.000001		
Total	15	0.000117				

Copyright and License Grant: CC By 4.0



DOI: https://doi.org/10.59122/174CFC14

ISSN (E): 2959-3921

(P): 2959-393X



# IV. Conclusion

This study investigated the optimization of PLA-based biocomposite material development using the application of Taguchi and regression model analysis. The fillers namely MCC and MTT, and Plasticizer S at various weight % loadings were considered with different T. Based on the experimental studies' results, the following conclusions could be made:-

- 1. The optimal factors in flexural strength are at 3%MCC, 9%MTT, 20%S, and 175°C. At these levels, FS is 96.5 MPa whereas for flexural modulus, 6%MCC, 9%MTT, 20%S, and 175°C. At these control factors, FM is 9.8 GPa.
- 2. The optimal factors in tensile strength are at 9%MCC, 9%MTT, 10%S, and 175°C. At these levels, TS is 85.2 MPa whereas for tensile modulus, 6%MCC, 9%MTT, 0%S, and 150°C. At these experimental runs, YM is 4.22 GPa
- 3. The optimal factors in hardness value are at 6%MCC, 9%MTT, 10%S, and 175°C. At these levels, HV is 138.2.
- 4. The optimal factors in water absorption are at 0%MCC, 0%MTT, 0%S, and 150°C. At these experimental runs, WA is 2.42% whereas for density, 9%MCC, 9%MTT, 30%S, and 175°C. At this experimental setup, D is 0.0427g/mm<sup>3</sup>.

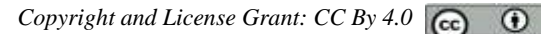
Finally, it was concluded that the inclusion of MCC, MTT, and S highly influences the performance characteristics of PLA. The PLA-based biocomposite developed using this approach is expected to be utilized for lightweight load-carrying applications

#### References

- O. S. Onyekwere, M. H. Oladeinde, and R. O. Edokpia, "Multi-Response optimization of bamboo fiber reinforced unsaturated polyester composites using hybrid Taguchi-grey relational analysis method," *Journal of Industrial and Production Engineering*, vol. 38, no. 2, pp. 98-107, 2021. DOI: 10.1080/21681015.2020.1848933.
- 2. T. Manu, A. R. Nazmi, B. Shahri, N. Emerson, and T. Huber, "Biocomposites: A Review of Materials and Perception," *Materials Today Communications*, vol. 31, art. no. 103308, 2022. DOI: 10.1016/j.mtcomm.2022.103308.
- M. Belkheir, M. Boutaleb, A. Mokaddem, and B. Doumi, "Predicting the effect of coconut natural fibers for improving the performance of biocomposite materials based on the poly (methyl methacrylate)-PMMA polymer for engineering applications," *Polymer Bulletin*, Issue 2, 2023. DOI: 10.1007/s00289-020-03183-7.

ISSN (E): 2959-3921 (P): 2959-393X

DOI: https://doi.org/10.59122/174CFC14





Volume 2, Issue 2, 2024

- 4. A. A. Mohammed, A. A. B. Omran, Z. Hasan, R. Ilyas, and S. Sapuan, "Wheat biocomposite extraction, structure, properties and characterization: a review," Polymers, vol. 13, no. 21, p. 3624, 2021. DOI: 10.3390/polym13213624.
- 5. V. Naik and M. Kumar, "A review on natural fiber composite material in automotive applications," *Engineered Science*, vol. 18, pp. 1-10, 2021. DOI: 10.30919/es8d589.
- 6. S. Bhambure and A. Rao, "Experimental investigation of impact strength of kenaf fiber reinforced polyester composite," Materials Today: Proceedings, vol. 46, Part 2, pp. 1134-1138, 2021. DOI: 10.1016/j.matpr.2021.02.055.
- 7. M. R. Ketabchi, M. Khalid, C. T. Ratnam, S. Manickam, R. Walvekar, and M. E. Hoque, "Sonosynthesis of cellulose nanoparticles (CNP) from kenaf fiber: effects of processing parameters," Fibers and Polymers, vol. 17, no. 9, pp. 1352-1358, 2016. DOI: 10.1007/s12221-016-5813-4.
- 8. A. El Amri, A. Ouass, Z. Wardighi, F. Z. Bouhassane, A. Zarrouk, A. Habsaoui, et al., "Extraction and characterization of cellulosic nanocrystals from stems of the reed plant large-leaved cattail (Typha latifolia)," Materials Today: Proceedings, 2022. DOI: 10.1016/j.matpr.2022.08.408
- 9. S. H. Sung, Y. Chang, and J. Han, "Development of polylactic acid nanocomposite films reinforced with cellulose nanocrystals derived from coffee silverskin," Carbohydrate Polymers, vol. 169, pp. 495-503, 2017. DOI: 10.1016/j.carbpol.2017.04.037.
- 10. A. Khenblouche, D. Bechki, M. Gouamid, K. Charradi, L. Segni, M. Hadjadj, and S. Boughali, "Extraction and characterization of cellulose microfibers from Retama raetam stems," Polímeros, vol. 29, no. 1, 2019. DOI: 10.1590/0104-1428.05218.
- 11. J. I. Morán, V. A. Alvarez, V. P. Cyras, and A. Vázquez, "Extraction of cellulose and preparation of nanocellulose from sisal fibers," Cellulose, vol. 15, no. 1, pp. 149-159, 2008. DOI: 10.1007/s10570-007-9145-9.
- 12. A. Kausar, S. T. Zohra, S. Ijaz, M. Iqbal, J. Iqbal, I. Bibi, S. Nouren, N. El Messaoudi, and A. Nazir, "Cellulose-based materials and their adsorptive removal efficiency for dyes: A review," International Macromolecules, 224, **Journal** of Biological vol. 1337-1355, 2023. DOI: pp. 10.1016/j.ijbiomac.2022.10.220.
- 13. M. Szymańska-Chargot, J. Cieśla, P. Pekala, P. M. Pieczywek, W. Oleszek, M. Żyła, Z. Szkopek, and A. Zdunek, "The Influence of High-Intensity Ultrasonication on Properties of Cellulose Produced from the Hop Stems, the Byproduct of the Hop Cones Production," *Molecules*, vol. 27, no. 9, p. 2624, 2022. DOI: 10.3390/molecules27092624.

Copyright and License Grant: CC By 4.0 📵



Volume 2, Issue 2, 2024

- 14. N. Reddy and Y. Yang, "Extraction and characterization of natural cellulose fibers from common milkweed stems," *Polymer Engineering & Science*, vol. 49, no. 11, pp. 2212-2217, 2009. DOI: 10.1002/pen.21469.
- N. M. Zeleke, D. K. Sinha, and G. A. Mengesha, "Chemical Composition and Extraction of Micro Crystalline Cellulose from Outer Skin Isolated Coffee Husk," *Advances in Materials Science and Engineering*, vol. 2022, Article ID 7163359, 2022. DOI: 10.1155/2022/7163359.
- H. S. Hafid, F. N. Omar, J. Zhu, and M. Wakisaka, "Enhanced crystallinity and thermal properties of cellulose from rice husk using acid hydrolysis treatment," *Carbohydrate Polymers*, vol. 260, Article ID 117789, 2021. DOI: 10.1016/j.carbpol.2021.117789.
- 17. G. Manimekalai, S. Kavitha, D. Divya, S. Indran, and J. Binoj, "Characterization of enzyme treated cellulosic stem fiber from Cissus quadrangularis plant: an exploratory investigation," *Current Research in Green and Sustainable Chemistry*, vol. 4, Article ID 100162, 2021. DOI: 10.1016/j.crgsc.2021.100162.
- D. Trache, M. H. Hussin, C. T. H. Chuin, S. Sabar, M. N. Fazita, O. F. Taiwo, et al., "Microcrystalline cellulose: Isolation, characterization and bio-composites application—A review," *International Journal of Biological Macromolecules*, vol. 93(Pt A), pp. 789-804, 2016. DOI: 10.1016/j.ijbiomac.2016.09.056.
- D. Haldar and M. K. Purkait, "Micro and nanocrystalline cellulose derivatives of lignocellulosic biomass: A review on synthesis, applications, and advancements," *Carbohydrate Polymers*, vol. 250, Article ID 116937, 2020. DOI: <u>10.1016/j.carbpol.2020.116937</u>.
- 20. H. S. Shekar and M. Ramachandra, "Green composites: a review," *Materials Today: Proceedings*, vol. 5, no. 1, Part 3, pp. 2518-2526, 2018. DOI: 10.1016/j.matpr.2017.11.387.
- 21. M. Zwawi, "A Review on Natural Fiber Bio-Composites, Surface Modifications and Applications," *Molecules*, vol. 26, no. 2, p. 404, 2021. DOI: <u>10.3390/molecules26020404</u>.
- 22. B. Debnath, D. Haldar, and M. K. Purkait, "A critical review on the techniques used for the synthesis and applications of crystalline cellulose derived from agricultural wastes and forest residues," *Carbohydrate Polymers*, vol. 273, Article ID 118537, 2021. DOI: 10.1016/j.carbpol.2021.118537.
- 23. G. Wang, D. Zhang, B. Li, G. Wan, G. Zhao, and A. Zhang, "Strong and thermal-resistance glass fiber-reinforced polylactic acid (PLA) composites enabled by heat treatment," *International Journal of Biological Macromolecules*, vol. 129, pp. 448-459, 2019. DOI: 10.1016/j.ijbiomac.2019.01.123.

Volume 2, Issue 2, 2024

DOI: https://doi.org/10.59122/174CFC14

(P): 2959-393X

ISSN (E): 2959-3921



Copyright and License Grant: CC By 4.0



- 24. K. Pongtanayut, C. Thongpin, and O. Santawitee, "The effect of rubber on morphology, thermal properties and mechanical properties of PLA/NR and PLA/ENR blends," *Energy Procedia*, vol. 34, pp. 888-897, 2013. DOI: 10.1016/j.egypro.2013.06.826.
- 25. A. Greco and F. Ferrari, "Thermal behavior of PLA plasticized by commercial and cardanol-derived plasticizers and the effect on the mechanical properties," *Journal of Thermal Analysis and Calorimetry*, vol. 146, no. 1, pp. 131-141, 2021. DOI: 10.1007/s10973-020-10403-9.
- M. Puthumana, P. Santhana Gopala Krishnan, and S. K. Nayak, "Chemical modifications of PLA through copolymerization," *International Journal of Polymer Analysis and Characterization*, vol. 25, no. 8, pp. 634-648, 2020. DOI: 10.1080/1023666X.2020.1830650.
- 27. K. Martinez Villadiego, M. J. Arias Tapia, J. Useche, and D. Escobar Macías, "Thermoplastic starch (TPS)/polylactic acid (PLA) blending methodologies: a review," *Journal of Polymers and the Environment*, vol. 30, no. 1, pp. 75-91, 2022. DOI: 10.1007/s10924-021-02207-1.
- 28. G. Rajeshkumar, S. A. Seshadri, G. Devnani, M. Sanjay, S. Siengchin, J. P. Maran, et al., "Environment-friendly, renewable and sustainable poly lactic acid (PLA) based natural fiber reinforced composites—A comprehensive review," *Journal of Cleaner Production*, vol. 310, Article ID 127483, 2021. DOI: 10.1016/j.jclepro.2021.127483.
- 29. R. Guo, Z. Ren, H. Bi, M. Xu, and L. Cai, "Electrical and thermal conductivity of polylactic acid (PLA)-based biocomposites by incorporation of nano-graphite fabricated with fused deposition modeling," *Polymers*, vol. 11, no. 3, p. 549, 2019. DOI: 10.3390/polym11030549.
- 30. M. Bocqué, C. Voirin, V. Lapinte, S. Caillol, and J.-J. Robin, "Petro-based and bio-based plasticizers: chemical structures to plasticizing properties," *Journal of Polymer Science Part A: Polymer Chemistry*, vol. 54, no. 1, pp. 11-33, 2016. DOI: 10.1002/pola.27917.
- 31. A. Alhanish and M. Abu Ghalia, "Developments of biobased plasticizers for compostable polymers in the green packaging applications: A review," *Biotechnology Progress*, vol. 37, no. 6, p. e3210, 2021. DOI: 10.1002/btpr.3210.
- 32. M. G. A. Vieira, M. A. da Silva, L. O. dos Santos, and M. M. Beppu, "Natural-based plasticizers and biopolymer films: A review," *European Polymer Journal*, vol. 47, no. 3, pp. 254-263, 2011. DOI: 10.1016/j.eurpolymj.2010.12.011.
- 33. M. Shahmaleki, F. Beigmohammadi, and F. Movahedi, "Cellulose-Reinforced Starch Biocomposite: Optimization of the Effects of Filler and Various Plasticizers using Design–Expert Method," *Stärke*, vol. 73, no. 9-10, Article ID 2000028, 2021. DOI: 10.1002/star.202000028.

ISSN (E): 2959-3921 (P): 2959-393X

DOI: https://doi.org/10.59122/174CFC14



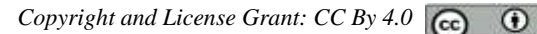


Volume 2, Issue 2, 2024

- 34. M. Liu, Y. Zhou, Y. Zhang, C. Yu, and S. Cao, "Physicochemical, mechanical and thermal properties of chitosan films with and without sorbitol," International Journal of Biological Macromolecules, vol. 70, pp. 340-346, 2014. DOI: 10.1016/j.ijbiomac.2014.06.050.
- 35. X. Ma, C. Qiao, J. Zhang, and J. Xu, "Effect of sorbitol content on microstructure and thermal properties of chitosan films," International Journal of Biological Macromolecules, vol. 119, pp. 1294-1297, 2018. DOI: 10.1016/j.ijbiomac.2018.08.034.
- 36. R. Rafiee and R. Shahzadi, "Mechanical properties of nanoclay and nanoclay reinforced polymers: a review," Polymer Composites, vol. 40, no. 2, pp. 431-445, 2019. DOI: 10.1002/pc.24747.
- 37. M. S. Nazir, M. H. Mohamad Kassim, L. Mohapatra, M. A. Gilani, M. R. Raza, and K. Majeed, "Characteristic properties of nano clays and characterization of nanoparticles and nanocomposites," in Nanoclay Reinforced Polymer Composites: Nanocomposites and bionanocomposites, M. Jawaid, A. el K. Qaiss and R. Bouhfid, Eds. Singapore: Springer Science Business Media Singapore, 2016, pp. 35-55. DOI: 10.1016/B978-0-323-39390-0.00002-4.
- 38. A. U. R. Shah, M. Prabhakar, and J.-I. Song, "Current advances in the fire retardancy of natural fiber and bio-based composites-A review," International Journal of Precision Engineering and Manufacturing-Green Technology, vol. 4, no. 2, pp. 247-262, 2017. DOI: 10.1007/s40684-017-0029-1.
- 39. G. Rajeshkumar, S. A. Seshadri, S. Ramakrishnan, M. Sanjay, S. Siengchin, and K. Nagaraja, "A comprehensive review on natural fiber/nano-clay reinforced hybrid polymeric composites: Materials and technologies," Polymer Composites, vol. 42, no. 8, pp. 3687-3701, 2021. DOI: 10.1002/pc.26125.
- 40. D. Rajamani, E. Balasubramanian, G. Dilli Babu, and K. Ananthakumar, "Experimental investigations on high precision abrasive waterjet cutting of natural fiber reinforced nano clay filled green composites," Journal of Industrial Textiles, vol. 51, no. 3, pp. 3786-3810, 2022. DOI: 10.1177/15280837211057684.
- 41. S. N. Shuvo, K. M. Shorowordi, and M. A. Islam, "Effect of nanoclay on jute fiber reinforced polyester composites," International Journal of Advanced Engineering and Nano Technology, vol. 2, no. 8, pp. 20-26, 2015. DOI: 10.2139/ssrn.2668083
- 42. J. Ferreira, L. Borrego, J. Costa, and C. Capela, "Fatigue behavior of nanoclay reinforced epoxy resin composites," Composites Part *B*: Engineering, 52, 2013. vol. pp. 286-291, DOI: 10.1016/j.compositesb.2013.04.003.

ISSN (E): 2959-3921 (P): 2959-393X

DOI: https://doi.org/10.59122/174CFC14





- 43. T. K. A. Bui, S. V. Hoa, T. D. Ngo, and M. T. T. That, "Effect of addition of nanoclays on properties of vinyl ester," in Design, Manufacturing, and Applications of Composites: Proceedings of the Eighth Joint Canada-Japan Workshop on Composites, 2010. DOI: 10.1007/978-1-4419-0733-5\_10.
- 44. A. S. Alex, R. Rajeev, K. Krishnaraj, N. Sreenivas, S. Manu, C. Gouri, et al., "Thermal protection characteristics of polydimethylsiloxane-organoclay nanocomposite," Polymer Degradation and Stability, vol. 144, pp. 281-291, 2017. DOI: 10.1016/j.polymdegradstab.2017.08.026.
- 45. R. Kurda, J. de Brito, and J. D. Silvestre, "CONCRETop-A multi-criteria decision method for concrete optimization," Environmental Impact Assessment Review, vol. 74, pp. 73-85, 2019. DOI: 10.1016/j.eiar.2018.10.006.
- 46. H. Kus, G. Basar, and F. Kahraman, "Modeling and optimization for fly ash reinforced bronze-based composite materials using multi-objective Taguchi technique and regression analysis," Industrial Lubrication and Tribology, vol. 70, no. 7, pp. 1187-1192, 2018. DOI: 10.1108/ILT-02-2018-0059.
- 47. D. Jena, R. C. Mohapatra, and A. K. Das, "Optimization of mechanical characteristics of rice husk particle reinforced polymer composites using Taguchi Experimental Technique," World Scientific News, vol. 124, no. 2, pp. 155-170, 2019. DOI: 10.1108/ILT-02-2018-0059.
- 48. O. Kelleci, D. Aydemir, E. Altuntas, A. Oztel, R. Kurt, H. Yorur, et al., "Thermoplastic composites of polypropylene/biopolymer blends and wood flour: Parameter optimization with fuzzy-grey relational analysis," *Polymers* and Polymer Composites, vol. 30. 2022. DOI: 10.1177/09673911221100968.
- 49. C. C. Ihueze, M. K. Achike, and C. Okafor, "Optimal Performance Characteristics and Reinforcement Combinations of Coconut Fibre Reinforced High-Density Polyethylene (HDPE) Polymer Matrixes," SSRN, 2015. DOI: 10.2139/ssrn.2902118.
- 50. S. Budin, N. Maiden, M. Koay, D. Ibrahim, and H. Yusoff, "A comparison study on mechanical properties of virgin and recycled polylactic acid (PLA)," in Journal of Physics: Conference Series, 2019. DOI: 10.1088/1742-6596/1372/1/012002.
- 51. D. Chandramohan and A. J. P. Kumar, "Experimental data on the properties of natural fiber particle reinforced polymer composite material," Data in Brief, vol. 13, pp. 460-468, 2017. DOI: 10.1016/j.dib.2017.06.045
- 52. R. Ramasubbu and S. Madasamy, "Fabrication of automobile component using hybrid natural fiber reinforced polymer composite," Journal of Natural Fibers, vol. 19, no. 2, pp. 736-746, 2022. DOI: 10.1080/15440478.2020.1761927.

Volume 2, Issue 2, 2024

ISSN (E): 2959-3921

(P): 2959-393X DOI: https://doi.org/10.59122/174CFC14

Copyright and License Grant: CC By 4.0



- 53. M. Kandasamy, A. Chandravathanan, and M. Mohan, "An investigation on tribological and mechanical properties of areca nut and BBorassus flabellifer fiber hybrid composite reinforced with epoxy," *Ind Eng J*, vol. 13, no. 2, 2020. DOI: 10.26488/iej.13.2.1217.
- 54. S. Kormin, F. Kormin, and M. Beg, "Effect of plasticizer on physical and mechanical properties of LDPE/sago starch blend," in Journal of Physics: Conference Series, 2019. DOI: 10.1088/1742-6596/1150/1/012032.
- 55. B. Dogu and C. Kaynak, "Behavior of polylactide/microcrystalline cellulose biocomposites: effects of filler content and interfacial compatibilization," Cellulose, vol. 23, pp. 611-622, 2016. DOI: 10.1007/s10570-015-0839-0.
- 56. R. Arjmandi, A. Hassan, M. K. Mohamad Haafiz, and Z. Zakaria, "Effects of micro- and nanocellulose on tensile and morphological properties of montmorillonite nano clay reinforced polylactic acid nanocomposites," in Nanoclay Reinforced Polymer Composites: Natural Fibre/Nanoclay Hybrid Composites, M. Jawaid, A. Qaiss, and R. Bouhfid, Eds. 2016, pp. 103-125. DOI: 10.1007/978-981-10-0950-1\_5.
- 57. M. Arief, A. Mubarak, and D. Pujiastuti, "The concentration of sorbitol on bioplastic cellulose based carrageenan waste on biodegradability and mechanical properties bioplastic," in IOP Conference Series: Earth and Environmental Science, vol. 679, no. 1, Article ID 012013, 2021. DOI: 10.1088/1755-1315/679/1/012013.
- 58. H. Tian, D. Liu, Y. Yao, S. Ma, X. Zhang, and A. Xiang, "Effect of sorbitol plasticizer on the structure and properties of melt processed polyvinyl alcohol films," Journal of Food Science, vol. 82, no. 12, pp. 2926-2932, 2017. DOI: 10.1111/1750-3841.13950.
- 59. O. M. Abel, S. Chinelo, and R. Chidioka, "Enhancing cassava peels starch as feedstock for biodegradable plastic," J Mater Environ Sci, vol. 12, no. 2, pp. 169-182, 2021.
- 60. J. Songok, P. Salminen, and M. Toivakka, "Temperature effects on dynamic water absorption into paper," Journal of Colloid and Interface Science, vol. 418, pp. 373-377, 2014. DOI: 10.1016/j.jcis.2013.12.003.
- 61. K. Olonisakin, R. Li, S. He, W. Aishi, F. Lifei, C. Mengting, et al., "Flame rating of nano clay/MCC/PLA composites with both reinforced strength and toughness," Journal of Polymer Research, vol. 29, no. 12, 2022. DOI: 10.1007/s10965-022-03110-1.
- 62. G. Lupidi, G. Pastore, E. Marcantoni, and S. Gabrielli, "Recent Developments in Chemical Derivatization of Microcrystalline Cellulose (MCC): Pre-Treatments, Functionalization, and Applications," *Molecules*, vol. 28, no. 5, 2023. DOI: 10.3390/molecules28052009

Copyright and License Grant: CC By 4.0 (a)



## Analyzing Mechanical Property and the Corresponding Power Output of **Bamboo Plant for the Construction of Vertical Axis Wind Turbine Blade**

Elias Alemu<sup>1\*</sup> and Degnet Abose<sup>2</sup>

<sup>1,2</sup>Arba Minch Institute of Technology, Arba Minch University, Ethiopia \*Corresponding Author's Email: eli alemu@yahoo.com

#### **Abstract**

Ethiopia has the largest bamboo plant coverage in Africa and has the third-largest wind power potential in Africa. These two factors inspired us to conduct this research. Use of Bamboo plant in Ethiopia is limited to a few common utilizations such as for furniture and civil construction. These applications resulted from less understanding of mechanical properties of the plant. Hence, this study aimed to determine the mechanical properties of bamboo, particularly tensile and fatigue strength. Mechanical properties were analyzed on lowland (Oxytenantheria abyssinica) and highland (Yushania alpina) untreated bamboo. Tensile test specimens were prepared from both species, and the test was conducted with calibrated universal testing machines (UTM). The expected outcome was to decide whether or not bamboo plant mechanical properties qualify for the construction of small-scale wind turbine blades. A total of 30 tensile specimens were prepared to conduct the test. Fatigue stress was calculated using the relationship between the tensile stress as various literatures revealed that fatigue strength equals 40 % to 60 % of the tensile stress. Experimental test output shows that lowland bamboo tensile strength is 178.1 Mpa while the corresponding fatigue strength is 71.24 Mpa. For highland bamboo, the tensile and the fatigue stresses are 122 Mpa and 48.8 Mpa respectively. This result confirmed that lowland bamboo has better strength compared to highland bamboo. This is because lowland bamboo is denser in fiber or microstructure than highland bamboo. This ensures that lowland bamboo has a larger load-bearing capacity. Fatigue stress (cyclic load) is the predominant stress for the failure of a structure when an intermittent load is subjected to the specific structure even if the exerted stress is below the yield stress of the component. Findings ensured that the bamboo plant has adequate strength for the construction of small-scale wind turbine blade production. In Ethiopia, the estimated wind power potential is nearly one Gigawatt, and the installed capacity is only 404 MW. Small-scale wind turbine installation was not offered sufficient attention. Integrating these two potential resources (bamboo as raw material and wind resources) will enhance and contribute to small-scale energy production.

Keywords: Fatigue Strength, Highland Bamboo, Lowland Bamboo, Tensile Strength

DOI: https://doi.org/10.59122/174CFC17

Volume 2, Issue 2, 2024

Copyright and License Grant: CC By 4.0 (a)





### I. Introduction

Ethiopian Standard Agency article ES-ES 6416:2021 defined Bamboo as: "tropical or semitropical grass having a tree-like character, usually hollow culms growing tall, enclosing lignin and having absence of secondary growth [1]. More than 1500 species of bamboo plants have been found worldwide [2]. In Ethiopia, two types of bamboo species are known as lowland (Oxytenantheria Abyssinia) and highland (Yushania alpina) [3]. In Ethiopia, lowland bamboo (nearly solid) and highland bamboo (hollow) cover nearly 1.4 million hectares [3, 4].

Lowland bamboo commonly grows in a warm and humid environment. This promotes rapid growth of the bamboo and in turn, it allows dense microstructures or fibers of the bamboo with cell thickness microstructure: For example, lowland bamboo in the Benishangul Gumuz region. On the other hand, highland bamboo grows in cooler and highland altitude environments. This permits slow growth of the cell wall with higher thickness as compared to lowland bamboo. This ensures that the structure has a higher thickness which carries more load than the thinner one. Therefore, bamboo growing in the lowland has better density which implies lowland bamboo has better mechanical properties than highland bamboo. In addition, it was observed from the experimental outcome, and it was compared with other plants [4].

#### Bamboo has the following amazing properties:

- It ranks first in absorbing a large amount of carbon dioxide and expelling out a large amount of oxygen, Bamboo is a crucial element in the balance of oxygen and carbon dioxide in the atmosphere. Bamboo releases 35% more oxygen than an equivalent stand of trees. Because of this, planting bamboo is a great way of reducing carbon footprint and helping fight global warming.
- It has excellent mechanical properties compared to other wooden plants.
- It has a fast-growing nature, growing 47.6 inches (1.2 meters) in 24 hours.

Research was conducted on locally available bamboo focusing on tensile, bending, and compressive stress by neglecting fatigue strength [5],[6]. The reason is that the common application of bamboo is for the construction of houses and furniture. In these situations, structures are naturally subjected to static loads. However, one can manufacture a component that is subjected to variable or intermittent loads such as wind turbine blades. In this case, it is essential to conduct and analyze the fatigue strength of the bamboo to determine its load and carrying capacity.

Bamboo in this report implies chemically untreated or not reinforced composite bamboo or not a single (bundle fiber), it is just natural bamboo. Locally available bamboo plant tests were conducted by considering its natural cylindrical geometry as specimens, without modifying shapes (Fig. 1).

Copyright and License Grant: CC By 4.0 (a)



The bamboo plant samples aged 3 to 4 years were collected from three different regions of the country, Benishangul Gumuz region (Assosa), Sidama Region (Arbegona), and Southern region (Chencha). This research work is specifically focused on preparing a standard tensile specimen as shown in Fig. 2 and conducting a tensile test followed by the corresponding fatigue stress using the two-stress relationship.

The middle culm of the bamboo was selected since it has a relatively better tensile strength as compared with the bottom and top part of the stem [7].

Specimens were prepared by splitting the bamboo into pieces and several numbers specimens were manufactured. The rough external surface of each of the specimens was smoothed by filing or rubbing with the help of various tools like file, sandpaper, or other similar tools. These specimens were not treated by chemical substances such as boric acid, hydrochloric acid varnish, and so on, which is common in treated bamboo.



Fig. 1.: Collected sample (highland) photo of bamboo-location Arbegona

Most research works supported by experimental tests and analysis were focused on the tensile, compressive, and bending stress of bamboo, even by considering the natural bamboo shape as a specimen. This ensures that tests did not consider how bamboo structures respond when it is subjected to impact or fluctuating loads. For example, if a structure is subjected to such types of loads, it will fail with a stess magnitude even below the yielding stress [8]. As a result, the component failure is early before the expected lifetime. This ensured that the effect of the corresponding fatigue test was neglected.

Volume 2, Issue 2, 2024

Copyright and License Grant: CC By 4.0



**DOI:** https://doi.org/10.59122/174CFC17

#### II. Materials and Methods

#### A. Introduction

(P): 2959-393X

The two species of bamboo were collected from different regions of Ethiopia which are potential sites such as Benishagul Gumuz (Assosa), Sidama Region (Arbegona), and Southern Region (Chencha). After preparing the standard tensile specimens, tests were performed using a Calibrated Universal Tensile Testing Machine at Addis Ababa Science and Technology University. Subsequently, data are systematically recorded and organized - scientifically for further analysis. Experimental test results were supported by graphs and tables to explore research outcomes.

#### **B.** Materials

1) Sample Preparation: 30 (thirty) Tensile test specimens were prepared with standard shapes and dimensions as noted in an international standard on ISO 22156 and [9],[10]. This standard recommends the suitable range of size and shape of the specimens for the tensile test of bamboo as indicated in Fig 2.

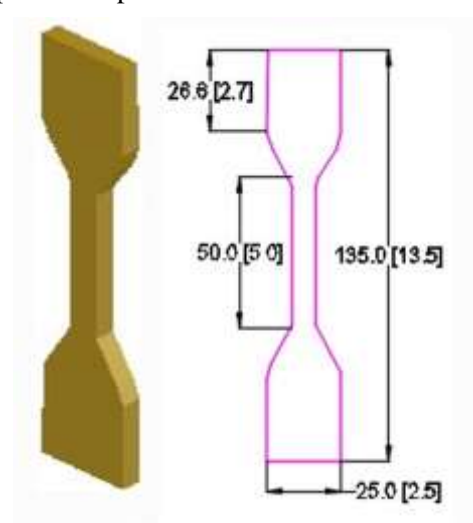


Fig.2.: Tensile test specimens with thickness = 4mm

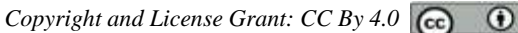
2) Specimen Preparation steps: To obtain accurate and irreproducible results, specimens were carefully prepared. Naturally, bamboo plants have different fiber distributions throughout their structure. For instance, its density or thickness increases as we go from the interior to the external surface. In addition, its mechanical property varies from the bottom to the top part of the culm. These factors were taken into account during the specimen preparation.

The following procedures were implemented for both species step-by-step to prepare the specimens.

*a)* Selection of Bamboo Culm: Bamboo culminating ages 3 to 4 years were selected. Too young culms have less strength while the aged ones also reduce their strength by propagating and cracking during testing.

Volume 2, Issue 2, 2024

DOI: https://doi.org/10.59122/174CFC17





- b) Cleaning the Bamboo Culm: Remove outer sheath (covering): The outermost shell of the bamboo cover was removed to expose smooth surfaces. In addition, file or remove any branches, knots, nodes, and surface imperfections.
- c) Cutting the Bamboo culm: cutting should be along the longitudinal cross-section of the fibers parallel to the applied load's direction. From the cylindrical bamboo culm, a rectangular cross-section was cut out with appropriate length and thickness. The length of the specimen should be sufficient to accommodate the elongation and failure length.
- d) Shaping the Specimen: using an appropriate tool sandpaper or file, rub off the surface of the specimen to avoid any irregularities or roughness. Finally, the required shape of the specimen was cut out according to the dimensions given in Fig. 2. Uneven surfaces are cases of stress concentration which mislead the accuracy of the results. The length of the specimens' thickness should be uniform throughout and consistent to overcome uneven load distribution.
- e) locating the grip region. During the griping of the specimen on the tensile testing machine, we have to control premature failure or slippage. So that the ends of the specimens were flattened and free from any notching.
- f) Mark the gauge length: the portion of the specimens between the gripping surfaces where the elongation of the specimens was measured. Here the gauge length is 50 mm,
- g) Check Uniformity: Finally, before conducting the test, such as dimensions, surface finish, straightness, and uniformity were checked to proceed to the next test setup.

#### C. Equipment

The experiment was conducted using the universal tensile testing machine, typically named as "WOW 100S Computer Controlled Electromechanical Universal Testing Machine". This UTM including its equipment was calibrated by conducting all significant tests, while outputs are recognized within the ISO ranges. In addition, the result generated during the experiment is partly included in this paper.

#### D. Test Procedures

The tensile test was managed by considering some of the important steps listed below.

The specimen was gripped properly between the jaws of the machine at the marked points.

- Tighten the jaws slowly and firmly.
- Ensured that the specimen was aligned between the top and the bottom jaws. This helps us to avoid any transversal loads on the specimens.



Copyright and License Grant: CC By 4.0 (a)



• Start the machine with a constant load rate. In our test, the speed rate of the machine was adjusted to 0.01 mm/s [9],[11].

Five best and most feasible reproducible test results were selected as indicated in this report. The rest of them have almost similar trend output and few of them show inaccurate output as a result of error during sample preparation and fixing on the UTM.

#### III. Results

Finally, tensile test results of two highland bamboos (Chencha and Arbegona) and three lowland bamboos from Assossa tensile are presented. As indicated in Fig. 3 and 4, selected test result data have a similar trend compared with other bamboo or fiberglass experimental outcomes.







(a) Lowland (solid) - Assosa (b) Highland (hollow) - Arbegona (c) Highland (hollow) - Chencha

Fig. 3.: Specimens before the test was conducted





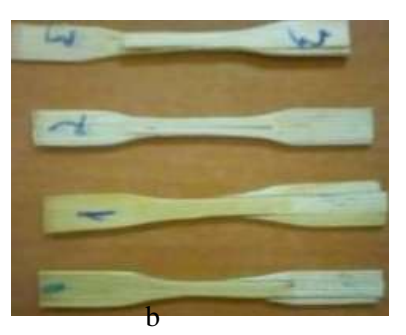


Fig. 4.: a) Conducting of the tensile testing (a) and the corresponding fractured specimens (b)

#### A. Result of the experimental Test

Results are tabulated in Table I which represents the stress vs. Strain test output of lowland bamboo and its corresponding graph of stress-strain diagram is indicated in Fig. 4. Similarly, Table II and Fig. 5 represent the highland bamboo of Arbegona.

Data are too large (1 to 1165) to include in the Table I, hence only a part of it is presented. Others are omitted by broken lines in the same table, but in the graph, data are incorporated.

Received: August 2024; Revised: 16 November 2024; Accepted: 28 October 2024; Published: 24 December 2024





Table I: Tensile test result of 01 lowland bamboo (stress in MPA)

N <u>o</u>	Stress	Strain	N <u>o</u>	Stress	Strain		
1	0	0	20	25.7	0.304		
2	0	0.004					
3	0	0.02					
4	23.85	0.036					
5	24	0.052					
6	24.2	0.07	1154	177.95	7.69		
7	24.4	0.086	1155	178.05	7.71		
8	24.55	0.104	1156	178.1	7.732		
9	24.75	0.12	1157	178.05	7.762		
10	24.95	0.136	1158	177.95	7.802		
11	25.15	0.154	1159	177.8	7.85		
12	25.35	0.17	1160	177.6	7.906		
13	25.45	0.188	1161	177.3	7.972		
14	25.55	0.204	1162	176.75	8.06		
15	25.55	0.22	1163	174.95	8.186		
16	25.6	0.238	1164	141.8	8.504		
17	25.6	0.254	1165	102.65	9.124		
18	25.65	0.27					
19	25.7	0.288					

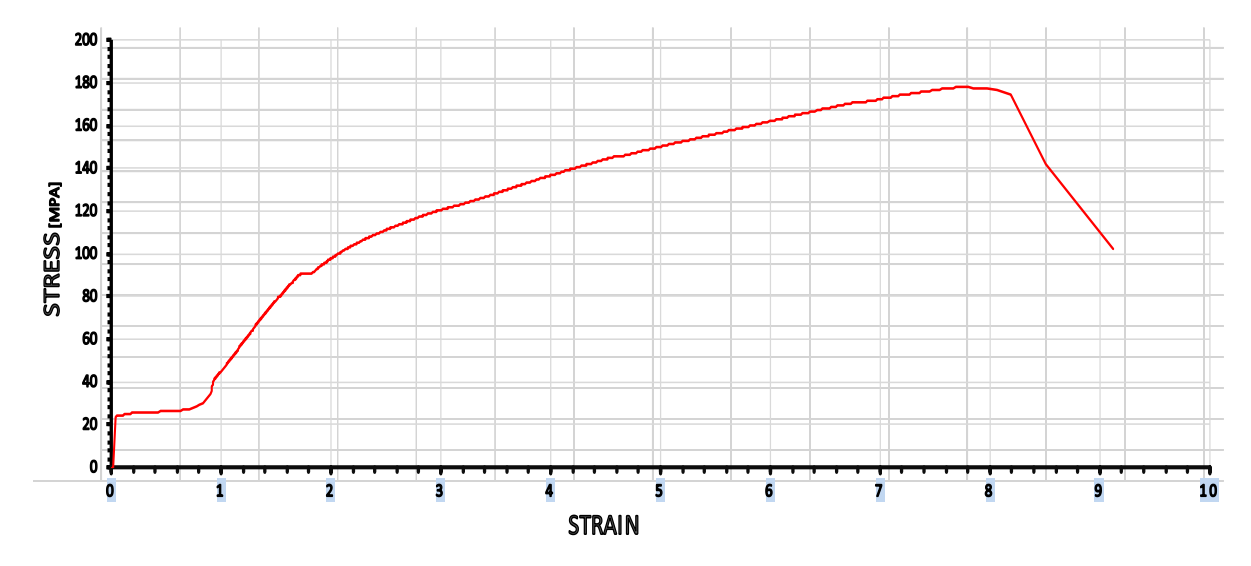


Fig. 5.: Stress-Strain diagram of 01 Lowland Bamboo (Benishangul Region - Assosa)

ISSN (E): 2959-3921

Volume 2, Issue 2, 2024 Copyright and License Grant: CC By 4.0





Table II: Tensile test result of 02 highland bamboo (Arbegona). Data ranges from 1 to 659

N <u>o</u>	Stress	Strain	N <u>o</u>	Stress	Strain
1	0	0	637	121	3.49
2	0	0	638	121.1	3.498
3	0	0.016	639	121.2	3.506
4	24.25	0.034	640	121.3	3.514
5	24.35	0.05	641	121.4	3.522
6	24.5	0.066	642	121.5	3.53
7	24.6	0.084	643	121.7	3.54
8	24.75	0.1	644	121.8	3.548
9	24.85	0.116	645	121.9	3.556
10	24.95	0.134	646	122	3.564
11	25.05	0.15	647	122	3.574
12	25.15	0.168	648	121.8	3.59
13	25.2	0.184	649	121.7	3.614
14	25.15	0.2	650	121.6	3.634
15	25.15	0.218	651	121.4	3.652
16	25.15	0.234	652	121.3	3.672
17	25.1	0.252	653	121.2	3.692
18	25.05	0.268	654	121	3.712
19	25	0.284	655	102.2	3.754
20	25	0.302	656	95.65	3.878
21	25	0.318	657	99.2	4.008
			658	98.2	4.126
			659	95.23	4.24



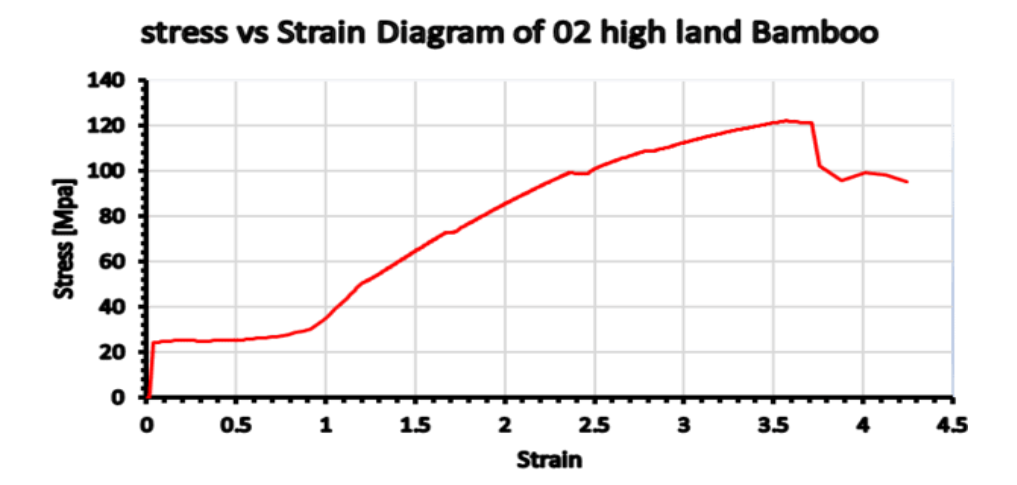


Fig. 6.: Stress vs Strain Diagram of 02 Highland Bamboo (Sidama Region - Arbegona)

#### IV. **Discussion**

As shown in the stress-strain diagram Fig. 6, the yield and ultimate stress are nearly at the same point. There is no significant clear point to distinguish them. In addition, the Fatigue life of the structure is highly dependent on the surface roughness of the material. If the roughness is high the fatigue life of the material decreases and vice versa [12].

From the experiment, we observed that sample 01 lowland (solid bamboo) has the maximum load carrying capacity = 7.124 KN, with the corresponding yielding strength ( $\sigma_v$ ) = 178.1 Mpa. As a result, the fatigue stress is 40% of the tensile stress which is 71.24 Mpa & Modulus of elasticity = 6 Gpa.

#### A. Sample 01 Lowland Bamboo (Assosa)

At the beginning of the tensile test, the stress-strain diagram shows that (Table I and Fig. 4) strain is very limited and has less response to elongation, however, stress is increasing significantly. From the origin of the graph, the yielding stress is nearly, close to 25Mpa and strain to 0.154, here also both the parameters have a direct relationship and satisfy Hooke's Law.

Between the stresses 25 Mpa and 40 Mpa, the stress-strain is not in a proportional limit; however, the strain is increasing significantly than the previous trend.

Yin as the test continued, the previous observation from the graph shifted considerably. The strain or elongation increased significantly, even with small increments in stress. This relationship is continuous up to the point where cracking is propagating nearly, and stresses and strain are equal to 178.1Mpa and 0.55 respectively.

Finally, the specimen completely failed at stress and strain nearly 102.65 Mpa and 7.732 respectively.

Received: August 2024; Revised: 16 November 2024; Accepted: 28 October 2024; Published: 24 December 2024





#### B. Sample 02 highland bamboo (Arbegona)

This trend is also similar to the lowland of bamboo with a basic difference of the proportionality and failure point as it is observed in the stress and strain diagram.

At the beginning of the test, the specimen is less responsive to elongation as stress is increasing significantly. Table II and Fig. 5 indicate stress 0 Mpa and strain 0. Stress increases up to the yielding stress nearly equal to 24.25 Mpa and strain is 0.034. In this range, both stress and strain have a direct relationship which satisfies Hooke's law as well.

Between the stresses 24.25 Mpa and 47.35 Mpa, the stress-strain is not in a proportional limit; however, the strain is increasing significantly than the previous values.

As the test continued, above the stress 47.35 Mpa and strain 1.16, both are in a proportional relationship. Cracking started to propagate near the stress equal to 121.4 Mpa and strain 3.652.

Finally, the specimen completely failed at stress and strain at nearly 95.23 Mpa and 4.24 respectively. Experimental Test result of the Tensile test and the corresponding Fatigue strength of bamboo specimens are given in the Table III.

Table III: Summary of the entire test result of low and highland bamboo

No	Types of	Logation			Fatigue Strength =	Modulus of
N <u>o</u>	samples	Location			40% *(σy) Mpa	Elasticity (Gpa)
1	01 lowland	Assosa	7.124	178.1	71.24	6
2	02 lowland		5.99	150	60	5
3	03 lowland	Assosa	4.586	114.65	45.86	4
4	01 highland	Chencha	4.846	121	48.4	4
5	02 highland	Arbegona	4.866	122	48.8	5

#### V. Conclusion

The specimens are free of any chemical treatment. If we apply such retting, certainly the strength of the bamboo increases [13]. The experimental data ensured that lowland bamboo (*Oxytenanthera abyssinica*) has better mechanical properties as compared to highland bamboo (*Yushania Alpina*). For example, 01 lowland bamboo has a fatigue stress equal to 71.24 Mpa, while sample 02 highland bamboo has a fatigue strength of 48.8 Mpa.

Finally, this study ensured that both species of bamboo which are locally available in Ethiopia qualify for the manufacturing of various components. For example, highland bamboo is the fittest to manufacture a component when it is subjected to a fluctuating load up to a fatigue stress equal to or less than 48.4 Mpa.

Volume 2, Issue 2, 2024

DOI: https://doi.org/10.59122/174CFC17

Copyright and License Grant: CC By 4.0 (a)



Similarly, the lowland bamboo can be applicable for manufacturing a component when subjected to stress up to 71.24Mpa.

Conversely, when subjected to a uniform load (continuous stress), bamboo structures can withstand higher stress levels, reaching 178.1 MPa for lowland and 122 MPa for highland varieties. The mechanical properties of bamboo are influenced by various factors, including species, culm position, age, and environmental conditions.

Lowland bamboo, typically grown in warm, humid climates, exhibits rapid growth, leading to denser microstructures and thicker cell walls. This is exemplified by lowland bamboo found in the Benishangul Gumuz region. In contrast, highland bamboo, cultivated in cooler, high-altitude environments, experiences slower growth and develops thinner cell walls compared to lowland bamboo [14] [15].

This ensures that the structure with a higher thickness carries more load than the thinner one. Therefore, as was observed from the experimental outcome, lowland bamboo has better mechanical properties than highland bamboo.

To sum up, experimental test data revealed that lowland bamboo available in Benishangul Gumuz regional state (like the Asosa zone) has better mechanical properties than highland bamboo (Chencha or Arbegona). Wind turbine blades are frequently subjected to intermittent or fluctuating wind loads. This leads to fatigue failure. For example, as an alternative material bamboo is applicable for the construction of small-scale wind turbines that generate electric power up to 6 kW. Hence, bamboo can be utilized for other lightweight components such as aerospace and piping systems when they are subjected to repeated loads.

The present study focused on the characterization of the mechanical properties of natural bamboo. Future studies can expand this research work on treated, hybrid, or composite bamboo materials and compare their output.

#### Recommendations

- 1. Extending the research by conducting tests on bamboo plants from different locations other than those listed in this report.
- 2. Extending the research by conducting additional fatigue tests which strongly confirm results.
- 3. Extending the research by polishing or using the chemical treatment on the external surface of the bamboo and analyzing the output of the study.
- 4. Extend the research for the Heat as the Heat Treatment also has a valuable impact on its strength.
- 5. Take into consideration that during tensile or fatigue testing, care should be given to avoid any external stress such as tightening of the specimen.

Volume 2, Issue 2, 2024

**DOI:** <u>https://doi.org/10.59122/174CFC17</u>



Copyright and License Grant: CC By 4.0



#### References

- 1. Ethiopian Standards Agency, Design of Bamboo Structures, 1st ed., 2021.
- 2. Bamboo: Origin, Habitat, Distributions and Global Prospective. Available: https://www.researchgate.net/publication/354206084.
- 3. United Nations Industrial Development Organization, *Bamboo Cultivation Manual: Guideline for Cultivating Ethiopian Highland Bamboo*.
- 4. Interesting Facts About Bamboo. Available: https://lewisbamboo.com/pages/interesting-facts-about-bamboo.
- 5. S. Woubshet and D. Addissie, *Investigation on Mechanical Properties and Suitability of Highland Bamboo (Yushania Alpina) for Use in Structural Truss Members*.
- 6. F. A. Muche and Y. M. Degu, "Experimental Investigation of Bending Strength of Oxytenanthera Abyssinica and Yushania Alpina Bamboos," Faculty of Mechanical and Industrial Engineering, Bahir Dar Institute of Technology, Bahir Dar University, Bahir Dar, Ethiopia.
- 7. S. Woubshet and D. Addissie, "Investigation on Mechanical Properties and Suitability of Highland Bamboo (Yushania Alpina) for Use in Structural Truss Members," *Science Development*, vol. 2, no. 2, pp. 23-29, 2021. doi: 10.11648/j.scidev.20210202.11.
- 8. Design Of Machine Element. Available: https://madeesay.in.
- 9. ISO/TR, Determination of Physical and Mechanical Properties of Bamboo Part 2: Laboratory Manual, 2004.
- 10. ISO/TR 22157-1, Bamboo Determination of Physical and Mechanical Properties Part 1: Requirement, 2004, pp. 1–8.
- 11. Bureau Of Indian Standards, *Indian Standard Method of Tests for Bamboo*, Manak Bhavan, 9 Bahadur Shah Zafar Marg, New Delhi 110002, 2008.
- 12. W.L. Xiao, H.B. Chen, and Y. Yin, "Effects of Surface Roughness on the Fatigue Life of Alloy Steel," Department of Modern Mechanics, University of Science and Technology of China, Hefei, Anhui 230026, China.
- 13. H. Chen, H. Cheng, G. Wang, et al., "Tensile Properties of Bamboo in Different Sizes," *Journal of Wood Science*, vol. 61, pp. 552-561, 2015.
- 14. Kidane, B., Mekonnen, Z., Getahun, A. et al., "Highland bamboo value chains development to enhance local livelihoods in Southern Ethiopia." *J Innov Entrep* 13, 50 (2024). https://doi.org/10.1186/s13731-024-00406-3
- 15. H. Huang and K.F. Chung, "Mechanical Properties of Bamboo as a Structural Material," *Journal of Materials Science*, vol. 43, no. 3, pp. 1069-1076, 2008.

(P): 2959-393X **DOI:** https://doi.org/10.59122/174CFC17



Copyright and License Grant: CC By 4.0



Volume 2, Issue 2, 2024

# Integrating Sustainability Frameworks for Assessment of Environmental Performance in Higher Education Institutions Via Energy, Fuel, and Waste Management Audits

Tsegaye Getachew Alenka<sup>1\*</sup>, Mulugeta Tadese Wotango<sup>2</sup>, Sileshi Kore Dube<sup>3</sup>

<sup>1, 2</sup>Wolaita Sodo University, Ethiopia

<sup>3</sup>State Owned Enterprises Standing Committee, FDRE, Addis Ababa, Ethiopia \*Corresponding Author's Email: tsegaye.getachew@ethernet.edu.et

#### **Abstract**

There are over forty-five universities in Ethiopia, with an expected increase in the upcoming years which necessitates studies on their environmental impact. However, the environmental impact of these large institutions, particularly regarding resource consumptions such as electricity, diesel fuel, and water remains largely uninvestigated. This study employed the IPCC SCOPE 3 approach to assess the environmental impact of selected Ethiopian universities. This study collects primary data through surveys and observations and complements this with relevant secondary sources such as government records, organizational data, and existing literature. It utilizes IPCC SCOPE 3 guidelines to comprehensively analyze emissions and sustainability in Ethiopian higher education. The finding revealed substantial resource consumption, with notable electricity use accounting for the largest proportion of total emissions. The university's transition to electric cooking primarily powered by hydroelectric energy has effectively decreased emissions from traditional stoves across two of its four campuses, impacting 75% of residents. Electricity still represents 78% of the greenhouse gas emissions followed by waste generation which is 17.81%. This highlights the urgent need for sustainable policies to mitigate environmental impacts. The research identified economic constraints and underlined the need for policy support to enhance sustainability and environmental outcomes. Existing youth engagement programs in solid waste sorting, composting, recycling, and water treatment for reuse or recycling of clean water are in their initial development stages. The study suggests strengthening these practices while recognizing the potential to integrate renewable energy sources with appropriate policies, which could significantly impact institutional sustainability efforts.

**Keywords:** Corporate Impact, Electricity Use, Emission, Environmental Impact Audit, Fuel Economy, Kilowatt Hour, Pollution

DOI: https://doi.org/10.59122/174CFC17

Volume 2, Issue 2, 2024

Copyright and License Grant: CC By 4.0





#### I. Introduction

Africa is one of the smallest contributors to global greenhouse gas emissions, accounting for only 4%. Climate change is a complex issue, and Ethiopia's technological advancements require ecological tradeoffs [1]. Universities in Ethiopia play a crucial role in shaping sustainable operations. The impact of corporate activities is essential for sustainable development goals, addressing direct impacts like electricity use, solid waste management, and emissions contributions [2].

According to the Paris Climate Agreement, the sustainable development of an institution involves consideration of the triple Ps (People, Profit, and Planet) in its functional activities aimed at attaining its economic, social, and environmental goals [3]. The BPIE 2022 report highlighted process optimization, standardization, and data-driven decision-making for sustainable operations. It proposed optimization of electricity demand and supply, addressing climate performance issues, and identifying energy-intensive utilities [4-8].

According to studies' reports, energy use is given a high priority in a corporate environmental impact audit, and it is consequently a significant CO2 producer, second only to automobile emissions [9]. The King Saud University (KSA) has implemented a machine learning-assisted building management system (BMS) to optimize HVAC energy consumption in higher education institutions. The system saved 3% in just two months, suggesting the use of smart buildings technology and adaptive BMS for further HVAC system optimization [10-11]. The authors proposed five subsequent clustering steps in ascending energy demand orders for an accurate and relevant energy audit for university buildings based on functional and weighed energy performance categories. The clusters include arts, sciences, hospitals, data centers, and research centers. The electricity use (E) of equipment is established in kilo-watt-hours (kWh) [10].

There are many techniques for incorporating automobile emissions, depending on the availability of data, monitoring technology, and vehicle technology. The European driving cycle consists of urban and extraurban categories with fuel consumption causing CO2 emissions. Researchers modified the rule-based control strategy, resulting in high energy content and power generation efficiency without pollution. Constraints introduced resulted in fuel saving and reduced stresses. Carbon Trust 2023 suggests global hydrogen-based integrated energy systems could reach "Net Zero by 2030", advising stakeholders to transition towards renewable energy generation [11-12]. Factors contributing to vehicle emissions include vehicle type, service status, fuel characteristics, driving conditions, and roads [13-14]. According to the research, fuel economy is inversely proportional to gasoline consumption, while the relationship is regarded as exponential. Fuel consumption is the amount of fuel consumed in a vehicle engine per trip distance,

Volume 2, Issue 2, 2024

(P): 2959-393X

**DOI:** https://doi.org/10.59122/174CFC17

4

Copyright and License Grant: CC By 4.0



whereas fuel economy is the amount of fuel used per 100 kilometers. In typical contexts such as Africa and Europe, the measure of fuel economy in fixed vehicle distance with a certain amount of fuel, is represented in liters per hundred kilometers (equal to the US's 235.2 miles per gallon) [15].

Educational institutions generate a variety of solid waste, including paper, cardboard, plastics, wood, food waste, glasses, metals, and hazardous waste. Effective food waste management strategies include source reduction, repacking, methane production, energy recovery, and incineration. Socio-economic factors contribute to food waste generation, necessitating proactive initiatives for food security. Challenges include improper segregation, inadequate policies, limited public awareness, and disregard for by-products [16].

Ethiopian universities are focusing on optimizing energy use to achieve independence and sustainability. They are encouraging open discussions about energy-intensive features and implementing dedicated operators and load forecasting systems to improve electricity consumption control, reduce monthly expenses, and maximize power generation. As Ethiopia undergoes a digital transformation, it is important to gather fact-based baseline data for future environmental performance assessments. The impact assessment should cover various business activities like solid waste management and energy use, including common energy-intensive features such as outside lighting and scientific equipment. This study aims to evaluate energy usage trends in a public Ethiopian university using data from multiple buildings, vehicles, and offices. The goal is to enhance baseline data for the adoption of best practices and ensure long-term university operations.

#### II. Methodology

According to Our World in data metrics, global territorial production annual emissions have increased dramatically, despite individual contributions have shown little reduction by 2021 compared to the previous year [8]. Another research reported an annual global per capita CO2 emission factor of 4.69 tonnes by 2021, compared to the global average of 4.69 tonnes. Emission Factors are calculated in appropriate units using emission factor data obtained from reputable sources such as Our World in Data, IRENA, UNFCC, and others [17-19].

Ethiopian higher education institutions have been classified over recent the five years as applied science, comprehensive, and research universities, with more than 45 public universities across the country [20]. Based on the idea from a study [10], the current research examines electricity consumption, fuel usage, and waste generation at four anonymous Ethiopian universities, employing primary and secondary data collection procedures and strategies to maintain institutional privacy and confidentiality. The data was

Volume 2, Issue 2, 2024

DOI: https://doi.org/10.59122/174CFC17



Copyright and License Grant: CC By 4.0



gathered from a public Ethiopian higher education institutions [14, 17] and included vehicle possessions, machinery, buildings, offices, students, waste, and staff. It utilizes a method to estimate total CO2 emissions from diesel vehicles, which serves as the basis for fuel use estimation, emissions analysis, waste generation rate, and energy. The estimation idea matches the estimations considered in the studies [21-22].

The building's impact assessment involved surveys observed lighting and electrical appliances, and verified information by cross-checking and consulting with electricians and technicians. The waste generation data was collected from student dormitories and staff apartments with a focus on liquid and solid waste. The method of data collection employed was structured questions, interviews, and field observations. This study attempts to identify trends and implement sustainable operations for higher education institutions. The information came from the university's website, which listed campuses, colleges, school offices, and other vital resources in the institution with 45,000 employees.

#### A. Analysis Description

The convenient standard value-chain-based emissions estimation prioritized category identification that requires: (1) considering risks and opportunities within the value chain, (2) prospective direction for sustainable operation, and (3) stakeholder engagement. The selection of the Scope 3 emissions calculation method is recommended considering the following factors: data-relevant parameters such as availability & quality of data, analysis cost, and amount of emissions. IPCC Scope 3 offers various formulae under fifteen distinct categories for almost all kinds of CO2 emission analysis. Major corporate activities identified based on the standard include the institutions building information with function, electricity use, employers' commuting, business travel, product transportation, and waste generation [2,10-11,14].

The data relevant for encompassing the listed activities collected include: lists of the university-owned vehicles and corresponding weekly distances covered by each, number of employees, working hours and shifts, lists of electrical appliances and relevant usage, number of annual events hosted as well as invited along with average business distances, annual products and goods recruitment with transportation distance, waste generation and treatment trends, etc. [10, 15]. Fig. 1 summarizes the IPCC Scope 3 enterprise/corporate requirements that have been carefully tailored to Ethiopian universities.

Volume 2, Issue 2, 2024

**DOI:** https://doi.org/10.59122/174CFC17

Copyright and License Grant: CC By 4.0



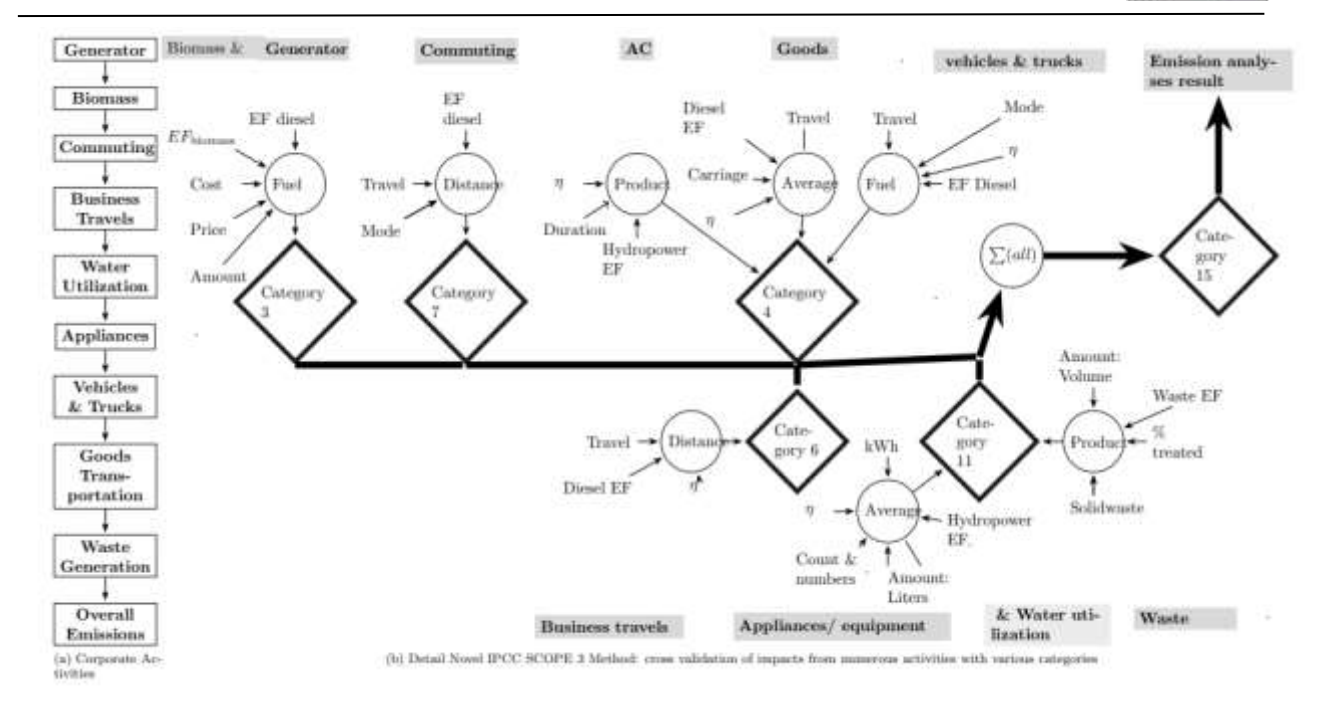


Fig. 1.: Corporate impact analysis based on IPCC SCOPE 3 Guidelines: (a) Typical corporate activities (b): Detail Scope 3 calculation method, Categories selected on relevance & attainability of dataset

The IPCC (Scope 3) accounting and reporting standard covers fuel-electricity and waste-related calculations, with categories 3, 4, 6, 7, 11, 13, and 15 included. The average-data method was chosen as illustrated in Fig. 1, and data was collected through a combination of processes/products. The SCOPE 3 methodology is based on relevant data presented in a visual chart and detailed in Appendix Table V. The circular shapes in Fig. 1 correspond to pertinent categories with leader arrows annotating data label texts. Appendix Table V summarizes the Scope 3 methodology employed and the activities involved.

#### III. Results and Discussion

#### A. Vehicles Travel and Fuel Consumption

The bus shift hours include morning employee's arrival, lunchtime travel to home & return, and evening departure for academic & admin staff where there are night shift office/class sessions. Vehicle travel information is summarized in Table I.



Copyright and License Grant: CC By 4.0



Table I: Weekly travel information and diesel fuel consumption of light duty (LD) & heavy duty (HD) vehicles and fuel expenditure of diesel generator

Items	Number	Standard	Amount	Unit
Generator (Stationary)	6	Fuel	5357	Liters
LD Automobile (Passenger)	12	Distance	370	km
LD Truck (pickups)	13	Distance	450	km
HD Truck (Bus & trucks)	14	Distance	214	km

When employees' entry outnumbers the vehicle seats, two rides in each travel along with early morning report & late evening departures of cafeteria transport services count four up to twelve runs counts. The turn for special purpose cars like ambulances depends on several emergencies and services that their average fuel bill converted into run counts to maintain consistency. The university's annual report for the academic year 2021/2022 reported a quarterly generator fuel cost of 6,000,000 birr and a monthly firewood expenditure of 1,000,000 birr. The local market price per an 18 m³ freshly cut eucalyptus was 11,500 birr. The research found that the experimental mean dry compact mass of eucalyptus (20% moisture) was 0.41tone/ m³. The amount of diesel oil purchased for emergency generators was 5,357 liters.

#### B. Electricity Consumption

The list of 36 electrical equipment items can be categorized into four functional themes based on their context. Recommendations for each theme should be aligned with the current operation, in contrast to generic approaches for classrooms, offices, laboratories, cafeterias, dorms, and residential areas. The equipment within each theme is ordered by their initial viability, from highest to lowest [4, 8, and 10]. The five-kWh classification of either generic clustering (arts, sciences, hospitals, data centers, and research centers) proposed or sophisticated grouping in five effective practical patterns (lighting, HVAC, electronics, laboratory, and appliances) can also be addressed but the latter methods can be effectively incorporated in the next phase of sustainable development of an institution after the baseline trend set in this study [1, 3-4, 7, 10, 24].

Two distinct patterns of electricity consumption were identified in addition to the established theme. The three major electric consumption themes are functional, usage, and categorical. The former captures administrative or facility management supervision structure while the last theme captures equipment types. Established studies grouped electric consumption in a categorical structure. However, the functional category provides a clearer view of practical resource management structure and utilities for potential integration with improvement schemes for similar higher education institutions. The marked distinction of



Volume 2, Issue 2, 2024

the functional theme confirms carefully designed approaches during the assessment. The effective management tool can be installed thereafter.

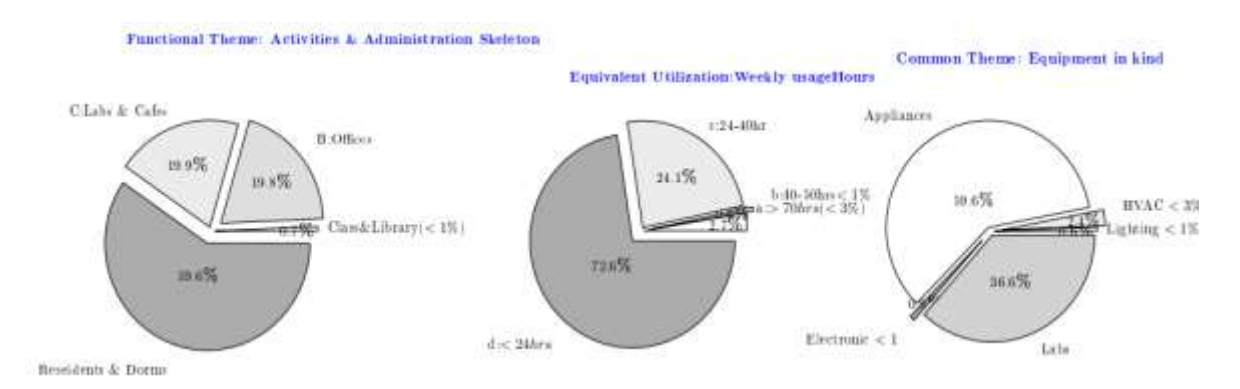


Fig. 2.: Electric consumption themes identified electric (in % use from total kWh)

The university's electricity consumption can be divided into three themes: functional, usage, and categorical. Functional themes include teaching, offices, cafes/labs, and residential/dorms providing consistent supervision but challenging-to-match assessment tools. The usage theme groups equipment based on weekly usage, while the categorical theme captures the type of equipment. The functional theme seems the most effective, with well-organized energy monitoring systems. The university consumes twenty times more electricity than the national average with residential appliances and dorms accounting for 60% of total consumption. Heavy-duty machines account for over two-thirds of total energy use. All kitchen appliances combined do not use as much electricity as heavy-duty machines.

#### C. Waste Generation

Cafeteria wastes include kitchen waste, vegetable oils, firewood ashes, and food waste that consists of leftovers and expired recipes to be measured using mass balance. Table II summarizes major waste generations by source & management scenario by sections. The existing solid waste management involved the temporary site collection of plastics through the youth's association for recycling, transportation, open destiny site disposal, drying, & firing.

Table II: Weekly waste trend of the institution

Types Waste Sources		Methodof Segregation	Truck Carrying	Total
• •			Capacity	(Weight/Volume)
Solid Waste	528 Dorms	Plastic Recycli-Temp.Store.	16.2 m <sup>3</sup> or 30 ton	129.6
		Dumping, drying, & burning		
Residential	328 Staff family	Plast. Recycling from Temp.	$16.2 \text{ m}^3 \text{ or } 30 \text{ ton}$	113.4
	rooms	Store. Dumping, drying, & Burning		

ISSN (E): 2959-3921

(P): 2959-393X

Copyright and License Grant: CC By 4.0





DOI: https://doi.org/10.59122/174CFC17

Cafeteria	3cafeteria,6lounges	Temp. Store. Dumping on farms	16.2 m <sup>3</sup> or 30 ton	113.4
Liquid wastes	fromall safety tanks	Temporary. Wastewater treatment & Recycling	10,000 liters	14,640,000

Note: 16.2 m<sup>3</sup> (about half the volume of a large U-Haul truck)

The university's solid waste collection from dormitories, residential compounds, and cafeterias showed a decrease in waste from over 600 rooms and 30,000 active students. The total solid waste from the university was 356.4 tons, slightly above the national average. The wastewater collected from these areas was transported to a wastewater treatment plant, resulting in 191 liters (about twice the volume of a mini fridge) per capita per day. The actual amount of treated waste is subject to the treatment plant's performance and future investigations [26-29].

#### D. Corporate Activities (Overall)

This study audited the university's weekly activities using the SCOPE 3 guidelines of WRI, WBC, and GHG Protocol. [2], and Carbon Trust. It evaluated corporate activities under fuel use & transport, energy use & kWh electric consumption, and waste management. The study found electricity kWh usage as the most significant corporate activity.

Table III: Sources of emission: university activities amount on a weekly base

Activitie	Business	Goods	Generator	University	Firewood	Electric	Wastewater	Solid
S	Travels	Transpirati	Fuel	Vehicles Fuel	Consumpt	Power	Generation	Waste
	in km	on in km	Consumptio	Consumption (	ion (kg)	Consumptio	(Liters)	(kg)
			n (Liters)	Liters)		n (MWh)		
Amount	2351	50	6.207	5877.056	116.352	38470.17	51912	117

The university's operational and emissions accounts show a significant reduction in biomass fuel usage, with a minimum of 9 m³ per week. This shift towards electric appliances has led to a significant reduction in biomass use for cooking. The university also has a low transportation of goods, with only 49.43 km a week of biomass fuel. Wastewater usage is minimal, mainly due to the university's functional treatment facility. The university covers 2,351 km (about half the width of the United States) per week for guests and employers, with a total weekly diesel fuel usage of 12,546 liters (about half the volume of a large U-Haul truck).



#### E. Corporate Emission Analysis Results (Overall)

The emission factors (EF) data relevant to the contexts were collected by consulting databases of credible journals and websites through convenient calculation of unit conversions. The review of the emission factor used is outlined in Table IV where the detailed calculation along with the source citations can be seen in Section 6 of Appendix in Table VII. Subsequent corporate analysis used emission factors summarized in Table IV.

Table IV: Emission factor used

Activities	Diesel	Passenger	LD	HD	kWh	SW	Waste
Activities	Generator	rassenger	trucks vehicles	K W II	2 W	water	
Emission	2.66kg	0.248kg	0.33kg	1.011kg	0.02kg	3.84kg	0.42kg
factor	$CO_2/L$	$CO_2/L$	$CO_2/L$	$CO_2/L$	$CO_2/kWh$	CO2/Lkg	$CO_2/L$

The following polar plot (spiral chart) in Fig. 3 portrays weekly equivalent CO2 emissions from the corporate activities and their relative importance from the stated emission analysis results. The axes that correspond to individual activities with distinct measurement units in subsection 4.4 compiled in Table III consistent system units of kg of CO2 to enable coherent comparison and adjusted in logarithmic scale to facilitate distinguishable visibility.

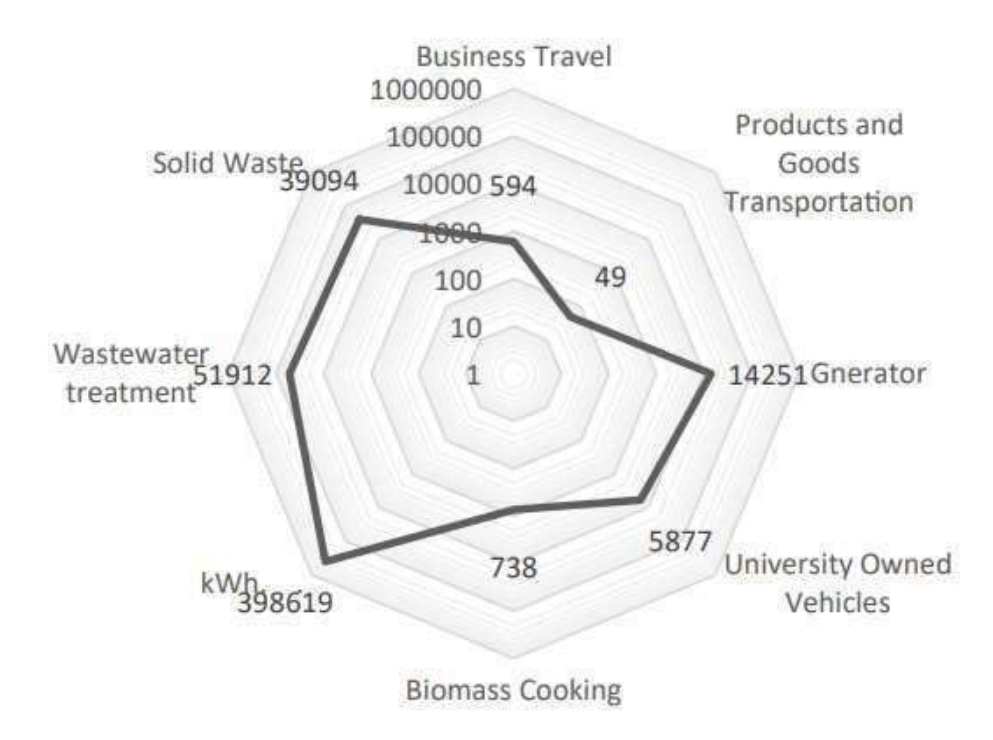


Fig. 3.: Corporate emission constituents of the Ethiopian university



The university's electricity usage was the most detrimental activity, emitting 398.86 tons of CO2e. Other major environmental adversities included wastewater, diesel generators, and solid waste generation. Vehicles had the worst environmental performance, accounting for 6 tons of CO2e emissions. Product transportation had the least emissions, with 49 kg CO2e. The majority of the university's total CO2e emissions, over 511 tons, comes from electricity kWh usage. The bar chart in Fig. 4 illustrates the relative importance of these activities. As discussed in the preceding analyses under Table III, the majority 78% of the university's total CO2e emission of over 511 tones comes from kWh usage of electricity.

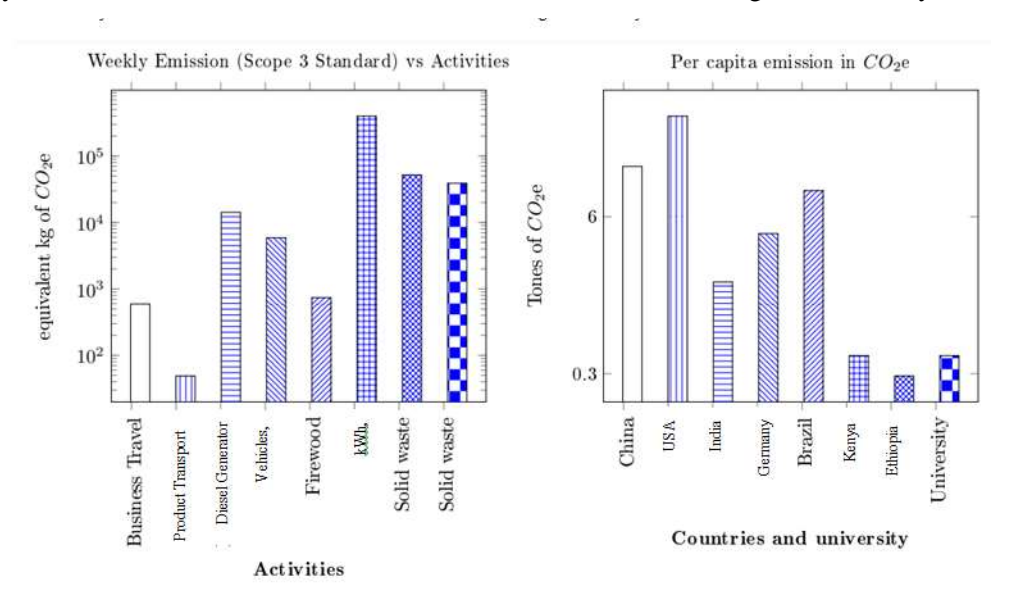


Fig. 4.: Sector emissions from various university activities

Waste sectors are the dirtiest remaining with wastewater contributing just over 10% followed by solid waste with 7.65% as seen in Fig. 4. The next significant polluting university operations of over 14 tons of CO2e (2.79%) emissions a week is contributed by electricity production via diesel generators while vehicles pollute 5.877 tones. The remaining three operations: firewood, product transportation, and business travel, constitute below 0.3% of the total emissions according to the results of the analysis. The two bar charts in Fig. 4 are added to aid the standard literature comparisons. The second bar chart in Fig. 4 is plotted by using per capita emission from Our World in Data considering five consecutive years' data of cumulative total emission data [22]. The total weekly corporate emission analysis of the university is estimated to be 511.114 tones (0.589 tones per capita per annum) as illustrated in Fig. 4 way beyond the national per capita emission of the year 2021, reported capita 0.15 kg CO<sub>2</sub>e according to previous research also illustrated in the second chart of Fig. 4. The emission data of the countries in Fig. 4 by energy consumption is extrapolated for the year 2021 from data corresponding to the previous four years using Lagrange polynomial estimation [9, 22].

Volume 2, Issue 2, 2024

DOI: https://doi.org/10.59122/174CFC17



Copyright and License Grant: CC By 4.0



Assuming all 45 government universities' emissions are virtually proportional, they contribute a substantial 6.3% of the national annual CO2e emissions total reported to be 19.04 million tones according to Our World in Data (see the second chart in Fig. 4. [22]. The baseline environmental performance assessment of the Ethiopian higher education institution revealed the need for policy development and review intervention in the supervision of kWh electricity usage and waste management sectors. The results implied that the integrated electricity system and introduction of digital control alongside assessment strategies established in this study have enormous potential for energy optimization and the environmental sustainability of Ethiopian universities according to references [3-7, 24].

Factors such as budget deficits and shortages, unplanned energy-intensive operations like the simultaneous use of heavy machinery in machine shops, mass cooking equipment in cafeterias, and cereal grinders significantly contribute to peak hour energy demands. Additionally, energy-inefficient practices in dormitories combined with waste mismanagement in residential areas and environmentally harmful behaviors within the community hinder the university's long-term objective of achieving efficient, sustainable, and eco-friendly operations.

The university's electricity consumption in the context of almost no air conditioning systems with significant consumption or zero cooling load was discovered to be twenty times higher than the national average. This is even though over 70% of the population reported a lack of access to electricity notwithstanding significant strides in increasing electricity access, highlighting Ethiopia's challenges in achieving universal electricity access. The result implies an increase in the significant potential for consumption reduction primarily through the implementation of energy-efficient practices and consideration of the use of renewable energy sources [25-29].

The finding also highlights insufficient efforts to improve energy access through renewable sources and decentralized systems, as reported in technical reports emphasizing the need for immediate intervention in decentralized energy solutions. Further, it demonstrates that urgency in resident-targeted behavior change campaigns can help reduce environmental impacts, particularly for kitchen appliances, as a secondary priority. Focusing on effective management practices can help avoid peak demand, particularly for heavy-duty machines such as manufacturing workshops that use more than two-thirds of total energy [28-30].

Furthermore, wastewater and solid waste generations of the Ethiopian university were identified as major potential areas for improvement and implementing established best practices. The study determined that waste management is a priority area of effective initiatives prioritizing waste management in Ethiopian universities. The benefit of environmental performance enhancement tools prioritizing waste management

Volume 2, Issue 2, 2024

DOI: https://doi.org/10.59122/174CFC17



Copyright and License Grant: CC By 4.0



as implied by the results of this study as a benchmark can have multifaceted gains such as biogas generation for cooking and electricity, fertilizer manufacturing, environmental protection, waste reduction, and overall sustainability [3,27-28,31].

#### IV. Conclusion

This study presents a preliminary integrated environmental impact assessment of Ethiopian higher education institutions, with the method illustrated in this research encompassing key activities such as fuel uses of diesel generators and vehicles, electricity consumption, transportation, and waste management. It employed a comprehensive methodology based on IPCC SCOPE 3 standards and relevant literature. Valuable insights were provided about the associated emissions, energy usage, and waste trends. The university has made significant strides in transitioning to electric cooking powered by hydroelectric energy, reducing emissions from traditional stoves for 75% of residents across two campuses. However, electricity still accounts for 78% of greenhouse gas emissions, with waste generation contributing 17.81%. This underscores the urgent need for sustainable policies to address environmental impacts.

Although the adoption of renewable energy sources like solar power may offer advantages, economic constraints pose challenges to integration. Weekly emissions from vehicle and generator fuel usage reach 6 tons of CO2e, while electricity consumption trends reveal four key utility themes, illustrating that residential and cafeteria facilities comprise 60% of the university's weekly total electricity usage of 1.931 GWh. Implementing integrated electricity-waste management systems could enhance energy efficiency and operational gains. Unplanned energy-intensive operations and inefficient practices hinder sustainable goals, indicating a need for supportive higher education policies to improve environmental outcomes. Moreover, focusing on waste sorting, recycling, and utilizing food waste could strengthen the university's sustainability initiatives, particularly through youth engagement.

The university's electricity consumption is alarmingly twenty times higher than the national average, despite the lack of significant air conditioning or cooling loads, indicating severe challenges in Ethiopia's pursuit of universal electricity access. More than 70% of the population still lacks reliable electricity, underscoring the need for energy-efficient practices and the adoption of renewable energy sources. There is a notable deficiency in efforts to enhance energy access through decentralized systems, calling for urgent interventions as highlighted in various technical reports. The urgency for behavioral change campaigns aimed at residents could facilitate a reduction in environmental impacts, particularly concerning kitchen appliances. Additionally, effective management strategies are essential to mitigate peak energy demand, especially from heavy-duty appliances that account for over two-thirds of total energy usage.



Copyright and License Grant: CC By 4.0



#### Acknowledgments

Our heartfelt gratitude goes out to the leaders, technicians, and facilitators from collaborating universities who provided invaluable guidance and professional expertise throughout the research process. Their years of institutional reports, technical advice, and contributions during observations and data collection were instrumental in this project's success. Without their support, this research would not have been possible.

#### References

- 1. E. Serene et al., "The role of clean hydrogen in achieving net zero," Carbon Trust, 2023. <a href="https://www.carbontrust.com/news-and-insights/insights/worth-the-hype-the-role-of-clean-hydrogen-in-achieving-net-zero">https://www.carbontrust.com/news-and-insights/insights/worth-the-hype-the-role-of-clean-hydrogen-in-achieving-net-zero</a>.
- 2. C. Cynthia et al., "Technical guidance for calculating scope 3 emissions (version 1): Supplement to the corporate value chain for accounting & reporting standard," World Resources Institute, World Business Council for Sustainable Development, GHG Protocol, & Carbon Trust, 2013. https://doi.org/10.22438/jeb/42/4(SI)/MRN-1534a.
- 3. F. Sofwan et al., "A systematic literature review: Determinants of sustainability reporting in developing countries," *Sustainability*, vol. 14, 2022. <a href="https://doi.org/10.3390/su141610222">https://doi.org/10.3390/su141610222</a>
- 4. G. Jesse and B. Rutger, "Industrial prefabrication solutions for building renovation June 2022 innovations and key drivers to accelerate serial renovation solutions in Europe," 2022.
- 5. S. Sibyl and R. Oliver, "Minimum standards, maximum impact: How to design fair and effective minimum energy performance standards," Buildings Performance Institute Europe, 2023. <a href="https://www.bpie.eu/publication/minimum-standards-maximum-impact-how-to-design-fair-and-effective-minimum-energy-performance-standards/">https://www.bpie.eu/publication/minimum-standards-maximum-impact-how-to-design-fair-and-effective-minimum-energy-performance-standards/</a>
- 6. B. Alfonso et al., "Energy optimization using a case-based reasoning strategy," *Sensors*, vol. 18, 2018. https://doi.org/10.3390/s18030865
- 7. S. Sergey et al., "Optimizing the energy efficiency of higher education institutions," *Web of Conferences*, vol. 244, 2021. https://doi.org/10.1051/e3sconf/202124411029
- 8. D. Florin, D. Otilia, and E. Elena, "Distributed power generation from renewable energy resources a framework for load forecasting in low voltage power grids," in *UKSim-AMSS 6th European Modelling Symposium*, 2012.
- 9. H. Hongwen et al., "Model predictive control with lifetime constraints-based energy management strategy for proton exchange membrane fuel cell hybrid power systems," 2020. <a href="https://doi.org/10.1109/TIE.2020.2977574">https://doi.org/10.1109/TIE.2020.2977574</a>

Copyright and License Grant: CC By 4.0



Volume 2, Issue 2, 2024

- G. Sonetti and D. Cottafava, "Enhancing the accountability and comparability of different campuses energy profiles through an energy cluster approach," *Energy Efficiency*, 2022. https://doi.org/10.1007/s12053-022-10024.
- 11. A.-D. Ahmad et al., "Multi-agent system for energy consumption optimization in higher education institutions," *Journal of Computer and System Sciences*, vol. 81, pp. 958–965, 2015. https://doi.org/10.1016/j.jcss.2014.12.010.
- 12. P. Hoornweg and D. Bhada-Tata, "A global review of solid waste management," World Bank, 2012. <a href="https://documents1.worldbank.org/curated/en/302341468126264791/pdf/68135-REVISED-What-a-Waste-2012-Final-updated.pdf">https://documents1.worldbank.org/curated/en/302341468126264791/pdf/68135-REVISED-What-a-Waste-2012-Final-updated.pdf</a>.
- 13. B. Aissa et al., "Improvement of autonomy, efficiency, and stress of fuel cell hybrid electric vehicle system using robust controller," *Sustainability*, 2023. <a href="https://doi.org/10.3390/su15075657">https://doi.org/10.3390/su15075657</a>.
- 14. G. Michael and H. I. José, "Real emissions, driving patterns and fuel consumption of in-use diesel buses operating at high altitude," *Transportation Research Part D*, 2019. <a href="https://doi.org/10.1016/j.trd.2019.10.004">https://doi.org/10.1016/j.trd.2019.10.004</a>.
- 15. W. Yiwei and M. Qing, "The impact of the corporate average fuel economy standards on technological changes in automobile fuel efficiency," *Resource and Energy Economics*, 2020. https://doi.org/10.1016/j.reseneeco.2020.101211.
- 16. M. Nuhu et al., "Food waste management current practices and sustainable future approaches: A Saudi Arabian perspective," *Journal of Material Cycles and Waste Management*, 2018. https://doi.org/10.1007/s10163-018-0808-4.
- 17. F. Asefa, "Ethiopia's third national communication to the United Nations Framework Convention on climate change (UNFCCC)," 2022. <a href="https://rb.gy/wo36z">https://rb.gy/wo36z</a>.
- 18. G. R. Darío and W. D. John, "Stationary combustion (EFDB emission factor database)," 2006. https://rb.gy/0s57w.
- 19. R. Hannah, R. Max, and R. Pablo, "CO2 and greenhouse gas emissions," *Our World in Data*, 2020. https://rb.gy/evrl3.
- 20. "Ethiopian University List 2023 ranking & top private and public university," 2023. <a href="https://www.neaea.com/ethiopianuniversity/">https://www.neaea.com/ethiopianuniversity/</a>.
- 21. K. C.G. et al., "Estimation of carbon footprint in Tamil Nadu agricultural university, Coimbatore," *Journal of Environmental Biology*, 2020. <a href="https://doi.org/10.22438/jeb/42/4(SI)/MRN-1534a">https://doi.org/10.22438/jeb/42/4(SI)/MRN-1534a</a>.

DOI: https://doi.org/10.59122/174CFC17

Copyright and License Grant: CC By 4.0



- 22. F. Teshome, "Municipal solid waste management in Ethiopia: The gaps and ways for improvement," *Mater Cycles Waste Manag*, pp. 18–31, 2021. https://bit.ly/3UL4cX9.
- 23. IRENA, "IRENA country energy profile (Ethiopia)," 2023, <a href="https://rb.gy/j1hhc.">https://rb.gy/j1hhc.</a>
- 24. H. Jochen et al., "Mobile combustion (EFDB emission factor database)," 2006. <a href="https://www.ipcc-nggip.iges.or.jp/public/2006gl/pdf/2%20Volume2/V2\_3\_Ch3\_Mobile\_Combustion.pdf">https://www.ipcc-nggip.iges.or.jp/public/2006gl/pdf/2%20Volume2/V2\_3\_Ch3\_Mobile\_Combustion.pdf</a>.
- 25. UNFCC, "Greenhouse gas emissions in Ethiopia," 2017. <a href="https://pdf.usaid.gov/pdf\_docs/pa00msr8.pdf">https://pdf.usaid.gov/pdf\_docs/pa00msr8.pdf</a>.
- 26. D. G. Pezzano, "Argentina unida diapositiva 1: Implanted forests," FAO, 2021. https://doi.org/10.1016/B978-0-12-804491-9.00003-3.
- 27. TRANSPOCO, "How is fuel consumption calculated?," 2023. <a href="https://www.transpoco.com/knowledge/how-is-fuel-consumption-calculated">https://www.transpoco.com/knowledge/how-is-fuel-consumption-calculated</a>.
- 28. A. Graham et al., "A global review of solid waste management," 2021. https://rb.gy/fow94.
- 29. R. Edward et al., "Country-level and gridded estimates of wastewater production, collection, treatment and reuse," *Earth System Science Data*, pp. 237–254, 2021. <a href="https://doi.org/10.5194/essd-13-237-2001">https://doi.org/10.5194/essd-13-237-2001</a>.
- 30. C. Gomez et al., "Adaptable model for assessing sustainability in higher education," *Journal of Cleaner Production*, pp. 1–11, 2014. <a href="https://www.elsevier.com/%20locate/jclepro.">www.elsevier.com/%20locate/jclepro.</a>
- 31. M. Meyer, "Eco-management and audit scheme (EMAS)," 2023. https://green-business.ec.europa.eu/eco-management-and-audit-scheme-emas.

Ethiopian International Journal of Engineering and Technology (EIJET)

(P): 2959-393X



Volume 2, Issue 2, 2024

DOI: https://doi.org/10.59122/174CFC17

Copyright and License Grant: CC By 4.0



#### **Appendix**

Table V: Standard Emission Assessment Tools & Relevant Activities

Selected IPCC Scope 3	Activity Measurement	Relevant Emission Factor	Method of analysis
Categories			
Category 3: Fuel based for Diesel	Annual fuel expenditure, price, and relevant unit conversion	kg of CO <sub>2</sub> per liter	$CO_2e = \sum (Expenditures/Price_i)*EF_i$
Generators	factors	diesel	
Category 4 i: Distance-based	Employees commuting per week, weekly work	kg of CO <sub>2</sub> per liter diesel for	$CO_2e = \sum [kmi * \eta_i(l/km)]$
for Commuting	hours, & vehicles models	HD trucks/buses	*Load/Capacity <sub>Maximum</sub> ]
Category 4 ii. Products-Based for goods	Products/goods, travel distance, amount	kg of CO <sub>2</sub> per liter diesel for HD trucks	$CO_2e = (Amount_i \times km \times EF_i)$
Category 4 iii: Average	Appliances & Weekly Usage to be used in Cat.7	kg of CO <sub>2</sub> per kWh	$CO_2e = (Amount_i \times Duration_i \times EF_i)$
Based for Appliances			
Category 6: Business	number of events hosted or invited, number &	kg of CO <sub>2</sub> per liter diesel for	$CO_2e = \sum [(kmi /\eta_i)^*]$
Travel (Events & re-	distance traveled by employees on third parties	HD trucks/buses	$(Number_{Passenger}/Number_{Employees})$
late)	owned vehicles		EF]
Category 7: vehicles	Distance traveled by each vehicle owned	kg of CO <sub>2</sub> per kWh liter fuel	$CO2e = P(km_{oneWay} \times Counts_i \times EFi)$
Category 11: Electricity	Work hours & no. of (bulbs, computers, printers,	kg of CO <sub>2</sub> per kWh	$CO_2e = P(kW_i \times hours_i \times no. \times EF_i)$
	stoves, lab. machines, microscopes etc.)		
Category 12: Waste	Amount of solid waste (SW) & wastewater (WW)	Kg of CO2 per kg of SW or	$CO2e = X(Amount_{Waste}.i \times$
		liter of WW	$\%WasteTreatd{i} \times EF_{i})$
Category 15: summary	All categories except construction projects	Results of the above categories	$Total\_CO_2e = \sum E_{CO2} i_s$

4

Ethiopian International Journal of Engineering and Technology (EIJET)

Volume 2, Issue 2, 2024

Copyright and License Grant: CC By 4.0



Table VI: Vehicles and Travel Information

DOI: https://doi.org/10.59122/174CFC17

Parameters	Buses	Medium bus	5Seat Station- wagen	5Seat Parado	Mini- bus, New	Minibus, Old	Light Duty Truck	Ambu- lance 4 Doors	Auto- mobile, Exec	HD Truck
Year/Model	2004- 2020	2020	2020	2009	2012	2020	2012	2010	2008	2015 & 2018
Avg. oneway in km	9	9	10	10	9	9	15	25	10	10
No. of Shift b/n stops	12	6	4	4	12	12	12	10	4	2
Daily avg. distance(km)	154	54	40	40	108	108	180	250	40	20
No. of vehicles	9		4	2	3	2	6	2	2	2

DOI: https://doi.org/10.59122/174CFC17



Ethiopian International Journal of Engineering and Technology (EIJET)

Volume 2, Issue 2, 2024

Copyright and License Grant: CC By 4.0



Table VII: Building Types & Numbers in the main campus and nearby staffs' residential compounds where short forms MFA, FR, CR, S, H, O & R designate multifamily apartment family room, class room, studio, Halls, office & rooms, respectively

Building	G+1	G+2 CR	G+3 CR	Labs	LH	Lib	G+2	G+4	G+2	G+3	G+4	Cafe	Lounges
Types (Col)/	CR	+ O	+ O				MFA	MFA	Dorms	Dorms	Dorm		
Parameters											S		
(Rows)													
Building	8	26	6	18	10	4	16	5	23	4	2	3	6
Count													
Room Count	8CR	10CR	16CR	2CR	20	1CD	12FR	20 FR	16R 1O	24R 1O	32R	2K 2.O 3S	1K 1.O 2H
	3Os	5Os	4Os 2S	2Ss 1H	1S	8O 3Ss	3S		1S	2Ss	1.0		
					1H	2H					3S		

Copyright and License Grant: CC By 4.0



Table VIII: Emission Factor: Source activities & corresponding emission factor identified in reputable publishing websites and peer-reviewed academic articles or calculated based on IPCC guidelines

Source (Rows)			
/Unit	D 4 LEE	<b>G</b> .	<b>EF</b> in Convenient Unit
Conversion	Reported EF	Conversion	EF in Convenient kg of CO <sub>2</sub> /Unit
(Columns)			
Energy use (Combined)		0.15 tones per capita a year [19]	0.15 tone CO <sub>2</sub> per capita
Diesel (Stationary)	74.1 kgCO <sub>2</sub> /GJ (Dar'10 and John)	0.03586 GJ/litre	2.66 kg/liter
Diesel (Passenger)	0.237 kg/km or 3.17231 kg/kg [24]	1 with advanced control	0.237 kg/ km
Diesel (Passenger l)	0.248 kg/km or 3.17231 kg/kg	1 with moderate contro	0.248 kg/km
Diesel (Passenger)	0.319 kg/km or 3.17231 kg/kg	1 uncontrolled	0.319 kg/km
Diesel (LD truck )	0.33 kg/km or 3.17231 kg/kg	1 advan./mod. Control	0.33 kg/km
Diesel (LD truck)	0.415 kg/km or 3.17231 kg/kg [24]	1 for uncontrolled	0.415 kg/km
Diesel (HD truck )	0.987 kg/km or 3.17231 kg/kg [24]	1 for advanced controlled	0.987 kg/km
Diesel (HD truck )	1.011 kg/km or 3.17231 kg/kg	1 for moderate controlled	1.011 kg/kmm
Diesel (HD truck )	1.097 kg/km or 3.17231 kg/kg [24]	1 for uncontrolled	1.097 kg/km
	$0.02 \text{ kg CO}_2/\text{kWh},$	ratio 93:4:2:1, Hydro	
Electricity	[17,22-23]	: Wind :	0.02 kg/kWh
		Geothermal:Diesel (23)	
Waste (Combined)	$3.876 \times 10^9 kg$ of $CO_2$ a year	Solid waste (SW) to wastewater ratio 18.2 : 1	

Volume 2, Issue 2, 2024

(P): 2959-393X **DOI:** https://doi.org/10.59122/174CFC17



Copyright and License Grant: CC By 4.0

60	<b>①</b>
	24

	$CO_2e EF = (Waste \times$		
Solid Waste (Landfill)	%degradable) ×(1 –		200 kg CO2/kg a year
	CH4 Oxid <u>n</u> Factr.) ×	$CO_2e EF = 0.15 \times 0.5 \times 0.5 \times 0.5 \times 0.4 \times (1 - 0) \times (16/12) \times (1 - 0)$	
	CH <sub>4</sub> Cor <u>rection</u>		
	Factor.×(1 –		
	Recovery)x(16/12)		
Wastewater (treated)	$0.202 \times 10^9 kg$ of $CO_2$ a year	$CO_2e$ $EF = O_2$ DemandWaste $\times$ $CH_4$ Correction Factor. $\times$ $CH_4$ emissn Factor	EF=0.06*0.1*0.25*28=0.42kg CO <sub>2</sub> /year [17,25]
Firewood	CO <sub>2</sub> e EF = $(44/12) \times$ Cal. Value <sub>net</sub> × $(1 - \eta \text{stove}) \times (1 + H \psi) \times (1 +$	CO <sub>2</sub> e EF = $(44/12) \times 15 \times$ $(1 - 0.1) \times (1 + 0.2) \times (1 + 0.0067)$	6.06kgCO2/kg



# ETHIOPIAN INTERNATIONAL JOURNAL OF ENGINEERING AND TECHNOLOGY

#### About the EIJET

The Ethiopian International Journal of Engineering and Technology (EIJET) is a non-profit peer-reviewed open-access research Journal of Arba Minch Institute of Technology under Arba Minch University, Ethiopia. The scope of the Journal covers multidisciplinary and cross-disciplinary areas of research in engineering and technology. The Journal is indexed in Google Scholar. The Journal publishes all types of quality research papers, case studies, review papers, experimental and empirical papers, shortened thesis/disertations in the broad area of engineering, technology and the other converging areas.

The Journal is specificaly dedicated to publish novel research outcomes, contributions and inovative research ideas in the following fields of enginering and technology:-

- Intelligent Computing and Information Technology
- Mechanical and Metallurgy Engineering
- Architectural Design and Town Planning
- Civil and Transport Engineering Systems
- Electrical Engineering and Power Electronics
- Emerging areas of Renewable Energy

Papers related to allied disciplines, emerging technologies, and future-generation engineering paradigms will be given priority for publication.

The Journal publishes papers from worldwide sources, especially for covering the emerging issues of engineering and technology from developing and developed countries. The Papers from African continent countries having localized problem-solving research will be given priority.

Arba Minch University Arba Minch Institute of Technology Arba Minch, Ethiopia Phone: +251 46 881 4970

Fax: +251 46 881 4971